A Non-intrusive and Non-destructive Technique for Condition Assessment of Transformer Liquid Insulation

A Thesis
Submitted in Partial Fulfillment of the Requirements for the Award of the Degree of

Doctor of Philosophy (PhD)

By

Sangineni Rohith

School of Energy Science and Engineering
Indian Institute of Technology Guwahati
Guwahati, Assam-781039 India
May 2023

TH-3272_186151014

Dedicated

To

My Guruji

Prof. Sisir Kumar Nayak,

My Parents

Mrs. Harileela and Mr. Venkateshwarlu Sangineni,

my sister and brother-in-law **Mrs. Roshini and Mr. Rajesh Karupakala**

for their love and support

TH-3272_186151014

Declaration

I hereby certify that the work presented in this thesis entitled '**A Non-intrusive and Non-destructive Technique for Condition Assessment of Transformer Liquid Insulation**' is entirely my own account of research performed under the guidance of Dr. Sisir Kumar Nayak. Any part of this work has not earlier been submitted for the award of any degree, diploma, associate-ship, fellowship, or its equivalent to any University or Institution.

Date: 25.05.2023

S.Rohith

(Sangineni Rohith)
Registration No. 186151014
School of Energy Science and Engineering
Indian Institute of Technology Guwahati
Guwahati – 781039, Assam, India

TH-3272_186151014

School of Energy Science and Engineering
Indian Institute of Technology Guwahati
Guwahati – 781039, India

Certificate

This is to certify that the thesis entitled "***A Non-intrusive and Non-destructive Technique for Condition Assessment of Transformer Liquid Insulation***", submitted by Sangineni Rohith (186151014), a research scholar at the School of Energy Science and Engineering, Indian Institute of Technology Guwahati, for the award of the degree of Doctor of Philosophy, is a record of an original research work carried out by him under my supervision and guidance. The thesis has fulfilled all the requirements as per the regulations of the institute and in my opinion, has reached the standard needed for submission. The results embodied in this thesis have not been submitted to any other University or Institute for the award of any degree or diploma.

Date: 25.05.2023
Place: Guwahati

Dr. Sisir Kumar Nayak
Professor,
Department of EEE,
Indian Institute of Technology Guwahati
Guwahati – 781039, Assam, India

TH-3272_186151014

Acknowledgements

The first and foremost gratitude goes to my supervisor **Prof. Sisir Kumar Nayak** for his valuable guidance, support, love, empathy, and motivation throughout the research work. I am forever indebted to him for his encouragement in the laboratory as well as in sports. I would like to thank him for investing his valuable time in improving my technical, sports, and interpersonal skills. I would also like to acknowledge my sincere gratitude to my doctoral committee members, **Prof. Santosha Kumar Dwivedy**, **Prof. Harshal Bhalchandra Nemade**, and **Prof. Rakhesh Singh Kshetrimayum** for their precious suggestions and advice throughout my research work. Further, I express my sincere gratitude to Dr. Marley Becerra of KTH Royal Institute of Technology, Sweden for his precious suggestions for improving my research.

I would like to thank the Ministry of Education, Government of India, for providing the Prime Minister's Research Fellowship (PMRF) to pursue a PhD. I extend my thanks to the PMRF review committee, Prof. Senthilvelan, Prof. K. V. Krishna, Prof. V.S. Moholkar, Prof. K. Mohanty, and Prof. V. V. Goud of IIT Guwahati for providing a smooth platform to perform my research. I would like to thank all the faculty members, staff, and security personnel of the School of Energy Science and Engineering, for rendering their whole-hearted cooperation and support during my journey. I am grateful to SERB, DST, for bestowing me with International Travel Support and providing financial support to present a technical paper at the Conference on Electrical Insulation and Dielectric Phenomena held in Denver, CO, USA, from 30 October to 2 November 2022. I am thankful to the IEEE Dielectric and Electrical Insulation Society for awarding me the 2022 IEEE DEIS Graduate Student Fellowship.

I would also like to extend my gratitude to Dr. Thirumurugan Chandrasekaran of Vellore Institute of Technology, Mr. Manas Chakraborty of Regional Testing Laboratory – Central Power Research Institute, Guwahati and Central Instrument Facility, IIT Guwahati for their support in availing various test facilities. I am thankful to my laboratory members Dr. Mrutyunjay Maharana, Dr. Niharika Baruah, Dr. Amit Kumar Baghel, Ms. Sujita Srichandana Dey, Mr. Shashank Satish Kulkarni, Mr. Vivek Kumar, Mr. Kanumuri Deepak, and Mr. Ambuj Kumar for their valuable suggestions and cooperation during my PhD.

My special thanks to my friends Mr. Maturi Krishna Chaitanya, Mr. Uday Boddepalli, Mr. Sumanth Veerapuram, Ms. Sunanda, Mr. Ravi Kiran Dokala, Mr. Rakesh, Mr. Arun Kumar

TH-3272_186151014

Reddy, Mr. Rabindra Banik, Mr. Sampreet Kalita, Mr. Bhasker Kethireddy, Mr. Cilaveni Satish Chandra, Mr. G V N Chandra, Mr. Tholeti Aditya. My research and my personal life were enjoyable because of these people. I would also like to thank my neighbours Mr. Karan Kumar, Mr. Brij Nandan Tripathi, Dr. Debanjan Roy Chowdhury, Dr. Raveesh S, Mr. Sunil Kumar, Dr. Kaustubh Chandrakant Khaire, and Mr. Gangesh Gunjan with whom I had a great time growing up.

I would like to thank my parents, Mrs. Sangineni Harileela and Mr. Sangineni Venkateshwarlu, my sister and brother-in-law Mrs. Karupakala Roshini and Mr. Karupakala Rajesh for their love, support, and encouragement during my PhD journey. I would also like to thank my close friends Mr. Rajkiran Jaganmohan, Mr. Madasu Uttam Kumar, Ms. Jeevana Reddy, Ms. Pragatisheel Tiwari, Ms. Aradhana Priyadarshini, and Dr. Prajna Paramita Mohapatra for their never-ending love and cherishable memories. I feel proud of them for sacrificing their plans of spending time with me and letting me work. Lastly, I am and will always be thankful to God for guiding me through the tough and happy times of my life.

(Sangineni Rohith)
Registration No. 186151014
School of Energy Science and Engineering
Indian Institute of Technology Guwahati
Guwahati – 781039, Assam, India

TH-3272_186151014

Abstract

This thesis presents a high frequency signal based condition assessment technique that can detect and estimate the moisture content (MC) and total acid number (TAN) in insulating oil samples. It also addresses the applicability of the developed technique to various insulating oils such as mineral oil (MO), nanofluids (NFs), ester oil (EO), and blended oils (BO).

The MC and TAN are very important chemical properties that define the aging status of insulation. Conventional moisture and acid measurement devices are bulky, costly, immobile, and can be operated only in the laboratory environment due to their sensitivity and fragility. Moreover, conventional testing requires the sample to be carried over to the testing location, where waiting times may prevail for obtaining the test results. These factors may lead to delays in adopting corrective measures and may lead to equipment failure. Therefore, there is a need to develop a cost-effective and robust technique that can detect the physical parameters swiftly. In addition, the ability to detect more than one parameter makes the technique meritorious. A non-intrusive and non-destructive technique (NINDT) which uses an S-band horn antenna to radiate the signals onto the oil samples for detecting and estimating the MC and TAN in MO is developed. The reflected signal from the samples is analyzed to study the resonant frequency corresponding to MC and TAN. Electromagnetic interference on the measurements is avoided by placing the test setup in an anechoic chamber. Undesired reflections from the oil-test vessel boundaries are avoided by making the test cell with a material having impedance and relative permittivity close to that of the oil. The technique is applied to various laboratory-aged samples and linear prediction graphs are deduced from the obtained reflection coefficient. These linear prediction graphs are used to predict the MC and TAN in service-aged MO samples to evaluate the effectiveness of the developed technique. The chosen frequency band of 2.1 to 2.6 GHz is able to clearly differentiate MO samples with different TAN and MC. This technique is unaffected by the operating frequencies in the electrical substation due to its EMI-free design.

The EOs and BOs prove to be a good alternative to MO due to their excellent biodegradability, fire and flash points. BOs provide a middle ground by balancing the cost and properties. Moreover, an involuntary blending of MO and EO occurs when an old MO based transformer is retrofilled with EO. MO and a commercial EO (FR3) are mixed in various ratios to prepare BOs in this work. The electrical and physiochemical properties such as MC, AC breakdown voltage, dissipation factor, relative permittivity, specific resistance, flash points,

TH-3272_186151014

interfacial tension, and density of the BOs are studied. The long term performance of the BOs is also studied by oxidative aging them according to ASTM D1934. Since oils undergo electric stress in the transformer during their operation, partial discharge (PD) study of the EO, MO, and BOs helps in understanding their behavior under electric stress and gives an insight into their relative performance under electric stress. The PD in the fresh and aged oils is studied according to the IEC 60270 standard and the inception, extinction voltages, and phase resolved partial discharge patterns are presented.

The dissolved gas analysis (DGA) provides extensive information on the gas emission pattern of oils when subjected to thermal and electric stress. The fresh and oxidative aged MO, EO, and BOs are subjected to multiple electrical sparks and the gases produced are noted. The classical ratio methods such as Rogers, IEC, and Dornenburg ratios are used to predict the type and intensity of fault in the BOs from the collected data. Further, the prediction of the type and intensity of fault is attempted by using graphical methods such as Duval's triangles and pentagons. The total dissolved combustible gases produced in the oils are also presented. Further, solid insulation is aged in the EO to study the gelling phenomenon and the surface profile of the insulation. The retrofilling of an MO based transformer with FR3 or blended oil does not pose any danger to its operation. In addition, it provides better electrical and physiochemical characteristics. The amount of gases generated in BOs is different for individual combinations of MO and EO. The thermal aging of kraft paper in vegetable oil leads to the gelling of oil on the surface of the solid insulation at high temperatures.

The two-step method for preparation of the NFs is presented. The thermal conductivity of various NFs is studied by varying the concentration and temperature. The electric field around conducting, semi-conducting, and insulating nanoparticles (NP) under DC voltage is simulated by assuming all the NPs are spherical and have an equal diameter of 50 nm. The dielectric frequency response of insulating NP based NF with various concentrations of NPs is studied. Although extensive literature is available on the physiochemical and electrical properties of NFs, their magnetic behavior is unclear. Therefore, the magnetic response of the NPs, base oils, and NFs to the quasi-static and dynamic magnetic fields is studied at room temperature conditions, and various magnetic parameters of the NPs and NFs are extracted.

After extensive investigation and substantiation of the insulation, the NINDT and the linear graphs developed for MO are investigated for their applicability to detecting and estimating the MC and TAN in the NFs and BOs. Different test cells are used for each NF to

TH-3272_186151014

avoid the contamination of the subsequent samples. An attempt is made to age the NFs to prepare multiple samples with various TAN and MC. The EO and BOs are tested using the NINDT to predict the MC and TAN in them which are compared with the conventional test results. The percentage error between the predicted and actual value is reported, and the applicability of the NINDT for the BOs and NFs is commented upon.

TH-3272_186151014

Table of Contents

1. Introduction **1**

1.1. Introduction 2

1.2. Literature Survey 3

1.2.1. Types of liquid insulation 3

1.2.2. Aging and the importance of monitoring 6

1.2.3. Measurement tests and techniques for monitoring 6

1.3. Motivation 8

1.4. Objective of the thesis 8

1.5. Contribution of the thesis 9

1.6. Organization of the thesis 10

2. The non-intrusive and non-destructive technique for condition assessment of mineral oil **12**

2.1. Introduction 13

2.2. Materials and experimental technique 14

2.2.1. Sample preparation 14

2.2.1.1. Accelerated thermal aging 15

2.2.1.2. Oxidative aging 16

2.2.1.3. Inservice transformer sample 16

2.2.2. Test setup and calibration 17

2.3. Frequency response analysis of samples and validation of the technique 20

2.3.1. Frequency response of accelerated thermal aged samples 21

2.3.2. Frequency response of open beaker oxidative aged samples 23

2.3.3. Estimation of degradation of in-service transformer oil samples from frequency response 24

2.4. Non-isothermal thermogravimetric analysis of kraft paper 28

2.5. Summary of the chapter 33

TH-3272_186151014

3. Natural ester and blended oils as alternate transformer insulation **35**

3.1.Introduction 36

3.2.Materials and aging 37

3.2.1. Materials used in experimentation 37

3.2.2. Aging of samples 38

3.3. Physiochemical and electrical properties of the blended oils 38

3.3.1. Physiochemical properties and AC breakdown voltage 38

3.3.2. Partial discharge in blended oils 41

3.3.2.1. Test setup 41

3.3.2.2. Calibration and experimentation 43

3.3.2.3. PDIV and PDEV of fresh and aged blended oils 45

3.3.2.4. PD pattern and the minimum phase angle at PDIV 47

3.3.3. Gassing tendency of blended oils on subjecting to electrical sparking 52

3.3.3.1. Sample preparation and description of gas ratios 53

3.3.3.1.1. Sample preparation 53

3.3.3.1.2. Measurement of dissolved gases and description of gas diagnosis methods 53

3.3.3.2. Fault prediction from dissolved gases in blended oils 55

3.3.3.2.1. Fault analysis using gas ratios methods (IEC, Dornenburg's, and Rogers) 59

3.3.3.2.2. Fault analysis using Duval triangles and pentagons 60

3.3.3.2.3. Comparison of TDCG in BOs 63

3.4. Surface study of solid insulation aged in natural ester 64

3.5. Summary of the chapter 67

4. Nanofluids as alternate transformer insulation **69**

4.1. Introduction 70

4.2. Preparation of nanofluids 71

4.3. Thermal conductivity studies on the nanofluids 72

TH-3272_186151014

4.3.1. With variation in nanoparticle concentration 72
4.3.2. With variation in temperature 73
4.4. Simulation of electric field around nanoparticles dispersed in oil 74
4.5. Dielectric frequency response of nanofluids 78
4.6. Magnetic profiling of conducting, semi-conducting and insulating nanoparticles and their nanofluids 81
4.6.1. Introduction 81
4.6.2. Description of experimental techniques 83
4.6.2.1. Vibrating sample magnetometer spectroscopy 83
4.6.2.2. Electron spin resonance spectroscopy 83
4.6.3. Sample preparation 84
4.6.4. Magnetic profiling of nanoparticles and nanofluids 87
4.6.4.1. Magnetic study using vibrating sample magnetometer spectroscopy 87
4.6.4.2. Magnetic study using electron spin resonance spectroscopy 94
4.7. Conjecture on benefits of using vegetable oils and nanofluids over mineral oil 98
4.8. Summary of the chapter 99

5. The non-intrusive and non-destructive technique for condition assessment of alternate liquid insulating oils 102
5.1. Introduction 103
5.2. Non-intrusive and non-destructive technique for condition assessment of nanofluids 103
5.3. Non-intrusive and non-destructive technique for condition assessment of vegetable and blended oils 107
5.4. Summary of the chapter 111

6. Conclusion and future work 112
6.1. Summary of the present work 113
6.2. Contribution of the thesis 115
6.3. Suggestions for future research work 115

TH-3272_186151014

Bibliography 117

List of Publications 131

TH-3272_186151014

List of Figures

1.1	Milestones in the development of liquid insulation	4
1.2	Preparation of nanofluid	4
2.1	(a) Sealed beaker accelerated thermal aging setup and (b) Open beaker accelerated oxidative aging setup	15
2.2	(a) Closed beaker accelerated thermal aged samples (b) Open beaker accelerated oxidative aged samples and (c) In-service transformer oil samples.	16
2.3	Anechoic chamber for insulation monitoring. (1) Vector network analyzer (MS46122B, Anritsu) (2) Antenna placed over the testing vessel with no air gap.	18
2.4	Schematic representation of the experimental setup in the anechoic chamber.	18
2.5	(a) Dimensions of the pyramidal horn antenna and (b) radiation pattern of the antenna at 2.45 GHz.	19
2.6	Frequency response on the addition of HMWCA.	21
2.7	Frequency response of sealed beaker accelerated thermal aged samples.	22
2.8	Frequency response of open beaker accelerated oxidative aged samples.	24
2.9	Extrapolated linear fit for total acid content.	26
2.10	Extrapolated linear fit for moisture content.	26
2.11	Frequency response of in-service transformer oil samples.	27
2.12	Thermo Gravimetric Analyser.	30
2.13	Illustration of a ceramic pan filled with paper insulation in a TGA furnace with top-load balance.	30
2.14	Solid insulation samples (a) Vacuum oven dried fresh kraft paper (b) 300 hours oxidative aged kraft paper (c) 600 hours oxidative aged kraft paper (d) 900 hours oxidative aged kraft paper	31

TH-3272_186151014

2.15	(a) Empty ceramic cup (b) Ceramic cup filled with kraft paper samples (c) Ceramic cup with remainings after performing TGA.	31
2.16	Weight percentage vs temperature curve of the kraft paper samples from 30 to 900˚C.	31
2.17	Weight percentage vs Temperature of the kraft paper samples from 150 to 450˚C.	32
2.18	Derivative weight vs temperature of the kraft paper samples from 150 to 450˚C.	33
3.1	Hermetically sealed fresh and oxidative aged liquid insulation samples.	38
3.2	(a) Partial discharge measurement connection diagram and (b) Experimental setup with test cell.	42
3.3	(a) PD test cell with the needle (20 µm) and plane electrodes and (b) Illustration of PD test cell with dimensions.	42
3.4	(a) PDIV on reaching 100 pC and (b) PDIV on reaching 500 pulses/min.	46
3.5	(a) PDEV on reaching 100 pC and (b) PDEV on reaching 500 pulses/min.	46
3.6	PD pattern at 6 kV above PDIV for (i) A1 (ii) B1 (iii) C1 (iv) D1 and (v) E1 samples.	47
3.7	PD pattern at 6 kV above PDIV for (i) A2 (ii) B2 (iii) C2 (iv) D2 and (v) E2 samples.	49
3.8	(a) Duval triangle 1 for mineral oil and (b) Duval triangle 3 for FR3	55
3.9	Duval triangle 1 for fault prediction in blended oils.	61
3.10	Duval triangle 3 for fault prediction in blended oils.	61
3.11	Duval pentagon 1 for fault confirmation in blended oils.	62
3.12	Duval pentagon 3 for fault confirmation in blended oils.	63
3.13	Total dissolved combustible gases in sparked blended oils	64
3.14	Gel balls formed on the surface of the pressboard	64
3.15	(a) Gel balls (b) Single crystal X-ray diffraction of gel balls	65

TH-3272_186151014

3.16	(a) Fresh and dry solid insulation (b) fresh solid insulation subjected to moisture equilibrium with VO for 96 hours and (c) solid insulation aged for 500 hours at 180°C in VO	65
3.17	(a) 3D image of fresh dry solid insulation (b) 3D image of fresh solid insulation immersed in VO (c) 3D image of solid insulation after thermal aging for 500 hours (d) Topography of fresh dry solid insulation (e) Topography of fresh solid insulation immersed in VO (f) Topography of solid insulation after thermal aging for 500 hours.	66
4.1	Preparation of nanofluids.	71
4.2	Samples of (a)fresh MO (b)MO+0.01wt.%NP (c)MO+0.02wt.%NP (d)MO+0.05wt.%NP (e)MO+0.1wt.%NP (f) fresh FR3 (g) FR3+0.01wt.%NP (h)FR3+0.02wt.%NP (i)FR3+0.05wt.%NP and (j)FR3+0.1wt.%NP.	72
4.3	Thermal conductivity of base oils and nanofluids.	73
4.4	Samples of (a)fresh MO and (b)MO+0.01wt.%NP.	73
4.5	Thermal conductivity of MO and its nanofluid with increase in temperature.	74
4.6	Parallel plate electrodes with MO in between.	75
4.7	Electric field distribution in (a) MO (b) MO with conducting NP (c) MO with semi-conducting NP and (d) MO with insulating NP.	76
4.8	Electric field distribution along the electrodes in (a) MO (b) MO with conducting NP (c) MO with semi-conducting NP and (d) MO with insulating NP.	77
4.9	Samples of (a) MO (b) MO+0.01 %w/v Eh-BN (c) MO+0.05 %w/v Eh-BN (d) MO+0. 1 %w/v Eh-BN.	78
4.10	Impedance analyzer and dielectric interface for dielectric frequency response measurement.	79
4.11	Variation of (a) real and (b) imaginary relative permittivity of nanoliquids with frequency.	80
4.12	Variation in tanδ of nanoliquids with frequency.	81
4.13	(a) Experimental setup of VSM and (b) Schematic of VSM.	83
4.14	Experimental setup of ESR spectrometer.	84

TH-3272_186151014

4.15	Different kinds of nanofluids prepared in the laboratory (a) MO-Fe_3O_4 (b) MO-CuO (c) MO-Al_2O_3 (d) FR3-Fe_3O_4 (e) FR3-CuO and (f) FR3-Al_2O_3.	86
4.16	UV-visible spectroscopy of (a)MO-NFs and (b) FR3-NFs.	86
4.17	(a) Incident magnetic field, (b) Magnetic moment/mass of Al_2O_3 nanoparticle, (c) Magnetic moment/mass of CuO nanoparticle, and (d) Magnetic moment/mass of Fe_3O_4 nanoparticle.	89
4.18	M-H curve of nanoparticles.	90
4.19	M-H curve of MO and MO-NFs.	90
4.20	M-H curve of MO-NFs after removing the diamagnetic component due to base oil.	91
4.21	M-H curve of FR3 and FR3-NFs.	92
4.22	M-H curve of FR3-NFs after removing the diamagnetic component due to base oil.	94
4.23	ESR spectra of NPs and NFs.	95
4.24	Magnetic field lines in the presence of diamagnetic material.	99
5.1	Nanofluids prepared in the laboratory (a) MO-Fe_3O_4 (b) MO-CuO (c) MO-Al_2O_3 (d) FR3-Fe_3O_4 (e) FR3-CuO and (f) FR3-Al_2O_3.	104
5.2	Frequency response analysis of mineral oil based nanofluids.	105
5.3	Frequency response analysis of FR3 based nanofluids.	105
5.4	Fe_3O_4 nanoparticles adhered to the test cell after removing the nanofluid.	106
5.5	(a)Dried fresh pressboard (b) Pressboard aged in MO-Al2O3 NF (c) Pressboard aged in MO-CuO NF and (d) Pressboard aged in MO-Fe3O4 NF.	107
5.6	Hermetically sealed fresh and oxidative aged liquid insulation samples	108
5.7	Frequency response analysis of fresh MO, FR3, and their BOs.	109
5.8	Frequency response analysis of aged MO, FR3, and their BOs.	109

TH-3272_186151014

List of Tables

1.1	Physiochemical properties of a few natural ester oils	5
2.1	Specification of insulating oil procured.	15
2.2	Nomenclature of transformer oil samples obtained from substations of ASEB and IIT Guwahati.	17
2.3	Different types of Carboxylic acids	21
2.4	MC and TAN of sealed beaker aged samples.	22
2.5	MC and TAN of open beaker aged samples.	23
2.6	Coefficients, MAE, and R^2 of the first order polynomial for TAN and MC.	25
2.7	Predicted and measured results of MC and TAN of in-service transformer oil samples.	27
3.1	Samples of blended oils.	37
3.2	Physiochemical properties of blended oils.	40
3.3	Magnitude of highest discharge pulse at 10 kV, 15 kV, PDIV, and 6 kV above PDIV (100 pC)	50
3.4	Phase angle at PDIV (100 pC).	51
3.5	DG Interpretation according to IEC, Rogers, and Dornenburg ratios.	56
3.6	Dissolved gases in oils before and after sparking.	57
3.7	Gas ratios of oil samples after sparking	59
3.8	Fault indications using IEC, Dornenburg, and Rogers ratio analysis.	60
4.1	Specification of the liquid insulation.	84
4.2	Specification of the nanoparticles.	85
4.3	Moisture content in nanofluids.	87
4.4	Magnetic susceptibility of nanofluids.	92
4.5	Parameters extracted from ESR spectroscopy.	96
5.1	MC and TAN in nanofluids.	104
5.2	Samples of blended oils	107

TH-3272_186151014

5.3 MC and TAN in blended oils. 108
5.4 Predicted and measured MC and TAN in MO, EO, and BOs. 110

TH-3272_186151014

List of Acronyms

AC	Alternating current
ACBDV	AC breakdown voltage
AFM	Atomic force microscope
Al_2O_3	Aluminium oxide
ASEB	Assam State Electricity Board
ASTM	American Society for Testing and Materials
BDV	Breakdown voltage
BO	Blended oil
Cal	Calibrator
CAS	Chemical Abstracts Service
CC	Coupling capacitor
CG	Combustible gases
CGS	Centimeter Gram Second
CH_4	Methane
C_2H_6	Ethane
C_2H_4	Ethylene
C_2H_2	Acetylene
CIF	Central instrument facility
CIGRE	Conseil International des Grands Réseaux Electriques
CO	Carbon monoxide
CO_2	Carbon dioxide
CRGO	Cold rolled grain oriented
CGL	Crompton Greaves Limited
CuO	Copper oxide
CVD	Capacitive voltage divider
D1	Low energy discharges
D2	High energy discharges

TH-3272_186151014

DC	Direct current
DDF	Dielectric dissipation factor
DG	Dissolved gases
DGA	Dissolved gas analysis
DHE	Discharges of high energy
DLE	Discharges of low energy
DP	Degree of polymerization
DR	Dornenburg ratios
DT	Mixture of electrical and thermal faults
EC	European Community
EEE	Department of Electronics and Electrical Engineering
EHV	Extra high voltage
EMF	Electromotive force
EMI	Electromagnetic interference
EO	Ester oil
ESR	Electron spin resonance
FDDRM	Frequency domain dielectric response measurements
FDS	Frequency domain spectroscopy
Fe_3O_4	Iron oxide
FNF	Ferro nanofluid
FRI	Frequency response of liquid insulation
FTIR	Fourier transform infrared spectroscopy
GCT	Glass capillary tube
H_2	Hydrogen
HMWCA	High molecular weight carboxylic acids
HMWH	High molecular weight hydrocarbons
HV	High voltage
IEC	International Electrotechnical Commission
IEEE	Institute of Electrical and Electronics Engineers
IFT	Interfacial tension

TH-3272_186151014

IGR	IEC gas ratios
IITG	Indian Institute of Technology Guwahati
IN	Insignificant
IR	Infrared
L1	Minimum concentration limit
LMWCA	Low molecular weight carboxylic acids
MAE	Mean absolute error
MATLAB	Matrix laboratory
MC	Moisture content
MM	Mass magnetization
MO	Mineral oil
NEO	Natural ester oil
NF	Nanofluid
NMR	Nuclear magnetic resonance
NoP	No prediction
NP	Nanoparticle
ONAN	Oil natural air natural
PCB	Polychlorinated biphenyl
PCode	Process order number
PCTET	Polychlorotrifluoroethylene tube
PD	Partial discharge
PDC	Polarizing and depolarising current
PDEV	Partial discharge extinction voltage
PDIV	Partial discharge inception voltage
PDMS	Polydimethylsiloxanes
pH	Potential of Hydrogen
ppm	Parts per million
PRPD	Phase resolved partial discharge
PSW	Primary and secondary windings
PTFE	Polytetrafluoroethylene

TH-3272_186151014

RH	Relative humidity
RIE	Ratio of PDIV to PDEV
RMSE	Root mean squared error
RP	Relative permittivity
RPM	Rotations per minute
RR	Rogers ratios
RVM	Reverse voltage measurement
S	Stray gassing of oil at temperatures below 200°C
T1	Thermal faults below 300°C
T2	Thermal faults between 300°C and 700°C
T3	Thermal faults above 700°C
TAN	Total acid number
TC	Thermal conductivity
TDDRM	Time domain dielectric response measurements
TDCG	Total dissolved combustible gases
TF	Thermal fault
TGA	Thermogravimetric analysis
TR	Technical report
UVS	UV-Visible spectroscopy
VDE	Verband der Elektrotechnik
VNA	Vector network analyser
VO	Vegetable oil
VSM	Vibrating sample magnetometer
XRD	X-ray diffraction
ZnO	Zinc oxide

TH-3272_186151014

List of Symbols

$tan\delta$	*Dielectric dissipation factor*
S_{11}	*Reflection coefficient*
f_c	*Cut-off frequency*
ϵ_r	*Relative permittivity of the medium*
c	*Velocity of light in free space*
μ_r	*Relative permeability of the medium*
k	*constant*
x	*Independent variable*
y	*Dependent variable*
a	*Coefficient of independent variable*
b	*Intercept of the linear equation*
R^2	*Coefficient of determination*
ρ	*Resistivity*
E	*Test voltage*
K	*Cell constant in cm*
I	*Current through the sample in pA*
E_{max}	*Maximum electric field*
V	*Applied voltage*
r	*Radius of curvature of the needle tip*
d	*Distance between the needle tip and plane electrode*
$\%p_i$	*Percentage of i^{th} gas*
p_i	*Gas concentration in ppm*
R_1	*Ratio of concentration of ethene to ethane gas in ppm*
R_2	*Ratio of concentration of acetylene to ethene gas in ppm*
R_3	*Ratio of concentration of methane to hydrogen gas in ppm*
R_4	*Ratio of concentration of acetylene to methane gas in ppm*
R_5	*Ratio of concentration of ethane to acetylene gas in ppm*

TH-3272_186151014

ϵ	*Complex permittivity*
ϵ'	*Real part of complex permittivity*
ϵ''	*Imaginary part of complex permittivity*
σ	*Electrical conductivity*
ω	*Frequency of the input signal*
$\boldsymbol{B}$	*Magnetic flux density*
χ_p	*Mass magnetic susceptibility*
μ_0	*Absolute permeability of free space*
$\boldsymbol{H}$	*Magnetic field strength*
$\boldsymbol{F}$	*Magnetic force*
V_n	*Volume of nanoparticle*
g	*Lande's g factor*
$\Delta B_{p\text{-}p}$	*Peak-to-peak line width*
B_0	*Resonance flux density*
T_2	*Spin-spin relaxation time*
P	*Dependent variable*
ΔB	*Width at half height of the absorption peak*
A	*Area under the absorption curve*
α	*Asymmetry parameter*
$h(\hbar)$	*Planck's constant*
μ_B	*Bohr magnetron*
υ	*Frequency of electromagnetic radiation*

TH-3272_186151014

1

Introduction

Contents

1.1	Introduction	2
1.2	Literature survey	3
1.3	Motivation	8
1.4	Objective of the thesis	8
1.5	Contribution of the thesis	9
1.6	Organization of the thesis	10

TH-3272_186151014

1.1 Introduction

The transformer is a critical link in the power system and its reliability decides the quality of the power supply. Transformers have five major active components, namely magnetic, conducting, insulating, cooling, and structural elements. Among them, insulation is subjected to electric, thermal, chemical, and mechanical stresses simultaneously. Due to continuous multi-stresses acting on it, the insulation, being also structurally the weakest, forms the weakest link and dictates the reliability of the transformer. Hence, the transformer insulation needs to be monitored continuously to avoid catastrophic failures resulting in long power outages.

The insulation system of transformers is mainly categorized into three types:

1. Oil impregnated cellulosic solid insulation (OIP)
2. Gas insulated systems with cellulose replaced by Polypropylene and oil by SF6 gas and
3. Dry type transformers cast in epoxy resin.

With an overwhelmingly large population of transformers having paper and oil insulation systems, the work covered in this thesis is directed toward some reliability aspects of OIP transformers. Solid insulating materials commonly used in OIP transformers are kraft paper, pressboard, and fiberglass. MO is a vastly used liquid insulating material in transformers. MO serves multiple purposes, acting as a major insulation in conjunction with cellulose, as an impregnant to fill voids in solid insulation, and as a cooling medium.

The major disadvantages of MO are the low fire point and biodegradability. Also, being less hydrophilic than cellulose, it is more likely to give away moisture to cellulose rather than help to dry it. With the increasing stress on the use of green material, vegetable oil (VO) based esters are being investigated as a replacement for MO, which has the added advantage of low flammability. Moreover, the moisture saturation capability of VO helps keep the cellulose insulation relatively dry from moisture compared to MO. The ester oils produced either from natural resources or by synthesis are observed to possess better electrical characteristics compared to the MO. Further enhancement is sought with the use of nanofluids (NFs) prepared by the addition of nanosized particles into the mineral or ester oils, which have better thermal and electrical characteristics (partial discharge (PD) and breakdown) compared to the base oils. Irrespective of their origin, the insulation undergoes degradation over time due to various factors.

Temperature, moisture, contaminants, defects, magnitude, and duration of electric stress cause the aging of insulation and hence adversely affect its life. Among them, temperature and moisture are the foremost reasons for the faster deterioration of the transformer insulation.

TH-3272_186151014

Acids and moisture are formed in the insulation as by-products of degradation. As a result of aging, resistivity, dielectric strength, flash and fire points of the insulation decreases. Sludge formation occurs, and the viscosity increases, followed by a decrease in thermal conductivity (TC) and an increase in hotspot temperature. Defects being cumulative, increase the risk of insulation failure. Monitoring the condition of the aged insulation can reduce the risk of predicted failures by enabling pre-emptive corrective action to break up the cumulative action of defects.

Solid insulation, being closest to the conductor, is subject to the highest amount of electric and thermal stresses, which, in the presence of moisture, ages, resulting in lower electrical breakdown and mechanical strengths. Hence, it is important to monitor the aging of solid insulation. Since it is not possible to access the solid insulation directly for routine monitoring tests, oil serves as an agent for monitoring the condition of solid insulation. Several tests such as breakdown voltage (BDV), moisture content (MC), resistivity, *tanδ*, total acid number (TAN), furan content, dissolved gas analysis (DGA), interfacial tension (IFT), Furan content and particle content measurements are in vogue that not only detect the aging of oil itself but also indirectly that of the solid insulation. Each of these tests takes significant measurement time and yields only a single parameter. An instrument or a technique that can detect multiple parameters swiftly using high frequency signals and possess potential remote monitoring capability would be of immense value to the power system operator.

1.2 Literature survey

1.2.1 Types of Liquid Insulation

Oil in the transformer serves as an insulant, coolant, acoustic damper, and health indicator. Ideal insulation should have high resistivity, dielectric strength, thermal conductivity, oxidation stability, flash, and fire points. It should also be chemically and thermally stable with low viscosity, dielectric dissipation factor, and pour points. The development of various insulating liquids over time is presented in Figure 1.1. MO has been the most used dielectric fluid in transformers alongside pressboards and kraft papers for more than a century [1, 2].

MO is a complex mixture of hundreds of different organic compounds. The properties of MO may vary from one batch to another even though they are procured from the same supplier. MO is generally categorized as paraffinic, naphthenic, aromatic (unsaturated ring molecules), and mixed. Researchers felt the need to develop an alternative to MO due to its extinctive nature, non-biodegradability, and mediocre electro-thermal properties [3-7]. Liquid insulation

TH-3272_186151014

developed over time as an alternative to MO includes synthetic liquids, polychlorinated biphenyls (PCB), high molecular weight hydrocarbons (HMWH), Silicone oils, synthetic esters oils, natural ester oils (NEO), and Nanofluids (NF).

The NEOs have better electrical breakdown, moisture solubility, and aging characteristics compared to MO. Poor dissipation factor, oxidation stability, pour point, relative permittivity, and viscosity are their main disadvantages. NEOs are derived from plant sources and are completely biodegradable. A variety of them is available in the market, namely linseed oil, castor oil, corn oil, pongamia pinnata oil (karanji oil), soybean oil, punna oil, neem oil, jatropha curcas oil, palm oil, sunflower oil, olive oil, peanut oil, cottonseed oil, rapeseed oil (canola oil), coconut oil, honge oil, mustard oil, and hazelnut oil [8-16]. A few physiochemical and electrical properties of a few NEOs are presented in Table 1.1. The proper blending of VOs with MO may also be done to lower the pour point at the same biodegradability [17].

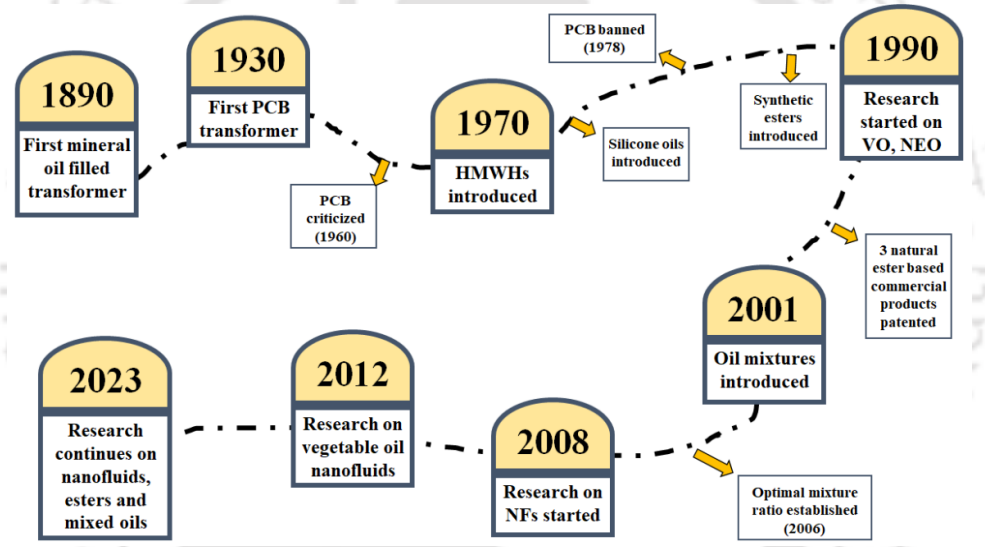

Figure 1.1: Milestones in the development of liquid insulation.

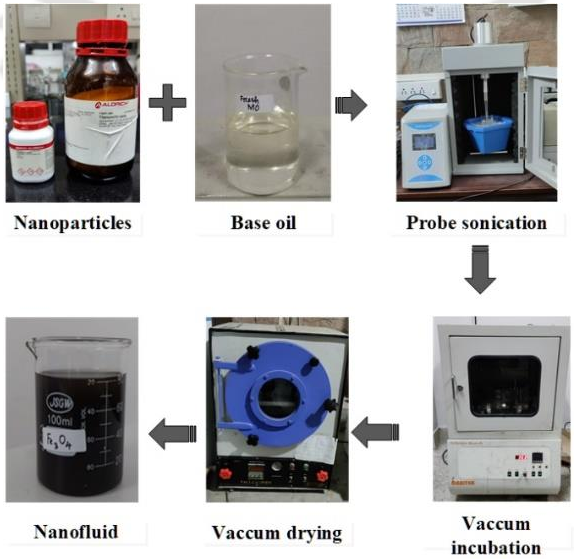

Figure 1.2: Preparation of Nanofluid.

TH-3272_186151014

1. Introduction

The development of innovative alternatives like NFs came to the forefront due to their better insulating and heat transfer properties than the conventional MO and ester oils [18, 19]. NFs are a new class of fluids developed by dispersing nanometer-sized materials (particles, nanofibers, nanotubes, nanowires, nanorods, nanosheets, or droplets) into base fluids in two step method as shown in Figure 1.2. The NFs can be used in cooling for engines, refrigeration, biomedics, and solar water heaters for efficient performance. Despite many NFs having good thermal conductivity, only a few NFs are suitable for insulating purposes [20-22].

Table 1.1: Physiochemical properties of a few natural ester oils [8, 12-14, 23-25]

Properties / Oils	Kinematic Viscosity at 40°C (cSt)	Flash Point (°C)	Acid Value (mg KOH/g)	ACBDV (kV)	Pour Point (°C)
Jatropha oil	33.8	260	0.06	73	-3
Crude Pongamia Oil	32	250	1.3	87.5	-25
Pongamia Oil Methyl Ester	12	284	0.9	82	-1
Rapeseed Oil	43	325	0.03	73	-18
Biovolt A (mineraltec)	36.1	312	0.05	55	-21
Soya Oil	33.1	318	0.08	42	-12
Rice Oil	32.4	318	0.04	37	-15
Sunflower Oil	38	312	0.06	37	-6
Coconut Oil	25.7	298	0.005 – 0.05	35	23
Honge Oil	116.62	298	--	42.8	--
Neem Oil	108.79	288	--	43	--
Mustard Oil	95.74	289	--	41.6	--
Punna Oil	129.66	280	--	42.3	--
Castor Oil	155.71	280	--	31	--
Palm Oil	5.06	186	0.005	81	-32.5

TH-3272_186151014

1.2.2 Aging and the importance of monitoring

The service life of mineral insulating oils is typically 30 to 40 years for power transformer applications [1, 26-28]. As mentioned earlier, insulation is subjected to electrical, magnetic, mechanical, chemical, and physical stresses during operation, resulting in its deterioration [29, 30]. Thermal stress is a result of fluxes interacting with the metallic body, normal and overloading of equipment, and ineffective cooling of the equipment. Electric stress is due to excitation, winding resonances, lightning, and switching transients. Mechanical stress is due to the short-circuit and inrush currents.

The insulating oil and paper undergo oxidation and pyrolysis under thermal stress, resulting in the formation of gases, sludge, etc., which accelerates the aging process. Thermal aging results in the reduction of life by 50% for an increase in operating temperature by 6 to 8°C. Chemical degradation, such as oxidation, promotes the formation of acids. The degradation eventually results in breakage in polymer chains of cellulose insulation and forms polar groups, which progressively damage the entire insulation system. Failing to determine aging ultimately leads to premature failure of the transformer, followed by loss of revenue and reliability of power supply to the consumers [27, 28, 31]. Therefore, it is essential to monitor the aging status periodically [18, 32-36].

Various tests are performed on the oil in laboratories to study and interpret the aging status of both solid and liquid insulation. Tests are also conducted to assess the gases, furans, phenols, cresols, and metal particles formed in the oil during its operation [27, 37]. Appropriate maintenance has to be undertaken on observing any deviation in the physiochemical and electrical properties from threshold values mentioned in ASTM, IEEE, and IEC standards. Condition based monitoring is preferred over time-based monitoring as it helps in cost cutting and saving time in attending to the equipment that is in need. It also helps in reducing catastrophic failures, unplanned outages, and downtime associated with them. To summarize, monitoring of a transformer should be done regularly while the maintenance is performed only if required.

1.2.3 Measurement tests and techniques for monitoring

With the knowledge gained on the need for monitoring and maintenance, the methods and techniques for monitoring are to be comprehended. The assessment of the insulation condition gives insight into its degradation status and the remnant life of the transformer. Although the transformer consists of both solid and liquid insulation, the solid insulation cannot be extracted from the desired locations during operation as it requires the opening of the

TH-3272_186151014

transformer. Therefore, liquid insulation is the best means to diagnose the condition of both solid and liquid collectively. Some of the most used diagnostic methods for oil are DGA, PD, MC, TAN, TC, dielectric dissipation factor (DDF), furan analysis, degree of polymerization (DP), BDV, insulation resistance, UV-Visible spectroscopy (UVS), frequency domain dielectric response measurements (FDDRM), and time domain dielectric response measurements (TDDRM) [27, 28, 31, 38].

DGA is a tool to predict the type and intensity of a fault occurring in the transformer based on the percentages and ratios of selected gases generated in the oil when subjected to stress. The breakdown of solid and liquid insulation leads to the formation of hydrogen (H_2), methane (CH_4), ethane (C_2H_6), ethylene (C_2H_4), acetylene (C_2H_2), carbon monoxide (CO) and carbon dioxide (CO_2) gases. There are multiple techniques such as Roger's, Dornenburg's, IEC, and IEEE ratios in addition to Duval's triangles and pentagons to predict the faults from dissolved gases (DG).

Electrical methods involve testing of BDV, insulation resistance, DDF, and PD. PD is said to happen when an electric discharge partially bridges the insulation between interturn or interphase or interwinding or conductor and metal parts when subjected to electrical stress. PD occurs due to local field enhancement and can be detected by optical, acoustic, electric, and chemical methods [27, 28, 31].

Optical spectroscopy methods such as UVS and Fourier-transform infrared spectroscopy (FTIR) provide reliable, easy, and affordable testing that unfolds information on different bonds and functional groups linked with the oil structure. Polarization and depolarization current measurement (PDC) and recovery voltage measurement (RVM) are important TDDRM techniques that are measured as a function of time. Frequency domain spectroscopy (FDS) is an important FDDRM technique and is measured as a function of frequency.

From the aforementioned literature, it is observed that the condition assessment of insulation for the reliable and efficient operation of the transformer is very complex, and the existing condition assessment devices provide a single parameter per device, which increases the testing times when multiple parameters are required. Therefore, a single device that predicts two or more parameters would be of benefit to various stakeholders. Further, techniques such as TDDRM and FDDRM have long measurement times. The longer time requires long power interruptions. Hence, higher frequency spectroscopy can be used as a new tool for insulation analysis and condition monitoring [39]. The studies show that the GHz frequency range is dominant on the dipolar polarization of the material, and hence, the moisture content can best be detected using GHz spectroscopy. The reflectometric, transmission, and resonance methods

TH-3272_186151014

were widely tested on the polar liquids for biomedical applications [40]. The studies report variations in oil properties are better studied at frequencies lower than X and Ku-band [41]. Electromagnetic waves are also used for the detection of PD in the oil [42, 43]. Microstrip antennas were developed to study the changes in liquid insulation permittivity with aging [44, 45]. Studies have shown that the usage of a ring resonator successfully detects transformer pressboard aging and moisture content [46, 47]. Therefore, high-frequency signals provide a means to measure the oil properties swiftly. With reference to this captivating theme of quick assessment of multiple parameters, a high frequency signal based non-intrusive and non-destructive technique is proposed in this thesis.

1.3 Motivation

Liquid insulation needs to be monitored to ensure reliable operation by initiating necessary action in case of deviation of properties from stipulated values. A technique that can detect the physiochemical parameters of the oil instantly and is potentially amenable to remote monitoring can reduce the testing times of insulation. Such a technique would also complement PD detection in addition to its regular function. The technical gaps found from the literature survey are as follows:

1. Conventional measurement devices yield a single physical or, chemical or electrical parameter per equipment. An equipment that can detect two or more parameters with a potential remote operability is beneficial.
2. Blended oils are finding applications as they inherit properties from both the base oils. The study of these blended oils is important as their gas generation rates, PD, and physiochemical properties are solely dependent on the blending ratio of these oils and are useful for utilities in choosing the best insulation and balancing the price and performance.
3. NFs are proving to be a promising alternative to MO because of their better electrical and thermal characteristics. The study of the response of these liquids to magnetic fields can help extract critical parameters that are useful in developing multiphysics models to simulate the in-service conditions.
4. A few conventional techniques, such as DGA, require elemental changes for their applicability to alternate insulating oils. A generalized technique that can detect two or more parameters with ease of applicability for MO and ester oils is of interest.

1.4 Objective of the thesis

This work focuses on developing a novel offline condition assessment technique for transformer liquid insulation. The objectives of the thesis are as follows:

TH-3272_186151014

1. Development of a non-intrusive and non-destructive condition assessment technique for condition assessment of MO.
2. Assessment of in-service transformers operating with MO to validate the developed non-intrusive and non-destructive condition assessment technique and comparison of the obtained results with those from existing oil testing methods.
3. Studying the physiochemical and electrical characteristics of the mixtures of MO and NEO to comprehend their performance as transformer insulants.
4. Studying the magnetic response of the nanofluids by subjecting them to various magnetic fields to comprehend their magnetic behavior which can be used to develop multiphysics models.
5. Assessment of nanofluids and mixed insulating oils by the developed technique to establish its applicability to the alternate insulating oils.

1.5 Contribution of the thesis

The major contributions of the thesis towards the realization of a novel condition assessment technique for liquid insulation are as follows:

1. A condition assessment technique comprising of an S-Band horn antenna operating between 2.1 to 2.6 GHz placed in an EMI free chamber is used to study the laboratory aged MO samples. The response obtained is used to derive linear prediction graphs for MC and TAN, which are further used to predict the condition of in-service transformer oil samples. The S_{11} parameter at the first and second resonance frequencies in the chosen band corresponds to the TAN and MC of the insulating oil sample, respectively, and the technique is able to clearly differentiate samples with respect to their TAN and MC.
2. Fresh as well as aged mineral, ester, and mixed insulating oils are studied for their partial discharge and dissolved gas generation behaviour. Apart from the above, multiple physiochemical properties of the mixed insulating oil that endorse the usage of the chosen oils for transformer applications are also studied.
3. The behaviour of Nanofluids subjected to quasi-static and dynamic magnetic fields and their magnetic response is plotted. Useful parameters such as magnetic relaxation time and magnetic susceptibility of nanofluids prepared from various nanoparticles are extracted from the magnetic response.
4. Nanofluids are studied using the non-intrusive and non-destructive setup to endorse the applicability of the developed setup. The effect of aging the nanofluids on the applicability of the developed technique is also studied.

TH-3272_186151014

5. Fresh as well as aged mineral, ester, and mixed insulating oils are studied using the non-intrusive and non-destructive setup to establish its applicability to alternate insulating oils.

1.6 Organization of the Thesis

This thesis is organized into six chapters as follows:

Chapter 2 focuses on the development of a condition monitoring technique using high frequency waves generated from an S-Band pyramidal horn antenna. The high frequency waves are incident on the insulating liquid and the reflected signal is analyzed for the resonances. Mineral oil samples with various moisture and acid content are prepared in the laboratory by two different aging apparatuses. These samples are analyzed in the frequency range of 2.1 to 2.6 GHz as two resonances, one corresponding to moisture and the other to the acid content present in the sample. The data from the analysis of laboratory aged samples is used to generate a linear prediction graph. These linear graphs can be used to predict the moisture and acid in any mineral oil sample. To validate the effectiveness of the developed setup, multiple in-service transformer oil samples are tested. The findings support the usage of the technique for mineral insulating oils for their condition assessment.

Chapter 3 proposes the usage of mixed insulation as an alternate insulation to mineral oil. The physiochemical, partial discharge, and dissolved gas behaviour of the oils are studied elaborately. The oils are aged to study their long-term behaviour to ensure their application in transformers. The results show that the mixed insulating oils do not pose any threat if they are used as an alternative. They also provide the added advantage of improved electrical characteristics. This study will be a guide to manufacturers and transmission system operators in choosing the appropriate insulation by balancing cost and performance.

Chapter 4 addresses the magnetic properties of the special alternate insulating oils known as nanofluids. Magnetic susceptibility and magnetic time constants are extracted from the results obtained from vibrating sample magnetometer and electron spin resonance spectroscopies. The nanofluids are also studied using frequency domain spectroscopy (FDS) for their low frequency behaviour. Insulating nanoparticle based nanofluids are also studied for their low frequency behaviour by varying the concentration of nanoparticles.

In Chapter 5, nanofluids and mixed insulating oils are tested using the non-intrusive and non-destructive technique for verifying the applicability of the developed setup. An effort has been made to study the aged nanofluids with an antenna. Due to the agglomeration and settling of nanoparticles on solid insulation, the aged samples could not be prepared with accuracy, implying the technique is unverifiable for nanofluids. Whereas, the fresh and oxidative aged

TH-3272_186151014

mixed insulating oil samples are studied for their response using non-intrusive and non-destructive technique. The results show that the developed technique can be used for condition assessment of mixed insulating oils with low moisture and acid content.

In Chapter 6, the conclusion of the thesis and the suggestions for the future scope of this research work are presented.

भारतीय प्रौद्योगिकी संस्थान गुवाहाटी • Indian Institute of Technology Guwahati •

TH-3272_186151014

2

The non-intrusive and non-destructive technique for condition assessment of mineral oil

Contents

2.1	Introduction	13
2.2	Materials and experimental technique	14
2.3	Frequency response analysis of samples and validation of the technique	20
2.4	Non-isothermal thermogravimetric analysis of kraft paper	28
2.5	Summary of the chapter	33

TH-3272_186151014

2.1. Introduction

MO has been traditionally used in transformers for insulation and cooling purposes for a century now. The insulation degrades over time in the combined or individual presence of high temperature, moisture, and oxygen. The high temperature is due to heat dissipated by the windings during the operation of the transformer. In contrast, moisture appears due to ingression from the atmosphere and the breakdown of cellulose. The moisture and oxygen form acids in the presence of heat leading to degradation of the paper insulation which in turn results in the formation of sludge. The sludge reduces the TC of liquid insulation and thus the operating temperature of the transformer will further increase. Therefore, due to aging, the acid, sludge, and other impurities in the oil increase [48]. Therefore, the monitoring of insulation integrity is important for the uninterrupted operation of the system [49]. The reliability of insulation depends on condition-based maintenance rather than time-based maintenance [27, 50].

The chemical methods used for condition assessment are MC, DGA, DP, furan content, and TAN analysis. A few electrical techniques are insulation resistance measurement, and dielectric loss factor measurement (*tanδ*). The popular TDDRM for insulation integrity assessment are PDC measurements and RVM [27]. The FDDRM for insulation assessment comprises *tanδ*, capacitance, and complex permittivity measurement as a function of frequency. The TDDRM and FDDRM are used to assess the condition of the insulation with respect to the state of aging or the moisture content [46]. The FDDRM is gaining popularity as it can characterize electrical properties in terms of frequency. Also, there is no unanimously accepted diagnosing technique over the globe to detect the degradation of oil [27].

All the techniques being developed are used to detect the aging in insulating oil. The aging of oil leads to an increase in contaminants which scale down the electrical properties of liquid insulation by generating free radicals. The studies have reported that the resonance frequency shifts toward a lower frequency for the aged oil as compared to fresh oil and it can be interpreted as an increase in the dielectric constant of aged oil [51].

Though high frequency techniques could establish a relation with aging, there are a few drawbacks concerning the reliability of the measurement, such as the antenna in [46] being held onto a pressboard using metal clips in the studies and the presence of metal clips closer to the antenna may affect the measurements. The other impediments of the high frequency measurement techniques are that either the antenna is to be immersed in the oil or the sample is to be placed precisely in the slot (for waveguide and cavity techniques) [51]. A small dislodgment may cause severe measurement errors.

TH-3272_186151014

Also, the degraded oil contains minuscule amounts of acids, dissolved gases, and other hydrocarbon chains. When an antenna is placed in the oil, the acid constituents of the oil may erode the sensor or antenna used for testing and if the same antenna is used for multiple sample assessments, it may contaminate the subsequent test samples and lead to erroneous results. The presence of an antenna in oil affects the conductivity of the oil in the region surrounding the antenna and may result in electrolysis and space charge development [44].

Considering the disadvantages of an antenna being inserted in the insulating oil, a new, reliable, non-intrusive, and non-destructive testing technique is introduced in this work. A horn antenna operating in the S-band is placed over an open top Polytetrafluoroethylene (PTFE) vessel filled with oil to study its characteristics. To avoid electromagnetic interference (EMI) and noise, the entire study is conducted in an anechoic chamber. The state of the oil is quantified in terms of the MC and the TAN. Both these parameters describe the state of aging of an oil sample. Based on some studies [52, 53], the samples were aged using two different processes, namely thermal and oxidative aging. Two different experimental setups for these aging processes were developed in the laboratory to age the transformer liquid insulation. The proposed method is tested initially on laboratory samples. The resonance in frequency response is correlated with the MC and TAN of the insulating oil. This study is further extended to predict the MC and TAN of in-service transformer oil samples obtained from various transformers belonging to the substations of Assam State Electricity Board (ASEB) and Indian Institute of Technology Guwahati (IIT Guwahati). The state of aging of in-service transformer samples is established by mapping the obtained reflection coefficient $|S_{11}|$ response with an established linear fit from the laboratory aged sample data. Later, an attempt is made to study the oxidatively aged solid insulation by using thermogravimetric analysis (TGA).

2.2. Materials and experimental technique

MO used in the present study was procured from M/s Savita Oil Technologies Limited and its properties are given below in Table 2.1. According to IEEE C57.106, this oil can be accepted for transformer applications [54]. The MO is degassed and dried in a vacuum oven to remove moisture and dissolved gases before experimentation as per IEEE C57.637 [55]. After removing moisture, the transformer insulation grade pressboard is immersed in MO along with copper conductor and proceeded for aging.

2.2.1. Sample Preparation

In the present study, MO along with pressboard and copper conductor is aged in closed beaker accelerated thermal aging and open beaker oxidative aging setup. All the samples

TH-3272_186151014

prepared in sections 2.2.1.1 and 2.2.1.2 are tested for TAN and MC following IEC 62021 and ASTM D1533 standards respectively, and the data is enlisted in Tables 2.4 and 2.5 respectively.

Table 2.1: Specification of insulating oil procured.

Parameter	Test Method	MO
Density (kg/m^3)	ASTM D1298	0.8180
Kinematic viscosity @ 27ºC (cSt)	ASTM D445	11.46
Interfacial tension @ 27ºC (N/m)	ASTM D971	47
Flashpoint (ºC)	ASTM D93	154
Pour point (ºC)	ASTM D97	-27
DDF @ 90ºC	ASTM D924	0.0045
Water content (ppm)	ASTM D1533	12.40

2.2.1.1. Accelerated Thermal aging

The oil needs to be aged at a faster rate to study the early, midlife, and afterlife properties of transformer insulation. An accelerated thermal aging setup was developed in the laboratory as shown in Figure 2.1a. In this setup, the oil sample, pressboard, and kraft paper in the ratio of 20:1:1 along with copper conductors are thermally stressed at a constant temperature of 140°C for 325, 650, and 975 hours. The samples are kept in a sealed beaker. As per IEEE C57.91, the age factor at 140°C is 17.1994, which gives the samples aged 3.4, 6.72, and 10.1% of their total life [56]. The reason for choosing these aging hours is to prepare oil samples with lower TAN and MC. The fresh and aged samples are shown in Figure 2.2a. The samples turn brown with aging and the color becomes darker with the increase in aging hours.

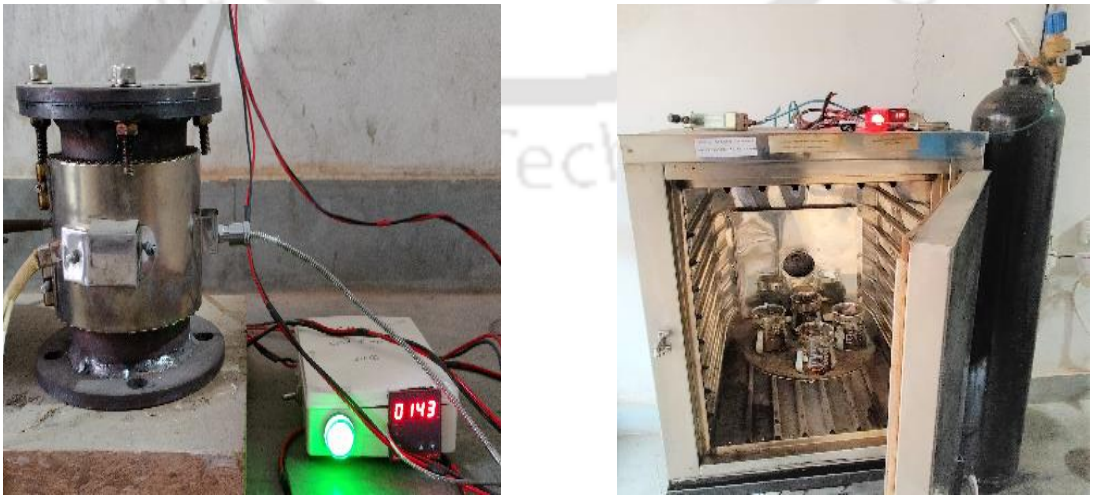

(a) (b)

Figure 2.1: (a) Sealed Beaker accelerated thermal aging setup and (b) Open Beaker accelerated oxidative aging setup.

TH-3272_186151014

2.2.1.2. Oxidative aging

In this aging process, oil, pressboard, and kraft paper are added to 300 ml MO in the ratio of 20:1:1 to the beaker along with a spirally wounded copper conductor (475 mm long). Open beakers are placed on a rotating platform inside the chamber, which is rotating at a speed of 2 RPM. The temperature inside the chamber is maintained at 115±1°C throughout the aging process following ASTM D1934 [57]. The aging is done for 500, 1000, and 1500 hours to prepare oil samples with higher TAN and MC. The open beaker accelerated oxidative aging setup developed in the laboratory is shown in Figure 2.1b. The fresh and aged samples are shown in Figure 2.2b. The oxidative aged samples turn crimson red in color with aging.

Figure 2.2: (a) Closed Beaker accelerated thermal aged samples (b) Open Beaker accelerated oxidative aged samples and (c) In-service transformer oil samples.

2.2.1.3. In-service transformer samples

The in-service MO based transformer insulation oil samples are obtained from operational transformers of 33 kV and 132 kV substations of IIT Guwahati and ASEB respectively. These transformers are of different age groups, and they have different voltage and power ratings.

TH-3272_186151014

Table 2.2. Nomenclature of transformer oil samples obtained from substations of ASEB and IIT Guwahati.

Name	Tr. A	Tr. I	Tr. II	Tr. III
Make	CGL*	EMCO	EMCO	EMCO
Affiliation	IIT Guwahati	ASEB	ASEB	ASEB
Operating Age (in years)	21	11	25	25
Power Rating	5 MVA, 33 kV	40 MVA, 132 kV	31.5 MVA, 132 kV	31.5 MVA, 132 kV
Winding Temp	65ºC	75ºC	60ºC	65ºC
Type of cooling	ONAN	ONAN	ONAN	ONAN
Oil Temp.	55ºC	58ºC	54ºC	58ºC
Oil Last Filtered	-	-	2013	2013

*CGL = Crompton Greaves Limited

The liquid insulation from transformers is sampled in accordance with ASTM D923 [58]. The liquid insulation samples are stored in air-tight glass bottles after sampling. The nomenclature of the samples is shown in Table 2.2 and the samples collected from the two different substations are shown in Figure 2.2c. The oil sample Tr. A belongs to the 33 kV substation at IIT Guwahati, and the samples Tr. I, Tr. II, Tr. III belongs to the 132 kV substation operated by ASEB.

2.2.2. Test Setup and calibration

To avoid external noise and the internal reflection of incident electromagnetic waves, the experiment is performed in an anechoic chamber of size $6 \times 4 \times 6$ m^3 erected in the Department of Electronics and Electrical Engineering (EEE), IIT Guwahati and is shown in Figure 2.3. The operating frequency range of this chamber is from 0.1 to 40 GHz for any polarization and incident angle with an isolation of -40 dB.

Since the frequency response of the insulating liquid is highly sensitive to temperature variation and humidity, the temperature inside the anechoic chamber is always maintained at 20°C using the temperature controller and humidity at 50% using the dehumidifier (AMDH 600, Advance International).

To study the reflection coefficient (S_{11}) of the prepared liquid insulation, the sample is filled in a PTFE vessel of inner dimensions of $142 \times 105 \times 40$ mm^3 since using the glass,

TH-3272_186151014

plastic, metallic, and fiberglass vessels for experimentation results in high reflections at the oil-vessel boundary due to impedance mismatch. As the permittivity of the PTFE and MO are nearly the same, the reflection of the wave from the boundary of the oil-vessel is minimized.

The testing vessel is molded with utmost care to match the aperture size of the S-band pyramidal horn antenna and is placed right below it such that there is no air gap between the aperture of the antenna and the oil sample. This effort avoids unnecessary reflections from the edges of the vessel. The prepared testing vessel can accommodate approximately 600 mL of oil.

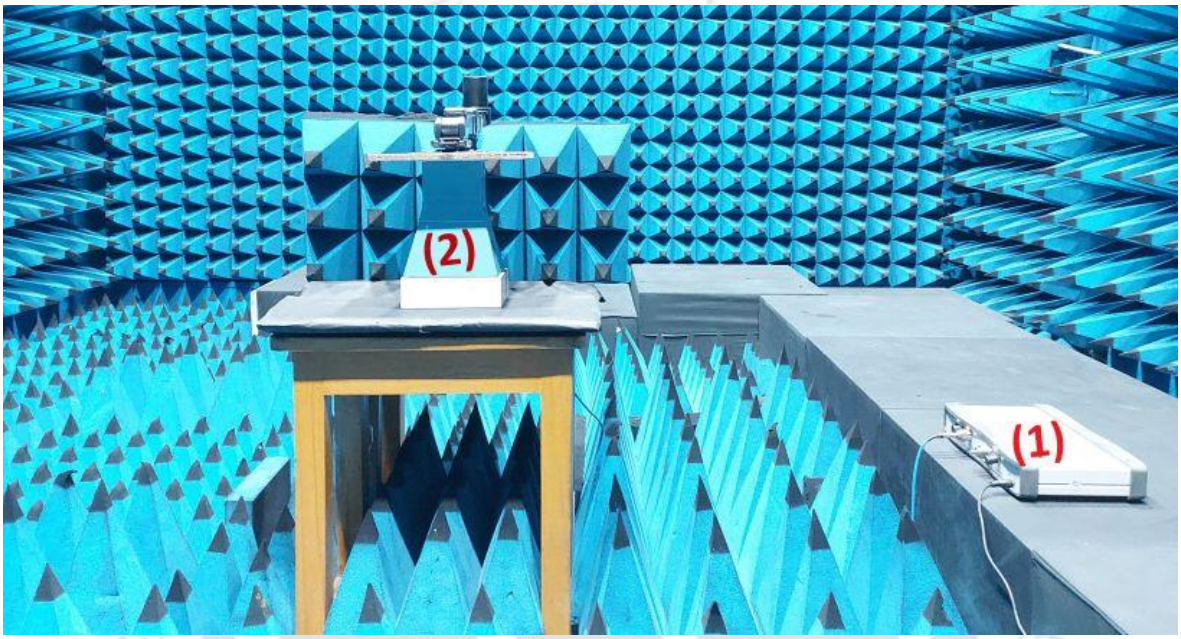

Figure 2.3: Anechoic chamber for insulation monitoring (1) Vector network analyzer (MS46122B, Anritsu) (2) Antenna placed over the testing vessel with no air gap.

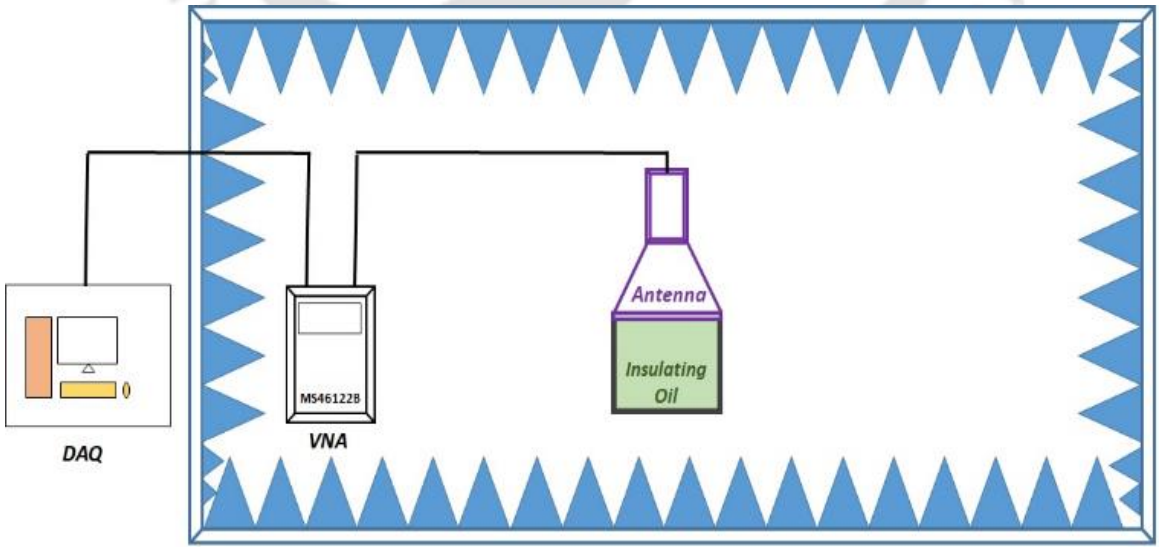

Figure 2.4: Schematic representation of the experimental setup in the anechoic chamber.

TH-3272_186151014

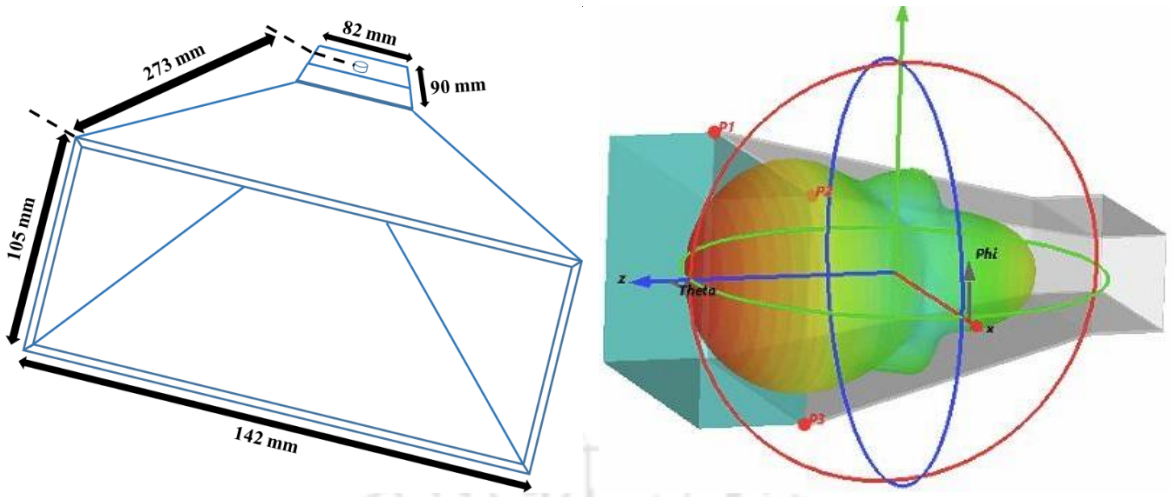

(a) (b)

Figure 2.5: (a) Dimensions of the pyramidal horn antenna and (b) radiation pattern of the antenna at 2.45 GHz.

A radiation absorber is placed in between the vessel and the table to avoid reflections, if any. The absorbers are also placed in between the antenna and the antenna mount stand. The schematic representation of the experimental setup placed in the anechoic chamber is shown in Figure 2.4. The dimensions of the pyramidal horn antenna are shown in Figure 2.5(a). The aperture of the antenna has an inner dimension of 142× 105 mm and the waveguide has a dimension of 90 × 82 mm. The distance between the radiating element and the aperture end is 273 mm. The horn antenna is chosen for this study because it has no resonance elements, making it operate smoothly over a wide frequency range of the S-band. This antenna also has an easy interface, high gain, simple construction, and high directivity. The output of the horn antenna is a linearly polarized wave. This antenna is designed with a center frequency of 2.45 GHz, which makes the antenna reliable and error-free for measurements in the band of 2 to 3 GHz. The antenna is connected to a vector network analyzer (VNA, MS46122B, Anritsu make) using cables and connectors. The cables used to connect the antenna and VNA are noise free. The testing vessel is designed in such a way that most of the radiation is focused on liquid insulation. Since radiation pattern in Figure 2.5(b) shows that radiation from the antenna is focused onto the liquid rather than the walls of the vessel. Thus, the walls of the vessel have a negligible impact on the scattering parameters obtained.

The VNA is calibrated for open, short, and loaded conditions before performing an experiment to avoid systematic errors. The main factors deteriorating the insulation of the transformer are moisture, temperature, and oxygen. Oxygen leads to oxidation of the liquid insulation, which in turn results in the formation of acids and sludge. These byproducts formed degrade the liquid insulation and they are conducting in nature. Hence these conducting

TH-3272_186151014

contaminants can be detected by the electromagnetic fields. The response in the frequency range barring 2-3 GHz cannot be relied upon with this designed antenna and testing vessel.

2.3. Frequency response analysis of samples and validation of the technique

This section presents the S_{11} parameter obtained from the experimentation of the fresh and laboratory aged insulating oil in the frequency range of 2.1 to 2.6 GHz. Every sample is measured three times for repeatability and a total of 301 readings are noted in the chosen frequency range. This frequency band is able to establish the status of the liquid insulation with the designed antenna and testing vessel deftly. The obtained results are used to predict the degradation level of in-service oil samples. All the measurements are performed at room temperature of 20°C and relative humidity (RH) of 50%. When oil degrades, the conductivity increases due to an increase in contaminants. The higher the amount of contaminants, the higher the degradation, the lower the impedance, the higher the conductivity, and the higher the reflections from the oil. Hence, the degradation of oil causes changes in the S_{11} parameter.

Low molecular weight carboxylic acids (LMWCA) such as formic, acetic, and levulinic acids and high molecular weight carboxylic acids (HMWCA) such as naphthenic and stearic acids are formed due to aging of the cellulose solid insulation and liquid insulation [59, 60]. The molecular weight and the formula of the acids are mentioned in Table 2.3. The degradation of oil gives rise to long chained acids, whereas the degradation of paper forms short chained acids [61]. LMWCA are adsorbed mostly by cellulose and are soluble in water. In contrast, HMWCA are absorbed by oil insulation and are not significantly water soluble [62]. Since the aging is done with pro rata liquid and solid insulation, both the LMWCA and HMWCA are formed in the laboratory aged samples as in transformers.

The LMWCA and HMWCA mentioned in Table 2.3 are added individually to the fresh mineral oil in various concentrations, followed by magnetic stirring, and the S_{11} parameter of the contaminated oil is studied. It is observed from the experiments that LMWCA concentration does not have any effect on the S_{11} parameter, whereas the S_{11} parameter of HMWCA shows a shift in the response at resonance frequency as the concentration of HMWCA increases. The frequency response on the addition of one such HMWCA (Naphthenic acid) to 580 mL of fresh mineral oil in different concentrations (100 µL, 500 µL, 1000 µL) is shown in Figure 2.6. The frequency response shows two resonance frequencies within the band of 2.1 to 2.6 GHz. As the horn antenna does not have any resonating components, the resonance is solely due to the oil response. It is observed from the figure that the change in concentration of HMWCA is reflected on the S_{11} parameter at the first resonance

TH-3272_186151014

frequency. As the increase in HMWCA content causes the increase of $|S_{11}|$, the first resonance frequency corresponds to the HMWCA content of the liquid insulation.

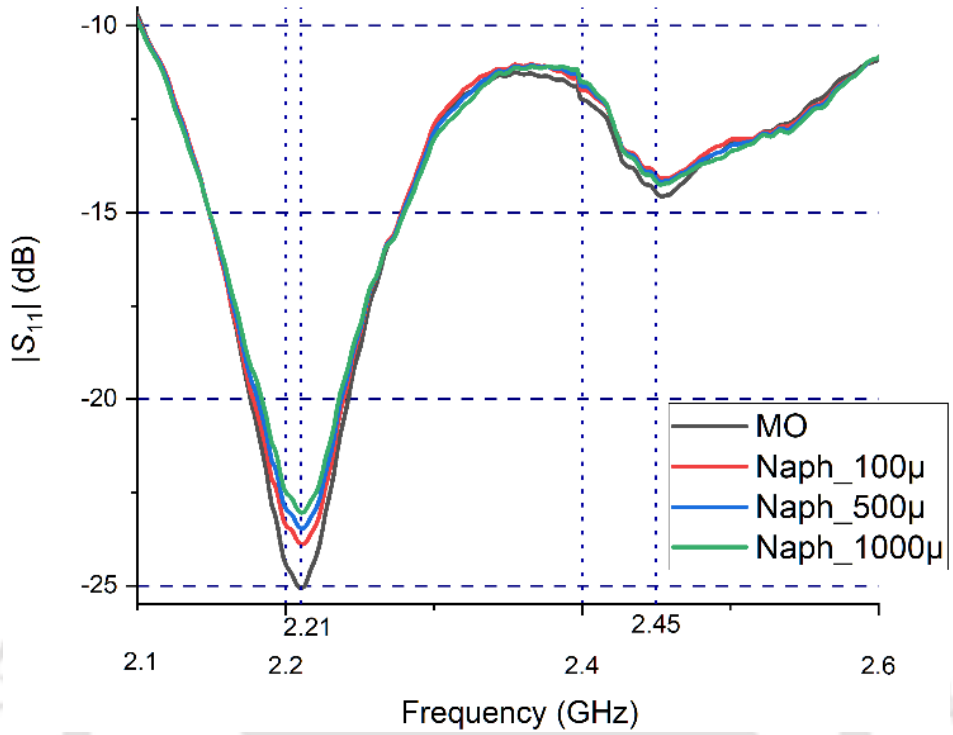

Figure 2.6: Frequency response on the addition of HMWCA.

The second resonance frequency at 2.45 GHz is related to structural changes in Van der Waal's bonds of the water molecule [63]. Hence, the second resonance corresponds to the MC of the liquid insulation. As the MC is not significantly changed during HMWCA addition, the response at 2.45 GHz remains nearly the same for various concentrations of HMWCA.

Table 2.3: Different types of Carboxylic acids [59].

Name of acid	Formula	Molecular weight	Acid dissociation constant
Formic	CH_2O_2	4	3.8
Acetic	$C_2H_4O_2$	60	4.8
Levulinic	$C_5H_8O_3$	116	4.6
Naphthenic	Variable	200-700	5.5
Stearic	$C_{16}H_{36}O_2$	285	10.5

2.3.1. Frequency response of accelerated thermal aged samples

The frequency response of the samples prepared in section 2.2.1.1 is plotted in Figure 2.7. The MC and TAN of the samples are shown in Table 2.4. It is observed from the figure

TH-3272_186151014

that the frequency response has two resonance frequencies. The fresh MO has the lowest $|S_{11}|$ for all frequencies. As the oil ages, the $|S_{11}|$ is observed to increase, indicating higher reflections from the oil.

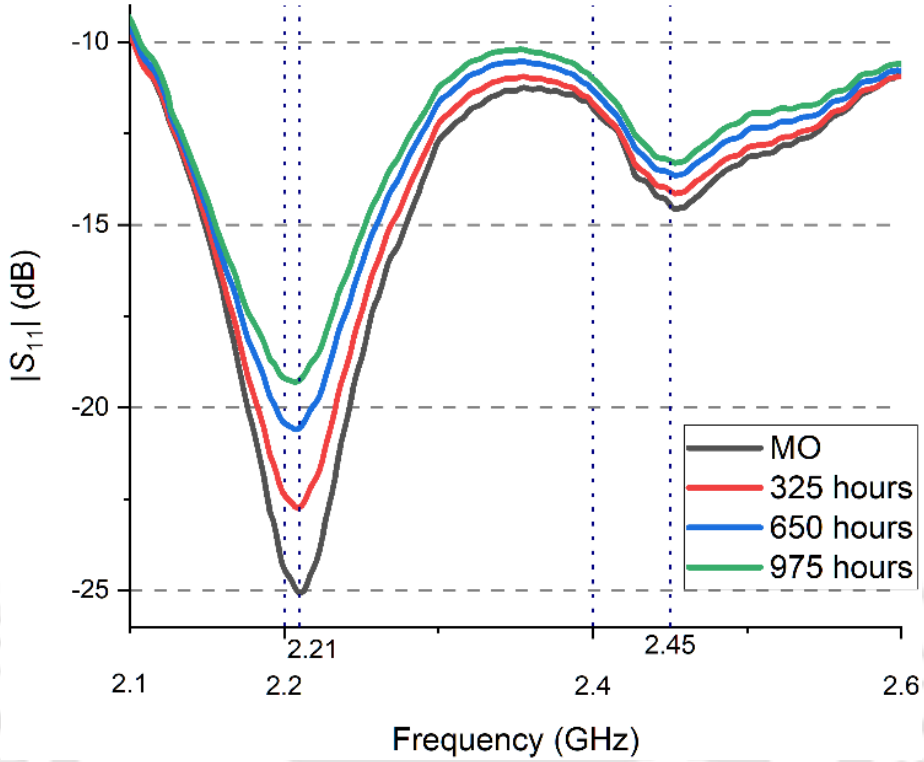

Figure 2.7: Frequency response of sealed beaker accelerated thermal aged samples.

Table 2.4: MC and TAN of sealed beaker aged samples.

MO sample	MC (ppm)	TAN (mg KOH/g)
Fresh	12.4	0.012
325 hours aged	22.1	0.0297
650 hours aged	25.5	0.0387
975 hours aged	28.9	0.0466

Fresh MO has lower contaminants and with aging, the MC and the TAN of the oil insulation are found to increase as indicated in Table 2.4. The frequency response in Figure 2.7 confirms the trend in Table 2.4 with higher $|S_{11}|$ scattering values at resonance frequencies for aged oil. The relationship between the cut-off frequency (f_c) of the horn antenna and the effective relative permittivity (ϵ_r) of the oil is given by (2.1).

$$f_c = \frac{k.c}{2\sqrt{\mu_r \epsilon_r}} \tag{2.1}$$

TH-3272_186151014

where k is a constant that depends on the dimension of the aperture and the mode of excitation of the antenna, c is the velocity of light in free space, and μ_r is the relative permeability of the medium. The frequency below the cut-off frequency at which the system and excitation resonate is the resonant frequency.

As the oil ages, the relative permittivity increases with an increase in moisture and other polar contents. Hence, there is a dwindle in the resonance frequency with aging, as shown in the figure. On account of the lower TAN and MC of the samples prepared in section 2.2.1.1, the shift in resonance frequency is also smaller for these oil samples. The obtained results are in accordance with the results obtained by other testing methods in [45-47]. The increase in $|S_{11}|$ at the first resonant frequency is observed to be proportional to the increase in the TAN which is established in Figure 2.6. Meanwhile, the increase in $|S_{11}|$ at the second resonant frequency is observed to be proportional to the increase in the MC.

2.3.2. Frequency response of open beaker oxidative aged samples

The frequency response of the samples prepared in section 2.2.1.2 is plotted in Figure 2.8. The MC and TAN of the samples are shown in Table 2.5. With the increase in aging hours, the MC and TAN increase at a higher rate in open beaker oxidative aging than in closed beaker accelerated thermal aging. This is due to the presence of oxygen in the aging chamber. The presence of oxygen amplifies the acid formation in the aging process. Further, data in Table 2.5 shows a higher MC and TAN with aging hours for the oxidative aged samples compared to the data provided in Table 2.4.

Table 2.5: MC and TAN of open beaker aged samples.

MO sample	MC (ppm)	TAN (mg KOH/g)
Fresh	12.4	0.012
500 hours aged	89.2	0.0319
1000 hours aged	120.5	0.0496
1500 hours aged	175.4	0.0551

On account of the higher TAN and MC of the samples prepared in section 2.2.1.2, the shift in resonant frequency is higher for these oil samples. Figure 2.5 illustrates the variation in resonance frequency with aging hours. The increase in $|S_{11}|$ at first resonance frequency is observed to be proportional to the increase in TAN and the second resonant frequency is observed to be proportional to the increase in the MC for the aged samples. The results obtained

TH-3272_186151014

in this section agree with the relation between f_c and ϵ_r in (2.1). The obtained results are also in accordance with the results obtained by other testing methods in [45, 46, 51].

Though the response curves of oxidative aged and thermally aged samples are similar, the magnitude of the reflection coefficient is different. This is because of the higher amount of contaminants in the oxidative aged samples. The higher the contaminants, the higher the reflections and the lower the $|S_{11}|$ are.

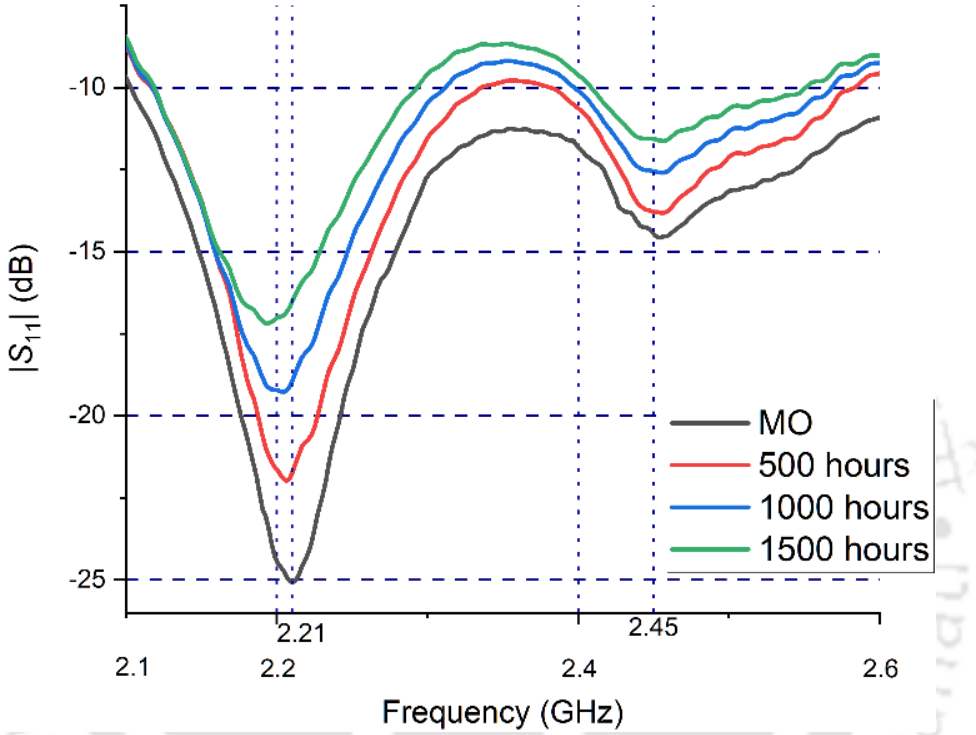

Figure 2.8: Frequency response of open beaker accelerated oxidative aged samples.

The difference in magnitude of $|S_{11}|$ measured between each oxidative aged sample is higher compared to $|S_{11}|$ measured between each thermally aged sample. This shows that the test setup developed can clearly distinguish the samples based on the amount of MC and TAN. With this comprehension, a linear prediction curve is generated from the above data which is later used to predict the MC and TAN of the in-service transformer oil samples.

2.3.3. Estimation of degradation of in-service transformer oil samples from frequency response

From the frequency response curves in Figures 2.7 and 2.8, the reflection coefficient $|S_{11}|$ at the first and second resonance frequencies are plotted as a function of the TAN and MC, respectively. A linear relationship is estimated to best fit the laboratory sample data points, according to (2.2).

TH-3272_186151014

The coefficients obtained from the linear curve fit are given in Table 2.6. The linear fit is extrapolated in MATLAB and the extrapolated curve is shown in Figures 2.9 and 2.10 with TAN and MC values of Section 2.3.1 and 2.3.2 overlapped. The linear fitting relation given in (2.2) and curves shown in Figures 2.9 and 2.10 correspond to a measurement temperature of 20°C and RH of 50%. Since the correlation of $|S_{11}|$ is done with absolute water content and acid content of the oil sample, it is relevant to plot and compare the MC and TAN data of laboratory aged and in-service samples in the same graph for Figures 2.9 and 2.10.

$$|S_{11}| = a \cdot x + b \tag{2.2}$$

where x is the independent variable (TAN/MC). The mean absolute error (MAE) root mean squared error (RMSE) and the coefficient of determination (R^2) mentioned in Table 2.6 indicate the goodness of fit.

These linear graphs are used to predict the TAN and MC of the in-service transformer oil samples. The frequency response of the in-service transformer oil samples obtained using the developed test setup is shown in Figure 2.11. The $|S_{11}|$ corresponding to the first resonance frequency in Figure 2.11 is then used to estimate the TAN of the in-service transformer oil samples from the best-fitting curve in Figure 2.9. Similarly, the $|S_{11}|$ corresponding to the second resonant frequency in the in-service transformer oil samples is used to predict their MC using the fitting curve in Figure 2.10. The estimated values of TAN and MC for these samples are given in Table 2.7. In order to compare these estimates with actual values, the TAN and MC for the in-service transformer oil samples are measured using conventional techniques following the IEC 62021 and ASTM D1533 standards respectively and the data is shown in Table 2.7. The percentage error between the estimated and measured values is calculated and shown in Table 2.7. The in-service oil samples are filtered using vacuum dried filter paper (pore size of 2 µm) to remove sludge and metallic solid contaminants in order to avoid their influence on the measurement and allow reproducibility.

Table 2.6: Coefficients, MAE, and R^2 of the first order polynomial for TAN and MC.

	TAN	MC
a	162.30863	0.01456
b	-27.11856	-14.3307
MAE	0.002	21.239
RMSE	0.00272	28.94945
R^2	0.98463	0.78779

TH-3272_186151014

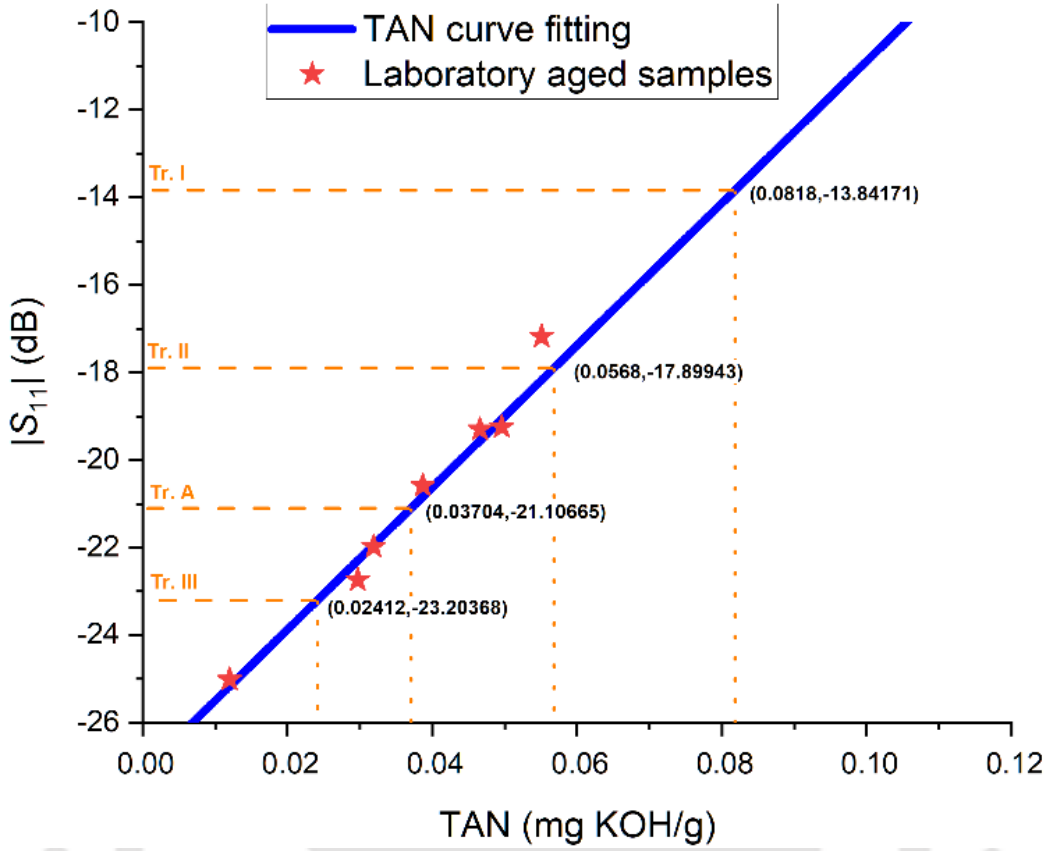

Figure 2.9: Extrapolated linear fit for TAN.

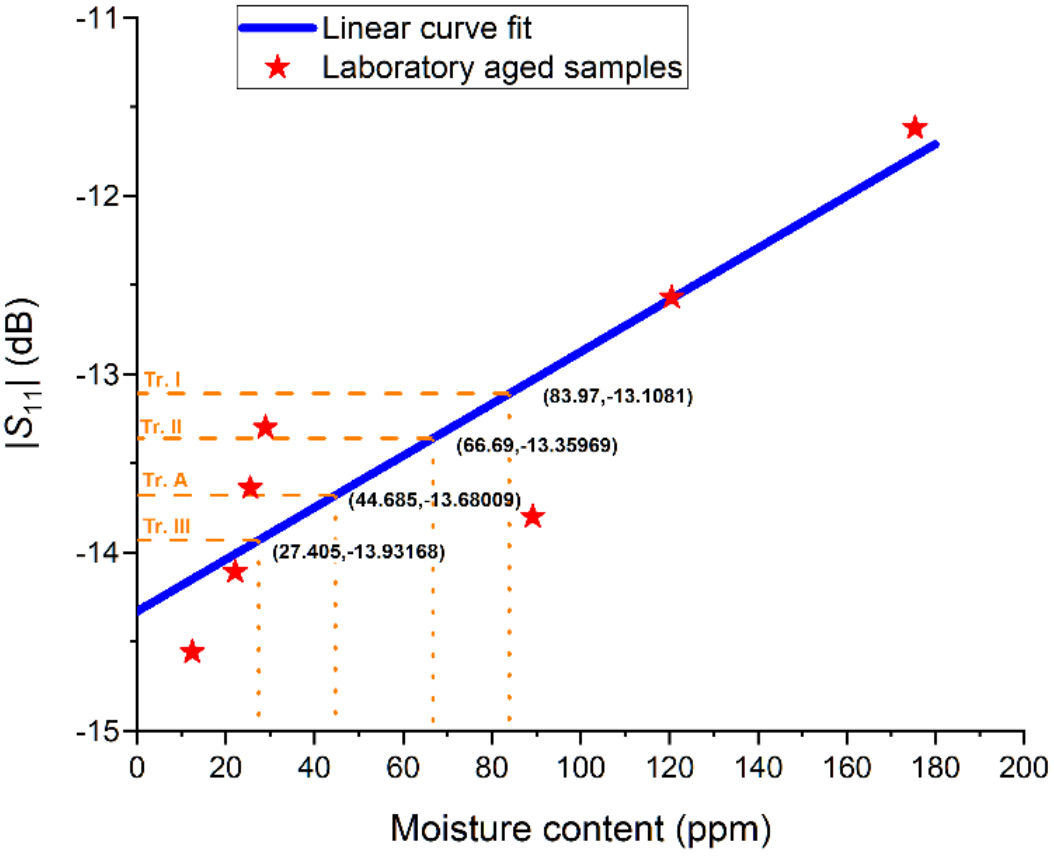

Figure 2.10: Extrapolated linear fit for MC.

TH-3272_186151014

Table 2.7: Predicted and measured results of MC and TAN of in-service transformer oil samples.

Sample	TAN (mg KOH/g)			MC (ppm)		
	Predicted value	Measured value	% error	Predicted value	Measured value	% error
Tr. A	0.03704	0.0364	1.78	44.685	38.6	15.7
Tr. I	0.0818	0.1019	19.72	83.97	89.8	6.49
Tr. II	0.0568	0.0735	22.72	66.69	70	4.73
Tr. III	0.02412	0.0222	8.65	27.405	36.3	24.5

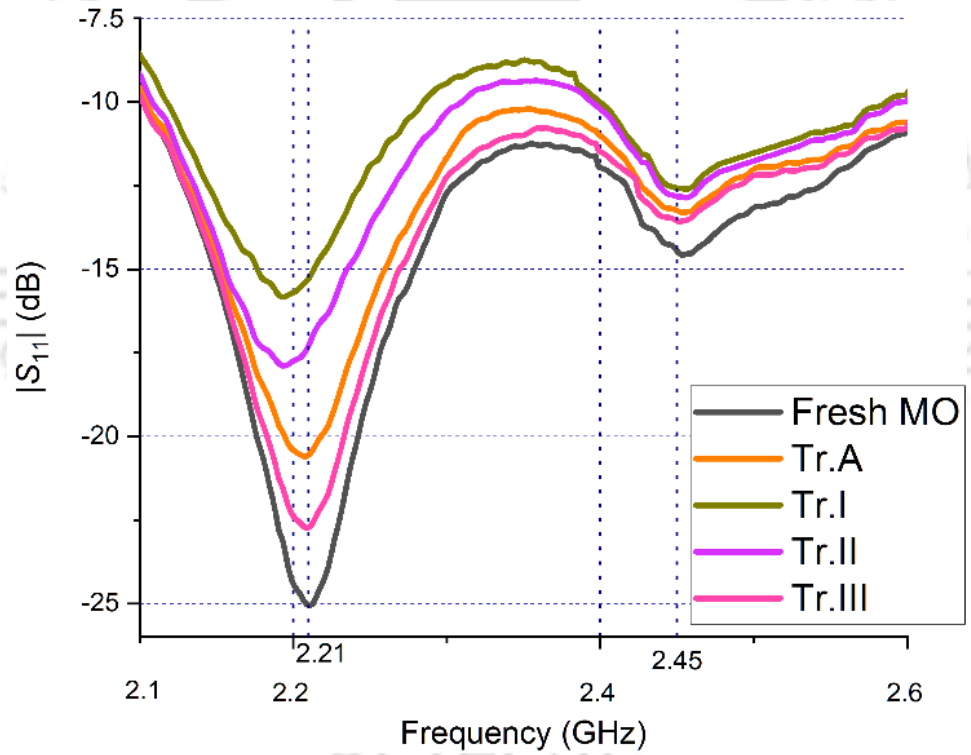

Figure 2.11: Frequency response of in-service transformer oil samples.

As per ASTM D974, the maximum limit for neutralization number (mgKOH/g) for accepting MO is 0.03. The percentage error for oil samples with TAN around and below 0.03 is less than 10% in Table 2.4, indicating that the linear prediction in Figure 2.9 is rational for MO samples with acceptable TAN. The mapped MC value is closer to the measured value for high MC content samples. The accuracy of the MC prediction at lower MC values can be further improved by having a larger data set.

TH-3272_186151014

Any alternate liquid insulation to mineral oil also has TAN and MC, and they increase with aging. The changes in TAN and MC of any liquid insulation can therefore also be detected with the developed setup after obtaining a suitable best-fitting curve. Making use of the MC in oil obtained from the experiment and the transformer operating temperature, MC in solid insulation can be derived using moisture equilibrium curves. Therefore, the relative state of moisture in solid insulation can also be predicted using this technique.

It is important to point out that the anechoic chamber used in the experimentation can be easily scaled to a smaller size to fit the antenna and testing vessel. This makes the experimental setup compact, lightweight, and portable. A customized portable VNA working in the frequency band established in this chapter will make this technique cost-effective. Therefore, using a customized portable VNA and a miniaturized testing chamber, the test setup can be made lighter and handy to carry out experiments on the field. This technique is useful in the fast identification of contaminants, reduces truck rolls, and is safe for the operating personnel. Therefore, the asset downtime can be minimized and the profitability can be increased.

2.4. Non-isothermal thermogravimetric analysis of kraft paper

Kraft paper is widely used as an insulating material in HV equipment. The degradation of paper as well as liquid insulation is due to the electrical and thermal stresses developed in the equipment. The degradation of solid insulation is irreversible and thus it is considered the end of the lifetime for equipment [64]. In addition to liquid insulation, solid insulation also provides extensive information on the aging and degradation status. There are several assessment techniques that determine the deterioration in paper namely, furan analysis, DP, and tensile strength of the paper. Among them, DP and mechanical strength tests on solid insulation are widely performed. The DP values and mechanical strength of paper can be correlated to each other and are mainly influenced by initial moisture, aging duration, and operating temperature of the insulation [65]. In this subsection, an attempt has been made to study the degradation of solid insulation using the non-isothermal thermogravimetric analysis (TGA) technique.

TGA is a technique in which the mass or mass degradation rate of a sample is studied by varying temperature in a predefined procedure over a defined time in a controlled atmosphere [66]. The mass or mass degradation rate of the sample is plotted as a function of temperature since the mass of the sample is dependent on the temperature applied to the sample. A Perkin Elmer TGA 4000 equipment shown in Figure 2.12 is used for this analysis. The schematic of the TGA experimental setup is depicted in Figure 2.13. The TGA equipment consists of a

TH-3272_186151014

sample pan made of ceramic that is supported by a vertical precision balance. The pan was placed in a furnace, which was heated during the experiment. The mass of the sample is monitored throughout the experiment by the vertical precision balance. An inert or reactive gas is filled in as purge gas to control the furnace environment [67]. This gas flows over the sample, surrounds it, and exits through an exhaust. The nitrogen gas is used in these experiments as an inert atmosphere, and it provides an oxygen free environment. This inert atmosphere avoids combustion of the sample due to oxygen. This ensures the degradation of the sample is only due to the temperature and not oxidation. The TGA analysis is performed in the temperature range of 30 to 900°C with an increasing ramp rate of 20°C/min. The nitrogen gas pressure is maintained at 1.8 bar and a flow rate of 20 ml/min. This flow rate is sufficient to maintain the oxygen free environment inside the instrument. The TGA analysis is generally used to study oxidation stability, filler contents, carbon contents, drying losses, volatility, moisture content, and many more parameters.

The kraft paper is subjected to oxidative aging, as shown in section 2.2.1.2, and the paper samples are extracted every 300 hours until a total of 900 hours. The samples of the kraft paper sampled and stored air tight in a polythene bag are shown in Figure 2.14. However, it is important to note that the oxidative aged kraft paper samples contain the oil that is impregnated in it during the aging process. TGA is performed on the fresh, dry, and oxidative aged kraft paper. This study focuses solely on the thermal degradation of the paper sample rather than on the amount of moisture present in the paper sample. Therefore, all the paper samples are dried in the nitrogen atmosphere at 100°C for 20 minutes before performing TGA to ensure the kraft paper is moisture free. Therefore, the TGA analysis performed here only gives a response with respect to paper aging status and not due to moisture. Figure 2.15 shows the empty ceramic pan, ceramic pan filled with kraft paper samples, and pan with remains after performing TGA in an inert atmosphere. Thermal degradation analysis is carried out and the results obtained are plotted for temperature versus weight percentage measurements.

The variation of the weight percentage of the sample with temperature is plotted in Figure 2.16. The results show that the response follows a similar trend for all the oil aged kraft paper samples and is different from the fresh kraft paper. The thermal degradation is not significant below 200°C. There is a huge degradation of the sample observed in the temperature range of 300 to 400°C. At temperatures beyond 400°C, the degradation is almost complete as the percentage weight loss is low.

To interpret the results in a better way, the results obtained in the temperature range of 150 to 450°C are focused and shown in Figure 2.17. There is an inverted hump in the response

TH-3272_186151014

of oil aged samples when compared to the dry paper sample. This inverted hump in oil immersed samples is observed in the range of 200 and 300°C. These temperatures are closer to the fire and flash points of the MO. The MO and karanji oil methyl ester degrade and evaporate in this temperature range [68]. Therefore, the loss in weight in this temperature range is due to the evaporation of the oil from the paper samples. As the dry paper sample does not have any oil, this trend is not observed in the dried sample.

Figure 2.12: Thermo Gravimetric Analyser.

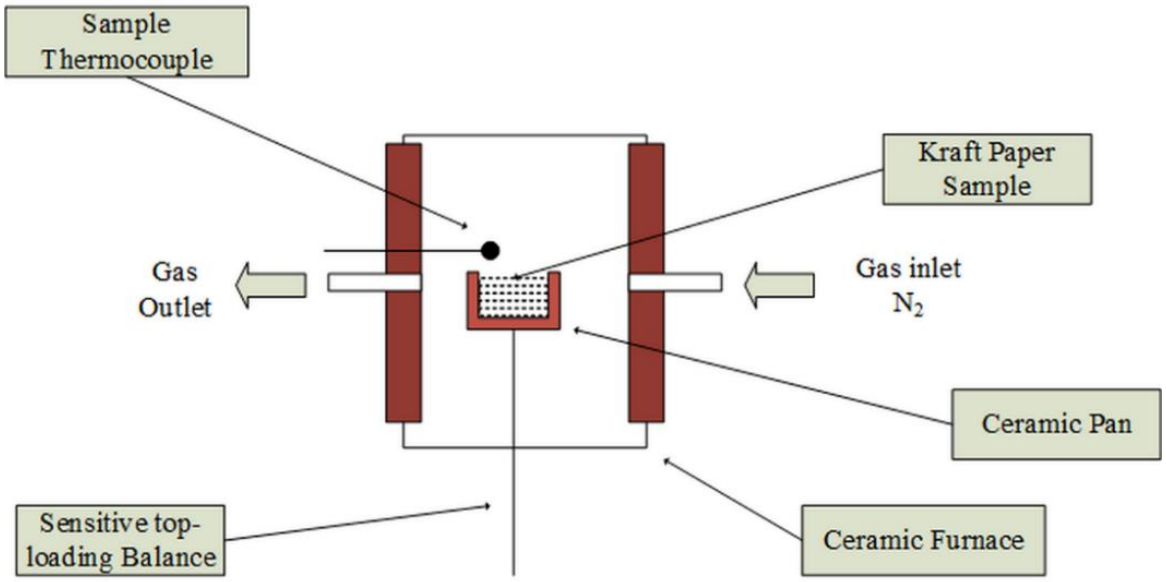

Figure 2.13: Illustration of a ceramic pan filled with paper insulation in a TGA furnace with top-load balance.

TH-3272_186151014

(a) (b) (c) (d)

Figure 2.14: Solid insulation samples (a) Vacuum oven dried fresh kraft paper (b) 300 hours oxidative aged kraft paper (c) 600 hours oxidative aged kraft paper (d) 900 hours oxidative aged kraft paper.

(a) (b) (c)

Figure 2.15: (a) Empty ceramic cup (b) Ceramic cup filled with kraft paper samples (c) Ceramic cup with remainings after performing TGA.

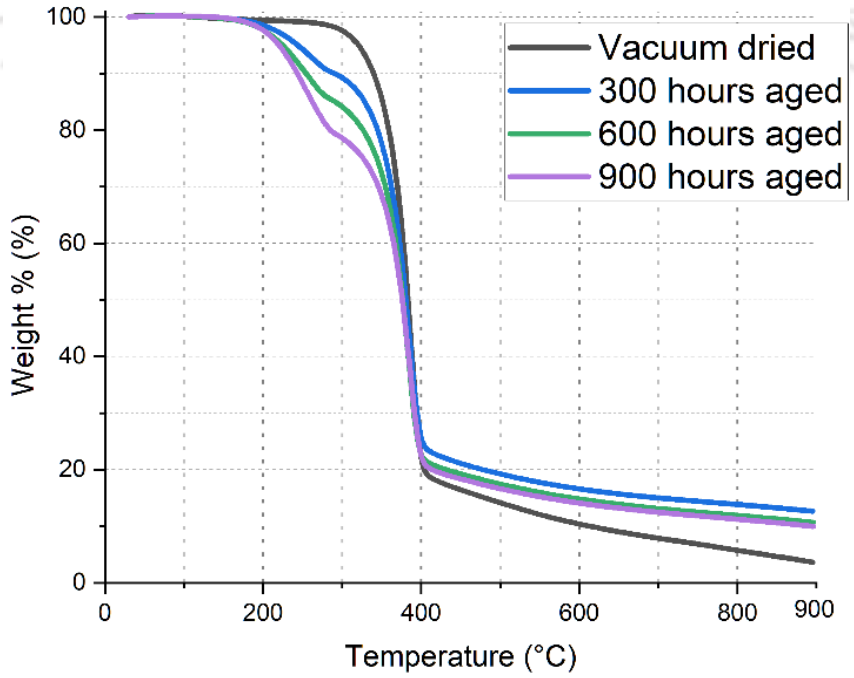

Figure 2.16: Weight percentage vs temperature curve of the kraft paper samples from 30 to 900˚C.

TH-3272_186151014

From Figure 2.17, it was observed that the percentage of weight loss in the temperature range of 200 to 300°C for the 900-hour aged sample is higher compared to the 600-hour aged sample followed by the 300-hour aged sample. To study the rate of weight loss with temperature variation, derivative weight is plotted in Figure 2.18. The derivative weight is the rate at which the mass is degraded. The units are mg/min.

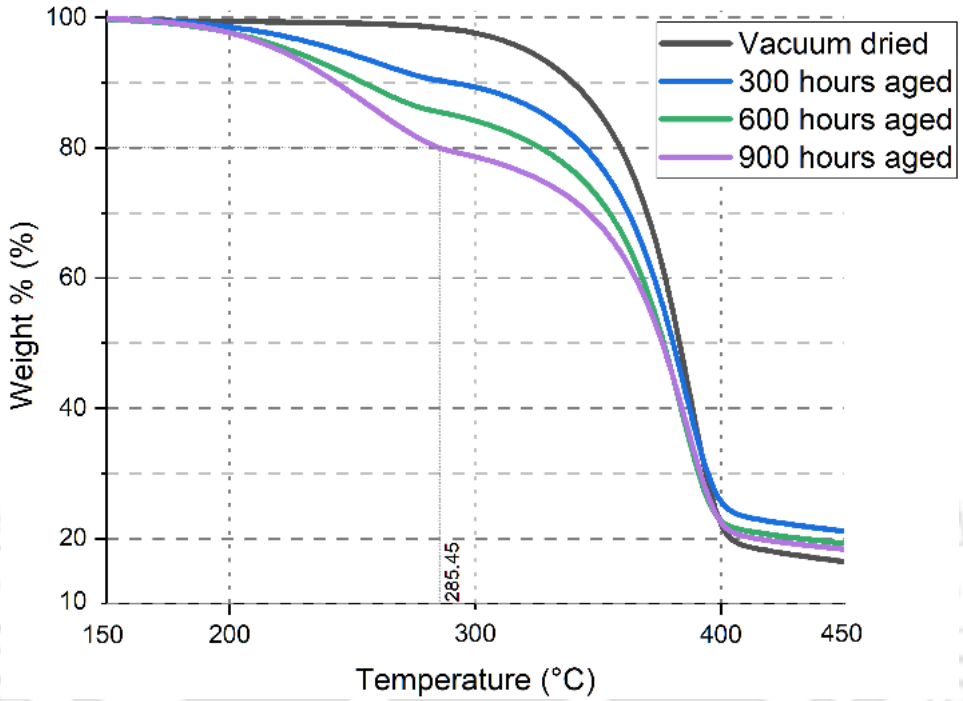

Figure 2.17: Weight percentage vs Temperature of the kraft paper samples from 150 to 450˚C.

The derivate weight graph is divided into two zones. Zone I for the temperature range of 200 to 300°C, and Zone II for the temperature range of 300 to 400°C. In Zone I, the rate of degradation is higher for the aged paper at a temperature close to 250°C, indicating the oil evaporation from the paper sample. The higher the aging status of oil, the faster the degradation rate. As the temperature increases beyond 250 to 300°C, the rate of thermal degradation reduces for the aged samples. It is noteworthy to mention that the dry paper is much more stable in zone I. In Zone II, the trend in degradation rate for the oil-aged samples is observed to be reversed in comparison to Zone I. The rate of degradation is higher for the 300-hour aged sample followed by 600 and 900-hour aged samples. The max degradation rate of the dry paper is closer to half of the max degradation rate of the 300-hour aged sample. Though the degradation rates are different, the max degradation for all the samples is found at 384.5±1˚C.

The TGA concludes that the thermal degradation of oil-aged samples in the temperature range of 200 to 300°C is due to evaporation of oil on the paper samples and the thermal degradation of dry paper starts after 300°C. The maximum degradation rate in the derivative

TH-3272_186151014

weight graph is found at 384.5±1˚C for all the samples. Since there is no significant difference in the temperature at which the maximum degradation rate of the paper occurs despite samples having various aging statuses, TGA cannot be used to define the aging status of the solid insulation precisely. It may be used in conjunction with other measurements or analyses to obtain a satisfying conclusion. Therefore, TGA will not be used hereon in the following chapters as an assessment technique and the focus is exclusively laid on the liquid insulation.

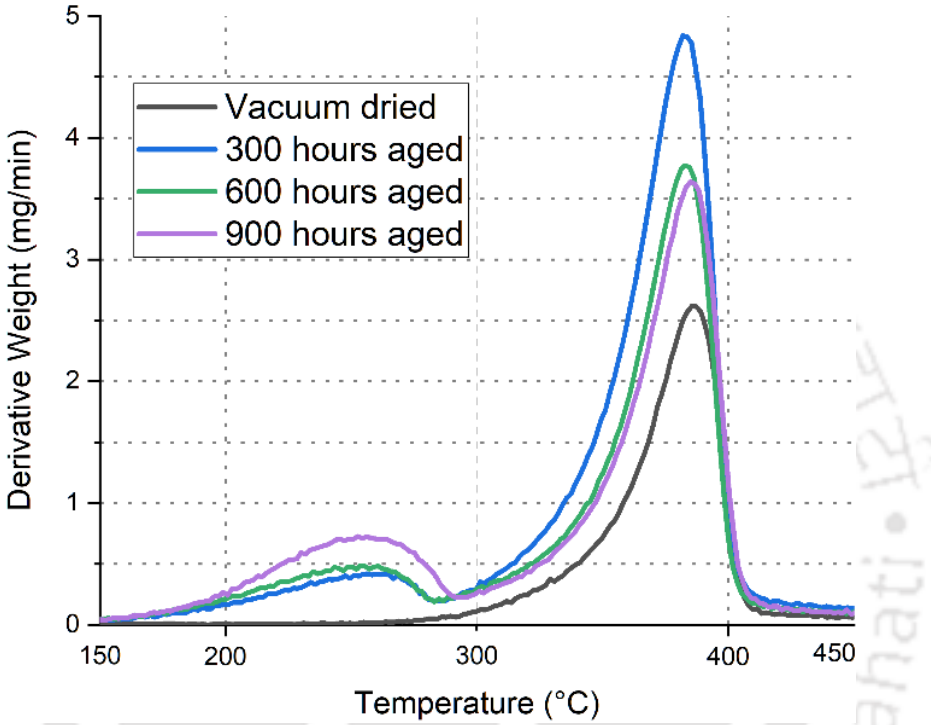

Figure 2.18: Derivative weight vs temperature of the kraft paper samples from 150 to 450˚C.

2.5. Summary of the chapter

An EMI free, non-intrusive, and non-destructive experimental setup is developed and optimized for testing of laboratory aged insulating oils. A first order prediction graph for TAN and MC is generated from the data obtained from laboratory aged samples and is used to predict the status of in-service transformer oils. Further, TGA is performed on fresh and oxidative aged solid insulation samples to study its performance. The outcomes of this chapter are as follows.

- The chosen frequency band of 2.1 to 2.6 GHz is able to clearly differentiate MO samples with different TAN and MC.
- Unlike LMWCA, the HMWCA is responsible for the shift in $|S_{11}|$ at the first resonance frequency in the chosen band.
- The S_{11} parameter at the first and second resonance frequencies in the chosen band corresponds to the TAN and MC of the insulating oil sample respectively.

TH-3272_186151014

- The TAN and MC of any unknown mineral insulating oil sample can be predicted by using the prediction graph.
- Scalable test setup is practically feasible, portable, and economical.
- This technique is unaffected by the operating frequencies in the electrical substation due to its EMI free design.
- TGA analysis alone is not sufficient to obtain the key aging status of the oxidative aged kraft paper.

This technique can be phenomenal in the swift and efficient detection of TAN and MC of transformer oil samples. Since the entire experimentation is performed in the anechoic chamber, the results are least affected by EMI interference. Therefore, this technique proves to be an effective way to estimate the degradation status of the transformer mineral oils. Since this technique is contingent on the MC and TAN of the oil sample, it could be applicable to alternative insulating oils, too. Alternative insulating oils are being developed for transformer application due to the exhaustible nature of MO and the demand for oils with higher electrical breakdown strength, flashpoints, and biodegradability. The following chapters deal with studying the fundamental properties of such alternative insulating oils and their response to the technique developed in this chapter.

Note: This work, "A Non-Intrusive and Non-Destructive Technique for Condition Assessment of Transformer Liquid Insulation," has been published in IEEE Transactions on Dielectric and Electrical Insulation, 2022, vol. 29, no. 2, pp. 693-700.

TH-3272_186151014

3

Natural ester and its blended oils as alternate transformer insulation

Contents

3.1	Introduction	36
3.2	Materials and aging	37
3.3	Physiochemical and electrical properties of the blended oils	38
3.4	Surface study of solid insulation aged in natural ester oil	64
3.5	Summary of the chapter	67

TH-3272_186151014

3.1. Introduction

MO has been used in transformers for a long time as an electrical insulation and thermal coolant [1, 69]. The vegetable oils (VO) manifest to be an alternative to MO with better electric breakdown characteristics, excellent fire safety, and environmental characteristics. The utilities are coming up with green transformers that use VO as a liquid insulant. The utilities also prefer to retrofill the aged transformers with the VO as it gives thermal stability to the solid insulation [28]. The above stated advantages of VO and the possibility of exhaustion of MO make the former the best potential alternative. When VO is retrofilled in MO based transformer, the blending of VO and MO occurs involuntarily as the latter cannot be completely drained from the transformer [28]. A small amount of the MO remains in the paper, pressboard, windings, core, tank, and radiators. However, most of the old insulant in solid insulation gets replaced by the new insulant within a few months of retrofilling [70, 71]. During this replacement time, there is a continuous change in the quantity of old and new insulants impregnated in the solid insulation. Hence, the blending ratio of these insulants closer to the conductors is unpredictable, and it affects the electrical properties at that particular location [70, 71]. Researchers have also come up with using blended oil (BO) as an alternative to MO due to the superior properties they inherent properties from both base oils [70, 72-74]. The blending leads to a synergy between the base oils and gives birth to a new structure that results in superior dielectric properties [70]. In addition, retrofilling with natural ester causes a rise in the number of hotspots and hotspot temperature [75]. Therefore, there should be a balance between the improvement in properties and the cost of insulant for commercialization. The balance between properties and cost can be achieved by BOs, so it is of interest to study the BO behavior in all aspects.

Many researchers have studied the dielectric performance of BOs prepared by mixing MO and VO in a ratio of 70%-30%. However, this ratio does not represent the exact scenario of the blending ratio of oils after retrofilling. Therefore, in an effort to understand the properties and nature of BO during transition, various ratios of MO and FR3 are mixed to produce five different types of BOs. These BOs are tested individually for their performance.

MO which is most used across the world for high voltage applications is blended with FR3 to produce BOs. Performance evaluation should be done before retrofilling the transformer to have a cognizance of the performance beforehand. During the operation of the transformer, the oil needs to be monitored continuously for insight into any imminent failure of transformer insulation. Hence, this chapter focuses on studying the physiochemical and electrical properties

TH-3272_186151014

with a special focus on PD trends due to needle-plane electrodes. Further, the gassing tendency of these oils subjected to continuous electric sparking is also investigated. In order to assess the short as well as long term performance, the tests are performed on fresh and oxidative aged oils. By identifying a proper blending ratio that balances the physiochemical and electrical properties, this study will help in cost cutting.

3.2. Materials and aging

3.2.1. Materials used in experimentation

MO used in the present study is procured from M/s Savita Oil Technologies Limited and FR3 from M/s Cargill India. The received oils are individually filtered using 2 µm pore size filter paper, followed by degassing and drying in a vacuum oven according to IEEE C57.637 [55]. This procedure removes moisture, dissolved gases, and organic contaminants (if any) from the fresh oils. The MO based transformer when retrofilled with FR3 has minute quantities of MO left in the windings, the FR3 will replace the MO and in turn, result in a different proportion of mixed insulating oil. The blending ratio in the close proximity of windings cannot be predicted and hence it is important to consider multiple blends of both oils. The fresh oils are used for preparing BOs. The blending is done in a glove bag filled with dry nitrogen gas to avoid the contamination of oil samples. The ratio of blending is mentioned in Table 3.1. After preparation, the fresh BOs are hermetically sealed and stored in a room with an RH of 35% and a room temperature of 20°C. All the oil samples prepared were found to be properly miscible and remained miscible for many weeks, even after experimentation. The miscibility of each sample is confirmed by testing the relative permittivity and dissipation factor at three different positions of the vessel [72]. The paper and pressboard are dried at a maximum permissible temperature of 110°C, which was later used in aging the BOs [76].

Table 3.1: Samples of blended oils.

Fresh sample	Sample code	Oxidative aged sample	Sample code
MO	A1	MO	A2
MO- FR3 (3:1)	B1	MO- FR3 (3:1)	B2
MO- FR3 (1:1)	C1	MO- FR3 (1:1)	C2
MO- FR3 (1:3)	D1	MO- FR3 (1:3)	D2
FR3	E1	FR3	E2

TH-3272_186151014

3.2.2. Aging of samples

IEC 60354 states the aging of insulation is mainly due to thermal stress. However, CIGRE and Electra 150 states that aging is accelerated by oxygen in addition to thermal stress [72]. Half of all the fresh samples prepared are aged using open beaker oxidative aging according to ASTM D1934. The oil, kraft paper, and pressboard are combined in a 20:1:1 ratio along with copper wire of length 475 mm wound spirally and filled in a beaker, and the beaker is placed on a platform rotating at a constant speed of 2 RPM [52]. The aging is done at a temperature of 115℃ for 96 hours. The fresh and aged samples are shown in Figure 3.1 and their sample codes are mentioned in Table 3.1 for easy interpretation.

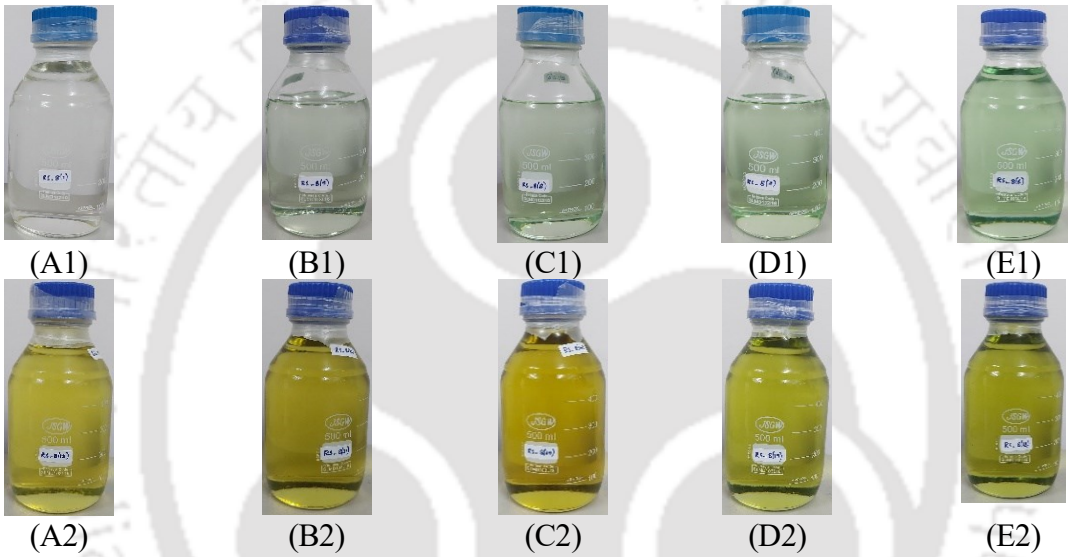

Figure 3.1: Hermetically sealed fresh and oxidative aged liquid insulation samples.

3.3. Physiochemical and electrical properties of the blended oils

3.3.1. Physiochemical properties and AC breakdown voltage

Various electrical and physiochemical properties of the BOs shown in Figure 3.1 are presented in Table 3.2. The moisture is measured by Coulometric Karl Fischer titration in accordance with ASTM D1533. This method uses a reagent that consists of Iodine and reacts instantly with the moisture. The amount of reduction in reagent is directly proportional to the amount of moisture present in the test sample and is detected amperometrically by the platinum electrodes. This method can detect moisture as low as 2 ppm. The AC breakdown voltage (BDV) is measured in accordance with ASTM D1816 using polished brass spherically capped Verband der Elektrotechnik electrodes. The test cup is filled with the sample and waited for a few minutes before applying voltage to let the air bubbles escape. Typical wait times are 5 minutes for MO and 30 minutes for VO according to ASTM D1816. Kindly note that the blended oils are also provided with a wait time of 30 minutes as they contain VO. Now, the

TH-3272_186151014

voltage is increased from zero at a rate of 0.5 kV/s until breakdown occurs and the corresponding rms voltage is noted. Five such breakdowns are performed on each sample with a wait time of 90 seconds between every test and the average is reported as ACBDV. The dielectric dissipation factor (DDF) and the relative permittivity are measured in accordance with ASTM D924 at 90°C by using a voltage source operating at power frequency. The DDF is a measure of the ratio of resistive current to capacitive current flowing through the sample on subjecting it to electric stress. Whereas the relative permittivity is a measure of the ratio of the capacitance of the test cell with the test sample as dielectric to the capacitance of the test cell with air as dielectric. The specific resistance of the liquid sample is measured in accordance with ASTM D1169. Direct polarity of the potential is applied to the sample, and the current through the sample is noted after a minute. Now, the terminals of the test cell are short-circuited for 5 minutes followed by polarity reversal and noting of current through the sample. The test voltage across the sample is also recorded. The individual resistivity for direct and reverse polarity is calculated from the recorded current and voltage using (3.1) and the average of both resistivities is reported as the specific resistance of the sample.

$$\rho = (VK)/I \tag{3.1}$$

where ρ is the resistivity, V is the test voltage in V, K is the cell constant in cm, and I is the current through the sample in pA.

The flash point is measured in accordance with ASTM D93 by a manual Pensky-Martens closed cup tester which can test flash points up to 370°C. The test sample is filled in a brass cup fitted with a cover and is heated while stirring at a specified rate. An ignition source is directed onto the brass cup at regular intervals with simultaneous interruption until a flash is noticed. The temperature corresponding to the occurrence of the first flash is reported as the flash point. The interfacial tension (IFT) is measured in accordance with ASTM D971 by the ring method. A ring with a 40 mm circumference made with a wire with a 0.3 mm diameter is used for the measurements. The instrument is calibrated by immersing it into a cup filled with water. The tension at which the film is adhering to ring ruptures is recorded as IFT. Now, to measure the IFT of the oil sample, it is spread onto the water and the ring is immersed into the oil. The ring is slowly moved and the tension at which the film adhering to the ring ruptures is recorded. The density of the oil samples is measured as per ASTM D1298 using the hydrometer method. In this method, the sample is loaded into hydrometer placed in a water bath maintained at the desired temperature. The observed hydrometer reading is the density of the sample.

The fatty acids in the VOs are deciding factors for the physiochemical properties of natural ester oils [77, 78]. Hence, blending them with MO in different ratios gives a unique oil

TH-3272_186151014

[72, 74]. The moisture content in Table 3.2 shows that with an increase in VO content, the MC in the fresh and aged oil increases. This increase in MC is due to higher moisture saturation value and percentage of VO. The increase in BDV is observed with an increase in VO content which is because of less free moisture.

The DDF, relative permittivity (RP), specific resistance, and IFT of the samples are observed to reduce with an increase in VO content. This is due to the polar molecular structure of the ester oil (EO). Also, it is notable that the change in IFT from new to aged ester oil is less compared to mineral oil as mentioned in IEC 62961 [79]. Though the ester oils have higher breakdown voltages, they have a higher charging tendency compared to MO due to their low resistivity [74].

Table 3.2: Physiochemical properties of BOs.

Property		MC (ppm)	ACBDV (kV)	DDF @90°C	RP	Specific resistance (Ω-cm)	Flash point (°C)	IFT @27°C (mN/m)	Density (kg/m^3)
Standard		ASTM D1533	ASTM D1816	ASTM D924		ASTM D1169	ASTM D93	ASTM D971	ASTM D1298
Fresh sample	A1	8.2	92.5	0.00167	2.012	234.80×10^{12}	163.5	47.81	0.817
	B1	38.3	95.5	0.00401	2.211	17.84×10^{12}	184.4	28.13	0.830
	C1	71.1	97.6	0.00780	2.478	6.64×10^{12}	219.7	23.52	0.864
	D1	91.5	98.9	0.01006	2.630	2.27×10^{12}	256.6	22.86	0.872
	E1	99.2	100.2	0.03583	2.904	926.20×10^{09}	320	20.09	0.913
Aged sample	A2	29.9	88.9	0.00187	2.034	132.60×10^{12}	160.5	17.88	0.822
	B2	72.8	90.3	0.01155	2.238	4.94×10^{12}	178.5	15.69	0.838
	C2	112.9	91.3	0.01606	2.472	1.80×10^{12}	208.4	19.19	0.878
	D2	163.2	91.9	0.03002	2.658	862×10^{09}	231.4	20.05	0.893
	E2	316.4	92.9	0.04881	2.960	78.68×10^{09}	289.6	20.06	0.934

The flash point and density of the oil samples are found to increase with the increase in VO content. The increase in these properties is due to the long chain fatty acids in VO. All the above properties show that VO has both advantages and disadvantages over MO. The agreement between the oils is observed in BOs. Therefore, BOs have a very high potential as an alternative insulation. In addition to the above properties, the non-destructive characteristics such as PD and DGA give insight into the behaviour of these oils during operation. The

TH-3272_186151014

following sections deal with the PD and DGA of blended oils when subjected to selective electric stress.

3.3.2. Partial discharges in blended oils

Monitoring needs to be done for the reliable operation of assets in the power grid and to save on downtime costs. Power failures occur due to insulation failure. The impending insulation failures can be detected by the PD measurements [80]. PD is an electric discharge occurring in the insulating medium between two conductors that does not completely bridge the two conductors. Continuous and long-term PD results in degradation of the insulation and leads to erosion, aging, and early failure of insulation [31, 81]. The PD test of the oil insulation gives an insight into the aging status of the transformer and necessary action may be initiated at the early stages of failure [81, 82]. The important attributes that can be established from the PD study are PD inception and extinction voltage, apparent charge of pulse, phase angle of pulse, pulse repetition rate, accumulated apparent charge, average discharge magnitude, peak discharge magnitude, average discharge current, discharge power, quadratic rate, phase resolved PD pattern (PRPD) and pulse resolution time [31, 83]. PD inception voltage (PDIV) is controlled by the local applied field rather than the average field across the insulation [84]. PDIV can be reasonably reproduced. PD occurs at both AC and DC voltages. However, as most of the power and distribution transformers in the power system network operate on HV alternating current, this work focuses on studying the PD in BOs due to AC voltage.

PD occurs due to the high stress zones created by surface defects in conductors, floating metals, trapped air, poor earthing, and contaminants in the oil [28, 76]. Concentrated PD occurs on the sharp edge of electrodes and also in the oil ducts when stress exceeds the limits of PDIV [76]. The contaminants in oil tend to migrate to areas of high electric stress faster in a low viscosity oil [76]. It indicates a higher viscosity oil could be better for usage in transformers bushings and capacitors. But as higher viscosity causes a reduction in TC, the BOs provide a feasible solution in balancing the viscosity and electric stress. To ascertain various theories and establish the relation between the blending ratio and PD, this subsection focuses on studying PD in various BOs.

3.3.2.1. Test setup

The test setup consists of a high frequency filter, discharge free HV source (230V/100kV, 10 kVA), capacitive voltage divider (CVD), PD test cell, connecting wires, quadripole, coupling capacitor (CC) (1000 pF), data acquisition and processing system connected as shown

TH-3272_186151014

in Figure 3.2(a). An isolated power supply supplies power to the HV source through high frequency filter. The PD happens only in small volumes around the highly stressed region. Therefore, PD signals can only be differentiated from external noise when noise to noise-to-signal ratio is significantly good. External noise such as EMI is mitigated by shielding the experimental chamber with interconnecting Aluminium sheets and earthing them. The earthing of the EMI shielding is essential as the metallic objects in the surroundings would otherwise produce noises [76].

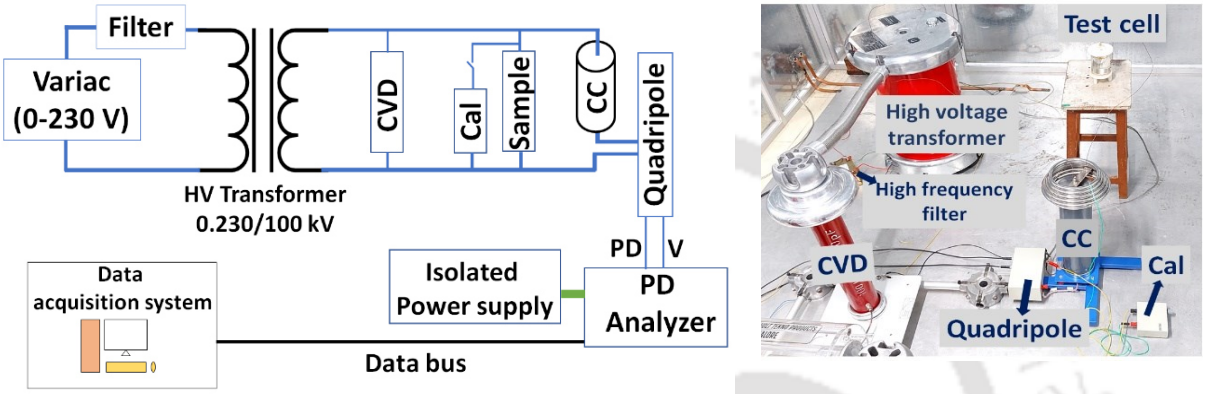

(a) (b)

Figure 3.2: (a) Partial discharge measurement connection diagram and (b) Experimental setup with test cell.

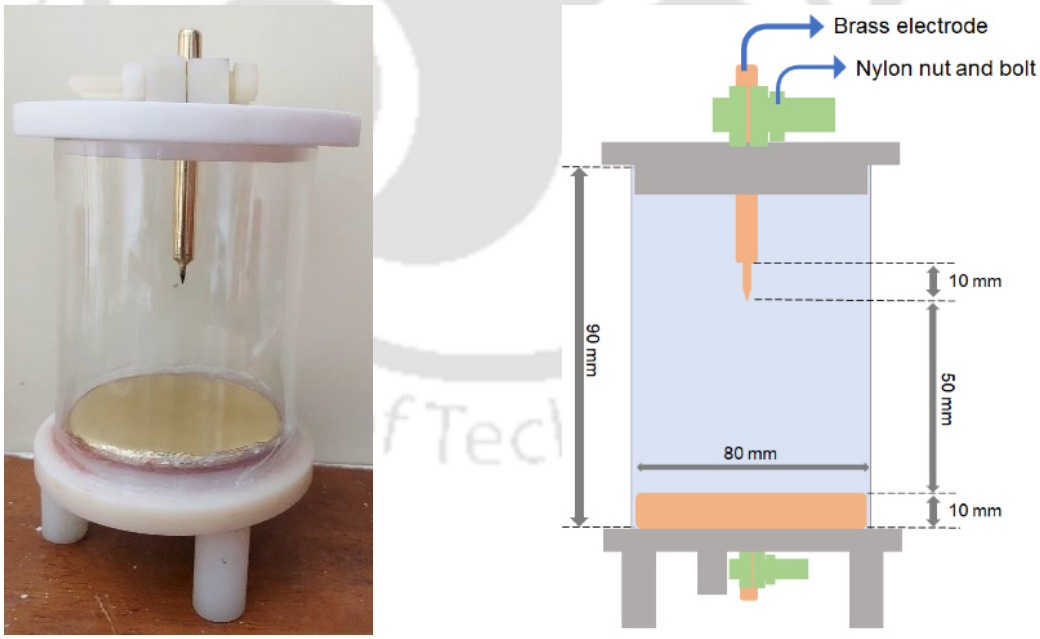

(a) (b)

Figure 3.3: (a) PD test cell with the needle (20 µm) and plane electrodes (b) Illustration of PD test cell with dimensions.

The test cell used for the PD study is shown in Figure 3.3. It is designed in such a way that there are no sharp edges other than the needle tip. A needle-plane electrode system with a

TH-3272_186151014

stainless steel needle of 20 µm tip radius is connected to a brass rod and placed at a distance of 50 mm from the brass plane electrode. The tip radius of needles is measured in a lab accredited by the National Accreditation Board for Testing and Calibration Laboratories (NABL) after production. The stainless-steel needle is brazed into the brass rod that connects it to the HV source. The brass rod and the plane electrode are buffed for a smooth outer texture. The needle and rod at the HV terminal are intentionally made of different materials to avoid the shaping out of the needle when welded into the rod. In this schema, the needle is brazed into the brass rod without melting or damaging the needle tip as stainless steel has a high melting point compared to the brass. The outer wall of the test cell is made of silica glass and fastened to the PTFE discs at the top and bottom with a provision for electrode placement. The HV and ground electrodes of the test cell are fastened to connecting wires using a nylon nut and bolt system to avoid sharp edges in the test cell and damage to the conductors. The nylon nut and bolt for fastening the HV electrode are shown in Figure 3.3(a). This unique design ensures the occurrence of PD is solely due to the needle.

3.3.2.2. Calibration and Experimentation

The test setup is calibrated according to ASTM D1868 using a standard pulse calibrator (CAL) whenever the needle is changed. The calibration is also performed every time the sample is replaced. The test setup without a needle is observed to be discharge free up to 48 kV for the developed test cell design. The PD pulses are recorded using a single channel commercial PD analyzer (PDC13, AES make). The sensitivity of the PD analyzer is 0.1 pC. The background noise of the measurement setup is observed to be 2.5 pC. The small background noise is achieved by providing earthing to a depth of 120 feet during the installation and commissioning of the PD analyzer. Based on studies conducted by various researchers and technical committees, a narrow band detector (300 kHz) is chosen to capture the PD activity in liquid [81, 85-87]. This measurement system is a wide band instrument according to IEC 60270. The wide band instrument is generally preferred for the detection of pulse bursts in liquids due to the dynamic nature of the voids [88].

The relative humidity of the testing atmosphere should be less than 60%, and the electrodes need to be coaxial during PD measurement. Otherwise, a correction factor is to be introduced [31]. The above two details are taken into consideration while designing the test cell and performing experiments. A constant room temperature of 20°C and an RH of 40% is maintained throughout experimentation. Care is taken to avoid the contamination of samples by hermetically sealing and placing the samples in a desiccator before and after

TH-3272_186151014

experimentation. The test cell is cleaned with laboratory grade methanol and rinsed twice with the test sample before each experiment. The sample is meticulously filled in the test cell to avoid bubbles and a stand time of 15 minutes is provided to let the trapped air escape before experimentation. Since this experimentation is non-destructive in nature, multiple measurements can be performed on one sample [85]. The experiments are repeated for two different fillings of the same sample with 10 PD measurements for each filling. A rest interval of one minute for MO, five minutes for BOs, and eight minutes for VO is provided between each measurement.

PDIV is interpreted in multiple ways by the researchers [89-92]. In this work, PDIV is interpreted in two ways. One of them is an apparent charge just exceeding 100 pC in accordance with IEC TR 61294 and the second consideration is the number of pulses with an apparent charge of each pulse greater than 5 pC exceeding 500 per minute [91, 93]. According to [91], the PDIV for insulating oils is nearly the same for 500, 1000, and 1500 pulses per minute. The need for a second PDIV consideration comes from the lack of interpretation of the PD pattern above PDIV by IEC TR 61294. The second consideration also satisfies the definition of PDIV by IEC 60270. The samples are stressed by applying the voltage at a rate of 1 kV/s until PDIV is reached in both cases. Further, the voltage is increased to 6 kV above PDIV and then gradually decreased at 1 kV/s to find the PD extinction voltage (PDEV) which is defined by upending the above two considerations for PDIV.

The voltage at the HV terminal is monitored by the CVD as well as the quadripole connected to the coupling capacitor. The behavior of the insulating liquids on the application of high stress is required to be studied to understand PD behavior at divergent field points. The insulating liquid with a higher ability to suppress the partial discharges would be the finest choice for the customer. PD occurs when insulating oil is subjected to a very high electric field. The electric stress in fresh and aged oil samples is generated using a needle-plane electrode system as shown in Figure 3.3. The needle tip is designed such that the electric field at the tip of the HV electrode is much greater than the dielectric strength of the liquid insulation. Just before PD happens, an interface is formed on the walls of the gaseous cavity as a result of Maxwell-Wagner polarization and when the potential across this cavity exceeds Paschen's minimum, the charges in the cavity are neutralized [31]. It leads to local discharges followed by the formation of gas bubbles and thereon partial discharges [31]. The electric field at the tip of the needle for this configuration can be determined using (3.2) derived by Eyring et al. [94].

$$E_{max} = \frac{V}{r ln(2\sqrt{((d+r)/r)})} \tag{3.2}$$

TH-3272_186151014

where V is the applied voltage, r is the radius of curvature of the needle tip, and d is the distance between the needle and plane electrodes. However, the electric field distribution across the gap is influenced by the conductivity and permittivity of the materials.

The following subsections present the results on PDIV, PDEV, minimum phase angle at which PDIV occurs, and PD patterns in the fresh and oxidative aged oil samples.

3.3.2.3. PDIV and PDEV of fresh and oxidative aged blended oils

PD takes place at the sites of field intensification and therefore to study the effect of intense fields on PD, a needle plane electrode configuration is preferred [95]. As discussed earlier, the PDIV is educed from two cases. Case 1 is the apparent charge exceeding 100 pC and case 2 is the number of pulses exceeding 500 per minute with each magnitude of pulse greater than 5 pC. Figure 3.4 shows the PDIV in fresh and oxidative aged oils for the above two cases. The PDIV results shown in Figure 3.4 are an average of 20 readings.

The PDIV results in Figure 3.4(a) show that with the increase in VO content, PDIV increases for the fresh oil samples with fresh FR3 having the highest PDIV. A smooth trend in the increase in PDIV is observed from sample A1 to E1. Volatile substances in the MO are released at lower temperatures compared to ester oils [73]. Therefore, the PDIV in MO and BOs with greater MO content is lower compared to VO among the fresh oils. However, the trend is not the same for the oxidative aged samples. The oxidative aging of oils produces organic acids, aldehydes, alcohols, saturated esters, ketones, peroxides, unstable products, lactones, polymerized hydrocarbons, sludge, and dissolved gases in addition to moisture [28]. These contaminants are collectively responsible for the change in PDIV and PDEV of the aged oils in comparison to fresh oils. Since the VO oxidizes and degrades faster in the presence of oxygen, pure VO has lower PDIV than BOs. A BO with an equal proportion of MO and FR3 has the highest PDIV. The reason for low PDIV for the VO among the aged samples is due to oxidation of EO in the presence of oxygen. The volatile substances in MO and the oxidation of VO are responsible for MO and VO having lower PDIV compared to their BOs.

When the applied voltage on the oil samples is increased gradually, case 1 is noticed first, followed by case 2. The PDIV recorded according to case 2 is presented in Fig. 3.4(b) and it can be observed that the PDIV for fresh oils follows the same trend as in case 1. However, the PDIV magnitude is higher in case 2. The BO with an equal proportion of MO and FR3 is observed to have the highest PDIV among the aged samples in case 2 as well. Similarly, an attempt is made to extract the PDEV values of the samples. PDEV in case 1 is construed as apparent charge to be less than 100 pC and pulse count less than 500 per minute with each

TH-3272_186151014

pulse greater than 5 pC in case 2. The average of 20 readings is presented in Figure 3.5. PDEV for fresh oil samples is found to increase with VO content with FR3 having the highest PDEV for both cases. The PDEV of aged oils is similar to their PDIV.

The ratio of PDIV to PDEV (RIE) is unity for ideal insulation. It is interesting to note that the RIE in case 1 is close to unity indicating that the oils behave as an ideal insulation. However, RIE in case 2 contradicts this ideal nature. The RIE is close to unity for sample A1 (1.0176) among fresh oils and for sample C2 (1.008) among aged oils in case 2. RIE is different for the same oils based on the inception and extinction criterion. RIE may be used in defining the PDIV for liquids as it clearly provides an understanding of the PD performance and the set criterion.

In addition, by weighing up the physiochemical properties in Table II with the PDIV of the oils, the BOs prove to be a better insulant balancing all the properties. The end life of transformers depends on the performance of aged oil. Therefore, considering PDIV and PDEV characteristics, the equal ratio of MO-FR3 blend proves to be the best alternative liquid insulation for transformer application in the long run.

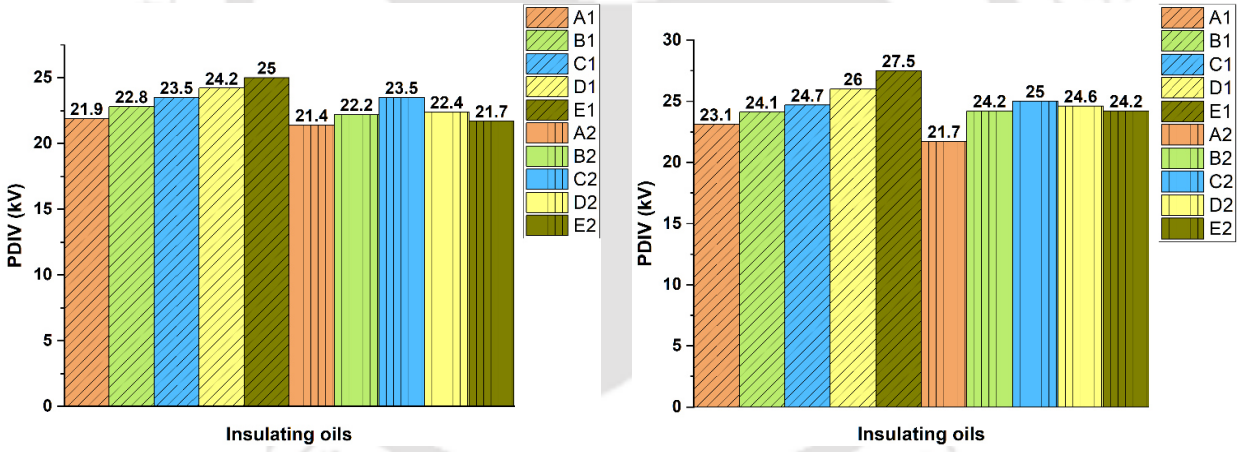

Figure 3.4: (a) PDIV on reaching 100 pC and (b) PDIV on reaching 500 pulses/min.

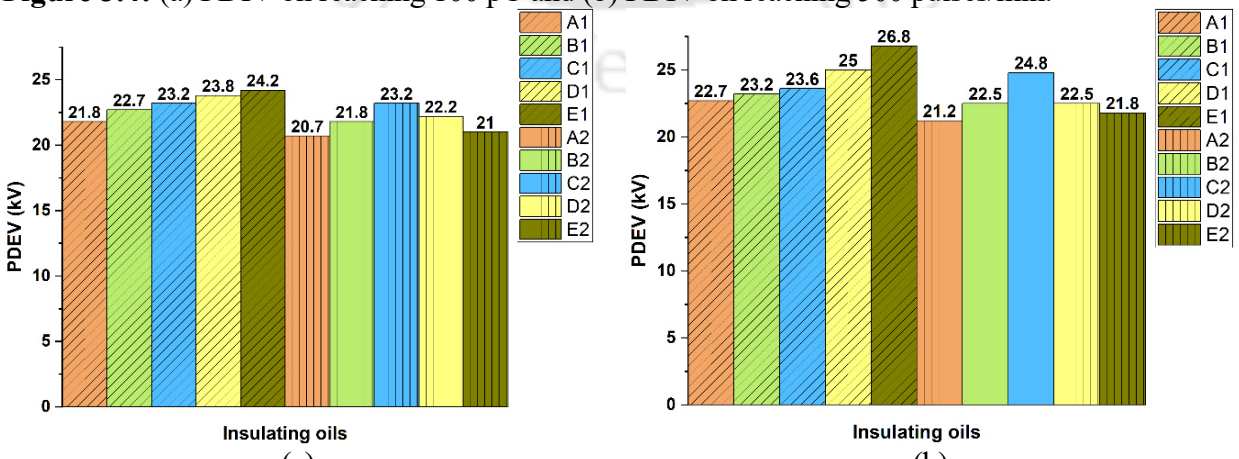

Figure 3.5: (a) PDEV on reaching 100 pC and (b) PDEV on reaching 500 pulses/min.

TH-3272_186151014

With knowledge of the PDIV and PDEV, there is a need to understand how the two cases are crucial in defining the PDIV and interpreting the devastating effects. This can be achieved by studying the PD pattern in the oil.

3.3.2.4. PD pattern and the minimum phase angle at PDIV

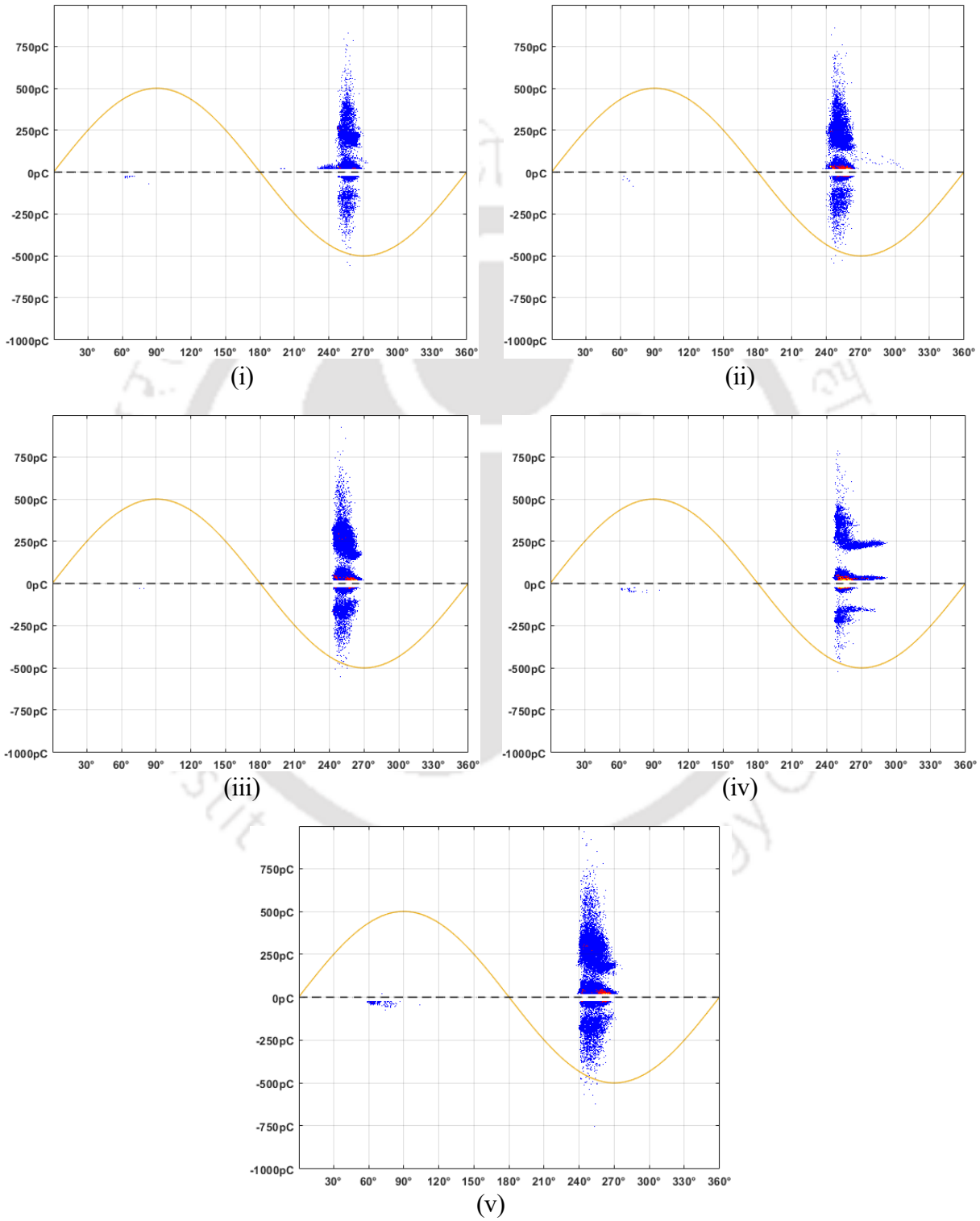

Figure 3.6: PD pattern at 6 kV above PDIV for (i) A1 (ii) B1 (iii) C1 (iv) D1 and (v) E1 samples.

TH-3272_186151014

The PD pattern provides insight into the magnitude, trajectory, frequency, and phase angle of the PD pulses with respect to voltage. They provide information on the intensity, type, and source of the PD. The shape and evolution features of the PRPD pattern are mostly identical for a sample in repeated tests. The discharge epoch is preferably observed at a certain voltage above the PDIV as it provides a more defined discharge pattern and a regular discharge character [87]. Also, the PD in liquid insulation is spasmodic in nature at PDIV. Therefore, the PRPD pattern in this work is presented at 6 kV above PDIV (case 1) of the respective liquid. As the PDIV of case 1 is lower, it ensures safe operation and discharge magnitudes within the detectable range of equipment. This enables a better comparison of the discharge epoch in liquid insulation. Therefore, the PRPD patterns presented in this section are at 6 kV above PDIV according to case 1.

The PRPD pattern in fresh and oxidative aged oils at 6 kV above their respective PDIV for 1500 cycles are shown in Figures 3.6 and 3.7 respectively. The discharge density in all samples is observed to increase with the increase in voltage above PDIV. The discharge rate, phase, and magnitude are asymmetrical for positive and negative half cycles. It is noteworthy to observe that a larger number of discharges are found to occur in the negative half cycle for fresh and aged oils as observed by other researchers [88]. The greater number of discharges in the negative half cycle is due to the abounding electron injection from the needle tip to the dielectric liquid. When subjected to electric stress, all insulating oils exhibit pulse burst characteristics [90, 96]. Therefore, each data point of the PD pulse shown in Figures 3.6 and 3.7 corresponds to an integrated response of the total charge transfer of a pulse burst occurring at that moment. Pulse amplitude and repetition rate indicate the severity of the defect. The discharges in MO are smaller in magnitude compared to other fresh oils. The PD magnitude and pulse count of the A1 sample are observed to increase almost linearly with the voltage. Whereas, for the E1 sample, heavy discharge magnitudes are found at PDIV and above. For all other samples, a lower discharge magnitude is observed up to PDIV and the discharge magnitude increases exponentially beyond that. The PRPD pattern of all the oils is found to be stochastic, erratic, and have sudden high magnitude discharges suggesting pulse bursts [90]. This indicates the severity of PD is large in fresh VO and all the aged oils. IEC TR 61294 states that PDIV is mostly related to the chemistry and not the conditioning of the liquid insulation as the PD is a local phenomenon. The PD pattern and PDIV suggest that there may be a chemical change in the structure due to the blending of oils. The magnitude of the highest discharge pulse for all the samples at 10 kV, 15 kV, PDIV, and 6 kV above PDIV is presented in Table 3.3. The magnitude of discharges for samples A1, B1, A2, and B2 increase

TH-3272_186151014

proportionally with voltage up to PDIV and above PDIV. Whereas, the discharge magnitude for samples C1, D1, E1, C2, D2, and E2 is consistently low up to PDIV and increases impulsively after PDIV. The higher discharge magnitude and higher number of pulses in VO indicate a catastrophic performance. Although the PD magnitude and pulse count are low in MO, the small PDIV values are of concern.

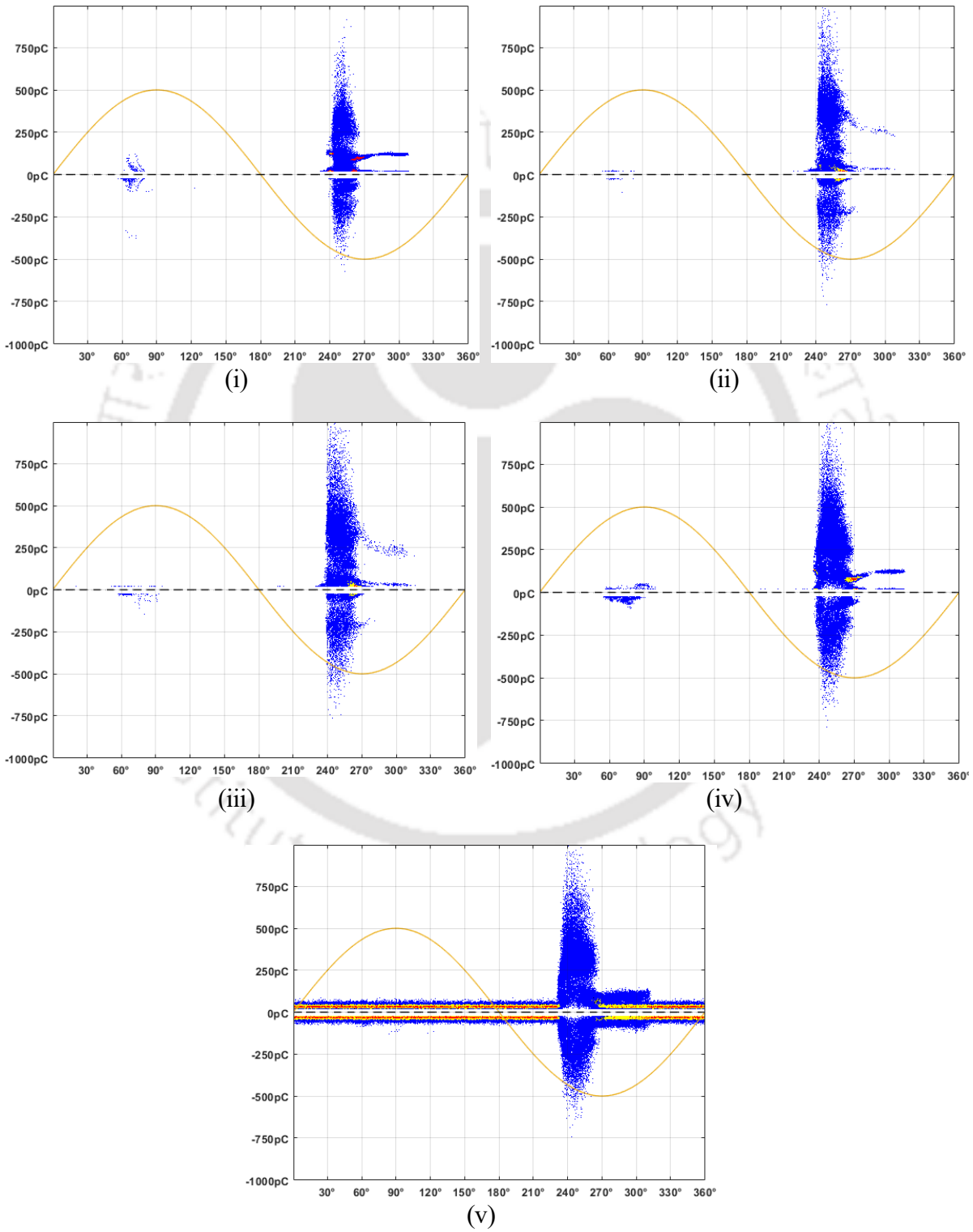

Figure 3.7: PD pattern at 6 kV above PDIV for (i) A2 (ii) B2 (iii) C2 (iv) D2 and (v) E2 samples.

TH-3272_186151014

The trend of the PD pattern is more important than the magnitude of the PD pattern. The comparison of the PRPD pattern of fresh and aged oils shows that the PD pattern is vertically elongated for the aged oils. This is due to the higher contaminants in aged oil, leading to higher discharges. The ascending PRPD in aged oils indicates a large number of discharge sites. The higher discharge magnitude and steep PRPD pattern in VO could also be a consequence of a large number of discharge sites. The PD amplitude is an indicator of the quality of insulation. The lower the PD magnitude, the better the quality of the insulation [28, 31, 80, 82]. All the fresh oil samples are observed to have approximately the same discharge amplitude. The aged oils have higher discharge magnitudes in comparison to fresh oils and enlarge vertically with the increase in VO content. The PD pattern and PDIV suggest that there may be a chemical change in the structure due to the blending of oils. The increase in pulse count for a few oils in comparison to others at a voltage greater than PDIV of case 1 indicates the need for introducing PDIV as an interpretation based on pulse count as it signifies the degradation. The magnitude of PD for samples A1, B1, A2, and B2 increases proportionally with voltage up to PDIV and above PDIV. Whereas, the PD magnitude for samples C1, D1, E1, C2, D2, and E2 is consistently low up to PDIV and increases impulsively after PDIV. It is of particular interest that the aged oils also have a broader PRPD pattern in addition to their vertical enlargement as shown in Figure 3.7. The broadening of PRPD can be visualized in two ways. The PRPD pattern of MO is observed to broaden towards zero crossing at 180° phase with aging (positive half cycle to negative half cycle) indicating a reduction in PDIV with aging. Whereas, samples D1, E1, and all aged samples broaden towards zero crossing at 360° phase (negative half cycle to positive half cycle) indicating lower PDEV. Samples C1 and C2 have narrow PRPD patterns among oils of the same nature. This confirms that the PDIV and PDEV of the sample with an equal ratio of MO and VO outperforms all other oil samples in the long run balancing the physiochemical and electrical properties.

Table 3.3: Magnitude of highest discharge pulse at 10 kV, 15 kV, PDIV, and 6 kV above PDIV (100 pC).

Voltage	Sample									
	A1	B1	C1	D1	E1	A2	B2	C2	D2	E2
10 kV	35	30	20	15	12	42	45	18	15	14
15 kV	60	50	32	28	22	75	72	32	30	25
PDIV	104	105	130	155	188	102	105	135	140	180
6 kV above PDIV	800	850	850	800	1000	875	1000	1000	1150	1200

TH-3272_186151014

Table 3.4: Phase angle at PDIV (100 pC).

Sample	>100 pC	Sample	>100 pC
A1	255.6°	A2	196.2°
B1	248.4°	B2	205.2°
C1	244.8°	C2	243.1°
D1	242.6°	D2	220.2°
E1	239.4°	E2	214.8°

The phase angle is a characteristic of PD which represents the structure of the PD cavity and the origin of PD [97, 98]. An effort is made to extract the information on the phase angle at PDIV from the experimental results using the AES Play Recording tool that was provided along with the PD analyzer. The phase angle at PDIV solely for case 1 is tabulated in Table 3.4 as it is not possible to extract the phase angle at PDIV for case 2 with the available software tool and the stored data. The phase angle at PDIV is only of concern as it is evident that the phase angle will reduce with a further increase in voltage [97]. Though it seems like the PD pattern of all oil samples is focused at the center of the half wave, the phase angle at which PDIV (case 1) occurs is found to be different. This could be due to the difference in cavity development times for different oils. With the increase in viscosity, the cavity development time decreases [99]. Therefore, viscosity is responsible for the decrease in cavity development times and thereby the inception phase angle for VO and BOs with VO content. The phase angle data in Table 3.4 for fresh oils show a decreasing trend with an increase in oil viscosity. However, the same trend is not observed in oxidative aged oils. This could be due to relatively higher moisture in MO resulting in PD cavity formation at a lower phase angle. Though the type of cavity developed is the same in all oils, the viscosity and moisture content could affect the cavity formation time and therefore the phase angle at which PD occurs.

This study is important in retrofilling MO based transformers with FR3 and vice versa. It is also useful for commercializing the blended oils. This study endorses the development and usage of blended oils in power apparatus. The increase in PD pulse count in a few oils in comparison to others indicates the need to interpret PDIV based on pulse count. This work benefits the transformer manufacturer and the transmission system operator in terms of cost cutting by choosing the apt insulation for a transformer based on the equipment's insulation requirement. This study supports the development, quality assurance, and condition monitoring of blended oil filled power apparatus.

TH-3272_186151014

3.3.3. Gassing tendency of blended oils on subjecting to electric sparking

Gases are generated in the transformer due to the decomposition of insulation owing to aging as well as the occurrence of thermal and/or electrical faults [100, 101]. Faults and aging result in the decomposition of insulation, followed by the formation of unstable radicals which rapidly recombine forming gases such as H_2, CH_4, C_2H_6, C_2H_4, C_2H_2, CO, and CO_2 [100-103]. Various compositions of the above seven gases can be correlated to the type of fault and its intensity. When the gas concentration is below the stipulated value and not significantly increasing, it is not considered a fault. On generation, a partial or an entire amount of these gases dissolve in the insulating oil depending on the solubility coefficients of gases as well as the type of oil. The attributes such as amount, change in concentration, and the rate of generation of gases obtained by performing DGA are helpful in the evaluation of the condition of the transformer [104].

DGA is a widely and frequently used promising technique for the assessment of transformer health. DGA is measured by three methods namely headspace, partial gas extraction, stripping gas extraction, and total gas extraction methods [104-106]. DGA is used for the diagnosis and tracking of faults by measuring the absolute and relative amount of key gases [107]. It also helps in monitoring the gas emission pattern in oil when subjected to individual or multiple simultaneous stresses. According to IEC 60599, faults are classified as partial discharges (PD), low energy discharges (D1), high energy discharges (D2), thermal faults below 300°C (T1), thermal faults between 300 and 700°C (T2), and thermal faults above 700°C (T3) based on the gases generated. Dornenburg ratios (DR), Rogers ratios (RR), IEC gas ratios (IGR), and the Duval triangle are the most commonly used methods to predict the type and intensity of fault [107-110]. The ratio of the amount of gases presents a very useful form of data for comparison and prediction of faults. The detection of fault at an early stage is important in prolonging the life of an equipment.

There is abundant documentation available on the gas evolving phenomena, evaluation, and fault identification using DGs for MO, nonetheless, the same methodology cannot be used directly for EO based transformers [29, 111, 112]. The EOs have a better electric breakdown, biodegradability, solid insulation endurance, and flash and fire point characteristics compared to MO making them a sustainable alternative [113-115]. Each EO has its own gassing rates and tendencies for a similar fault [101].

Small amounts of DGs are produced when PD occurs and are seldom detectable by DGA [116]. However, decomposition due to immense and short duration electric stress can be detected and analyzed using DGA [112, 116-118]. Sparking could be a low temperature fault

TH-3272_186151014

in some oils while it could be a high temperature fault for other oils. Sparking at voltage above oil BDV results in a relatively higher amount of DG generation. Multiple sparkings need to be performed to ensure sufficient concentration of fault gases [111, 112, 119]. Sparking at least 200 times produces gases at a linear rate [119]. With the speculated increase in the application of EOs and BOs for power transformers, studying their DG generation tendency is of great importance. Studying the gassing tendency of insulation enables its possible field application by providing data for developing and regulating gas relays for error-free monitoring.

The aim of the work in this subsection is to study the gassing tendency of the BOs subjected to electric sparking at a laboratory scale. Multiple gas analyses using ratios and graphical methods are performed to validate their applicability to BOs. Also, in order to study their long-term performance, the BOs are oxidative aged and sparked.

3.3.3.1. Sample Preparation and Description of Gas Ratios

3.3.3.1.1. Sample Preparation

The oils are mixed in five different ratios to generate samples with wide mixing percentages as shown in Figure 3.1. Two sets of each sample are prepared; one of them is stored directly in airtight glass bottle after preparation and termed as fresh oil, while the other sample is oxidative aged in accordance with ASTM D1934, stored in airtight glass bottle and termed oxidative aged oil.

Each fresh as well as aged oil sample is subjected to 200 continuous electric sparks with a time gap of 3 minutes between each spark. Sparking is done by increasing the voltage at a rate of 1 kV/s up to the BDV of respective oil using a b2 electronics make breakdown analyzer (model BA 100) with Verband Deutscher Elektrotechniker (VDE) electrodes having a 2.5 mm spacing in between. The volume of the test cell is 400 mL and has a non-hermetically sealed top cover. After filling the test cell with oil, a settling time of 5 minutes for samples A1, A2 and 15 minutes for the rest of the samples is provided before sparking. All the oil samples are dried, aged, stored, and tested in the laboratory to avoid contact with sunlight and ultraviolet light [101]. These precautions ensure the gases generated in the oils are only due to aging and sparking.

3.3.3.1.2. Measurement of Dissolved Gases and Description of Gas Diagnosis Methods

Gases are generated due to multiple reasons. Decomposition of MO from 150 to 500°C produces mostly low molecular weight gases (H_2, CH_4, C_2H_4, C_2H_6). Whereas, C_2H_2 and high molecular weight gases are formed in addition to H_2 at high temperatures. Hotspots are indicated by the presence of significant amounts of methane and ethane. CO and CO_2 are

TH-3272_186151014

evolved on the decomposition of paper insulation. It is interesting to note that electric stress results in ten times lower gassing, whereas thermal stress results in three times higher gassing in EOs compared to MO [101, 115].

Thermal decomposition of kraft paper and pressboard in MO leads to the formation of CO, CO_2, and water vapor even at normal operating conditions. The increase in CO magnitude indicates degradation in cellulosic insulation. The CO_2/CO ratio is normally more than seven for normal operating conditions in MO. Overheating of cellulose impregnated with EOs also generates CO and CO_2. The CO_2/CO ratio is almost the same for MO and EOs. However, the thermal decomposition of EOs also results in CO production, which significantly exceeds CO production from solid insulation. Therefore, the CO_2/CO ratio at high temperatures does not provide quality information on cellulose degradation in EOs. The aging temperature in this work is 115°C implying that the CO generation (if any) is only due to the cellulose degradation in aged oil samples.

ASTM D3612 (headspace method) is defined to be used for the oils having a viscosity of 20 cSt or less at 40°C which means it cannot be applied for the EOs. However, IEEE C57.155 endorses the use of this technique for EOs. Nonetheless, there is no other reliable technique to measure DGs in EOs and BOs. Therefore, DGs in all the oil samples are measured in accordance with ASTM D3612 (headspace method) using a gas chromatograph procured from Agilent Technologies immediately after sparking in the same laboratory avoiding the need to transport and exposure to light. Each sample is tested three times for repeatability.

Various methods are available to analyze the measured DG content in oil. DR, RR, IGR, and Duval triangle methods are proposed by experts based on vast knowledge and experience unlike from intense scientific models ultimately resulting in different diagnosis by each method for the same sample [115]. Mineral and non-mineral oils show different gas levels for the same fault [117]. Some gas ratios such as $R_1 = C_2H_4/C_2H_6$, $R_2 = C_2H_2/C_2H_4$, $R_3 = CH_4/H_2$, $R_4 = C_2H_2/CH_4$, and $R_5 = C_2H_6/C_2H_2$ are majorly used by the ratio methods to interpret the faults.

The IGR method is based on IEC 60599 and uses ratios R_1, R_2, and R_3 to interpret the faults. This method is applicable to all types of equipment but is not very accurate in predicting faults due to the overlapping of ratio ranges. In the DR method, one of the gases (H_2, CH_4, C_2H_4, and C_2H_2) must exceed twice the minimum concentration limit ($L1$) mentioned in Table 4 of C57.104. In addition, at least one of the other two gases in any of the R_2, R_3, R_4, and R_5 ratios should exceed $L1$. Further, each ratio is compared in the order of R_3, R_2, R_4, and R_5 with Table 5 of [100] to interpret the faults. The RR method is similar to the IGR method and uses R_1, R_2, and R_3 ratios. Eventually, the ratios are compared with values in Table 6 of [100] to

TH-3272_186151014

identify the fault. Since this method is independent of the absolute content of each dissolved gas, it could lead to improper diagnosis as it happens with the DR method [100]. The ratios in IGR, DR, and RR methods are compared with the stipulated values in Table 3.5 for the fault identification.

$$\%p_i = \frac{p_i}{\sum_{j=1}^{3} p_j} \tag{3.3}$$

where p_1 = CH_4, p_2 = C_2H_4, and p_3 = C_2H_2.

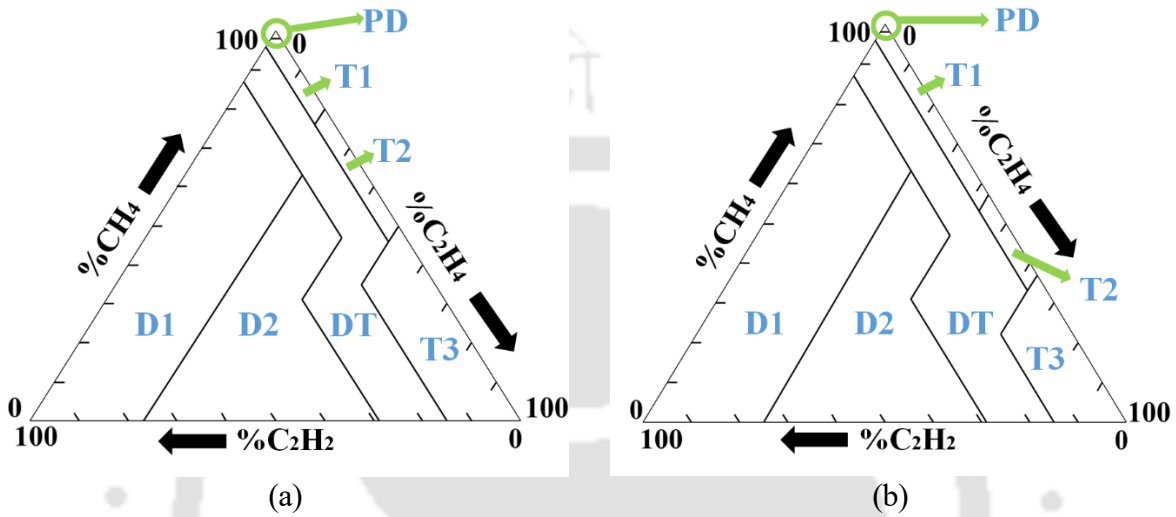

Figure 3.8: (a) Duval triangle 1 for MO and (b) Duval triangle 3 for FR3 [109, 118].

However, the ratio methods fail to diagnose multiple simultaneous faults in addition to their inapplicability to non-mineral oils. The above drawbacks can be overcome by using a graphical representation based Duval triangle method [115]. It uses absolute gas concentrations rather than ratios. The Duval triangle 1 and triangle 3 for MO and EO respectively are proposed based on the gas generation quantities in MO and non-MOs and are shown in Figure 3.8 [117]. Triangle 1 and 3 uses three gases (CH_4, C_2H_4, and C_2H_2) to detect the type of fault [101, 117]. The three gases form the three axes of the triangle with seven fault zones (PD, D1, D2, mixture of electrical and thermal faults (DT), T1, T2, and T3). The fault coordinates are found using the percentage concentration of the three gases obtained from (3.3) [116].

3.3.3.2. Fault prediction from dissolved gases in BOs

Certain gases (CH_4, C_2H_6, C_2H_4, C_2H_2, H_2, CO, and CO_2) which are imperative in detecting degradation are only considered for the diagnosis. Despite the fact that the gases generated in EOs under fault conditions are the same as those generated in MO, the production rates, ratios, and solubility of the gases are different [101]. Table 3.6 presents the DGs in the oil samples prior to aging, after aging, prior to sparking, and after sparking. To avoid the loss of gases generated during sparking and to ensure their quantity and composition remain intact, DGs are measured

TH-3272_186151014

immediately after sparking in the same laboratory. The exposure of EOs to ultraviolet rays from sunlight causes stray gassing [101]. Hence, certain measures such as performing experiments immediately after sparking and undertaking all experimental processes in the same lab assisted in reducing the stray gassing.

Table 3.5: DG interpretation according to IGR, RR, and DR methods [101, 108].

Name of Analysis		Ratios				
		R_1	R_2	R_3	R_4	R_5
IGR	Partial discharge (PD)	<0.2	IN	<0.1	-	-
	Discharges of low energy (DLE)	>1	>1	0.1 to 0.5	-	-
	Discharges of high energy (DHE)	>2	0.5-2.5	0.1 to 1	-	-
	TF of low temperature (T1)	<1	IN	>1	-	-
	TF of medium temperature (T2)	1-4	<0.1	>1	-	-
	TF of high temperature (T3)	>4	0.2	>1	-	-
RR	Normal operation	<0.1	>0.1 to <1.0	<1.0	-	-
	Low energy discharge (PD)	<0.1	<0.1	<1.0	-	-
	High energy discharge	0.1 to 3.0	0.1 to 1.0	>3.0	-	-
	Low temperature TF	<0.1	>0.1 to <1.0	1.0 to 3.0	-	-
	TF below 700°C	<0.1	>1.0	1.0 to 3.0	-	-
	TF above 700°C	<0.1	>1.0	>3.0	-	-
DR	Thermal decomposition*	-	<0.75	>1.0	<0.3	>0.4
	Low intensity PD*	-	IN	<0.1	<0.3	>0.4
	High intensity PD*	-	>0.75	>0.1 to <1.0	>0.3	<0.4

*ratios valid for oil; IN=insignificant; TF = Thermal fault;

TH-3272_186151014

Table 3.6: Dissolved gases in oils before and after sparking.

Sample	Sparking status	Dissolved gases (ppm)						
		H_2	CH_4	C_2H_6	C_2H_4	C_2H_2	CO	CO_2
A1	Before	<1	<1	<1	<1	<1	12	110
	After	156	6.6	2	11	180	12.2	120
B1	Before	<1	<1	<1	<1	<1	12	116
	After	122	6	1.5	16	158	15.4	124
C1	Before	5	<1	<1	<1	<1	15	140
	After	136.6	4	<1	13	64	28	167
D1	Before	<1	<1	<1	<1	<1	18	153
	After	125.1	2	<1	7	25	31.6	182
E1	Before	5	<1	<1	<1	<1	20	192
	After	119.4	1.5	<1	6	20	34	205
A2	Before	4.2	4	2	1	<1	23	112
	After	179	18	3	80	200	29	121
B2	Before	7.4	5	2	1.2	<1	46	206
	After	135	16	3	103	285	57	218
C2	Before	33	6	2	3.2	<1	54.4	324
	After	151.6	12	2.5	66	165	84	354
D2	Before	38	7	2	3.9	<1	106	387
	After	146.5	8.2	2.5	60	115	137	389
E2	Before	55	8.8	2.2	4.3	<1	223	481
	After	168	9	2.3	40	69	237	514

TH-3272_186151014

The fresh oils have all the gases within the limit according to Table A.2 of IEC 60599 and Condition 1, Table 1 of [100]. In aged oils, CO and CO_2 are found in higher quantities, whereas all other gases are within limits. CH_4, C_2H_6, C_2H_4, C_2H_2, and CO are generally termed combustible gases (CG). Despite the thermal aging of the oils, the CG are also within the limit as the aging temperature is not high enough for their generation. The carbon oxides are observed in fresh samples even before sparking. They could have formed due to the stray gassing of oils that occurred during the drying process. The carbon oxides are higher in EOs compared to MO as the degradation of the former results in carbon oxide formation. The gassing of insulating oils is enhanced in the presence of copper conductors irrespective of their proportion [120]. H_2 is formed when oil is aged in the presence of copper [120]. The production of H_2 on sparking is relatively higher in EOs. Since the scope of this work is limited to the evaluation of gases due to electrical faults, stray gassing is not investigated further.

For fresh and aged oils, the production of H_2 on sparking is highest for MOs (A1 and A2) and decreases with the increase in ester content. The EOs (B1 and B2) produce the lowest H_2. The same trend is observed for the CGs, too. The CGs are found to increase in sparked oils with the highest increase for MOs (A1 and A2) and the lowest for EOs (B1 and B2).

The sparking decomposes the insulation locally leading to the disruption of oil molecular structure. Low energy faults such as PD result in the scissioning of weak bonds (C-H) and the formation of H_2 gas. High energy is required to scission the (C-C) bonds and form C_2H_2. The C_2H_2 is thus formed when arcing occurs where the conducting channel is at several thousands of degrees Celsius. The C_2H_2 may also form at low temperatures but in low quantities [108]. In case of overheating, acetylene will represent a small portion of total dissolved combustible gases (TDCG). Partial discharges lead to high levels of hydrogen in comparison to acetylene and other CGs. Whereas due to arcing in MO, hydrogen, and acetylene are generated in almost the same quantities [100]. However, Hydrogen has a low Ostwald solubility coefficient in oil compared to acetylene [100]. Therefore, even though both H_2 and C_2H_2 are generated in the same quantities in MO during arcing, the C_2H_2 is observed to be higher in the arced MO sample. This is because H_2 escapes owing to small disturbance to the oil which cannot be avoided. Despite the efforts to minimize the disturbance in oil from preparation to testing, there is a scope during the sampling of oil into the syringe resulting in hydrogen escaping. Therefore, the amount of hydrogen detected is slightly lower compared to the amount of acetylene for MO samples. This small variation can be neglected, and the analysis can be performed considering it to be an electric arc discharge. However, the CO and CO_2 gases are observed to increase in fresh BOs with the increase in ester content. With the knowledge of the reason for gas

TH-3272_186151014

generation and different types of gases generated, the type and intensity of fault are interpreted from fault gases of samples shown in Table 3.6 using various ratios and graphical methods. The IGR, DR, RR, and Duval triangle methods are explored in this work to evaluate the efficacy of these methods in predicting fault for BOs and to understand the discharge characteristics.

3.3.3.2.1. Fault Analysis using gas ratios methods (IEC, Dornenburg and Rogers)

The ratios R_1, R_2, R_3, R_4, and R_5 useful for IGR, DR, and RR methods are evaluated for all oils from the data available in Table 3.6 and are presented in Table 3.7. Despite the drawbacks of the Dornenburg and Rogers ratios methods, an effort has been made to interpret the electrical faults in BOs by using them along with the IGR method. The DGs in sparked oils from Table 3.6 show that all the samples meet $L1$ criteria and the DR method is applicable. The faults in the sparked oils are evaluated by comparing gas ratios in Table 3.7 with the stipulated values in Table 3.5 and the findings are tabulated in Table 3.8. For the ratios that do not correspond to any fault, Table 2 of [108] is used to predict the fault.

Table 3.7: Gas ratios of oil samples after sparking.

Sample	Ratios				
	R_1	R_2	R_3	R_4	R_5
A1	5.5	16.36	0.042	27.27	0.011
B1	10.67	9.88	0.049	26.33	0.001
C1	13	4.92	0.029	16	0.016
D1	7	3.57	0.016	12.5	0.04
E1	6	3.33	0.013	13.33	0.05
A2	26.67	2.5	0.101	11.11	0.015
B2	34.33	2.77	0.118	17.81	0.011
C2	26.4	2.5	0.079	13.75	0.015
D2	24	1.92	0.056	14.02	0.022
E2	17.39	1.73	0.054	7.67	0.033

The visual inspection of the DG data in Table 3.6 suggests the occurrence of electric discharge in the oils [100, 101, 108]. The IGR method ratifies the formation of electric discharges in all oil samples. However, a clear distinction between high and low energy

TH-3272_186151014

discharge could not be achieved for most of the samples. It could clearly identify the discharge intensity only for two samples (A2 and B2). The RR method could not identify the fault in any of the BOs. The DR method also could not detect the fault in most of the BO samples, but it was able to predict for samples A2 and B2 indicating high intensity PD. The results show that only the IGR method could identify faults in all the samples among the ratio methods. The disproportionate rate of H_2 generation is responsible for the mismatch of results for gas ratio methods. It is noteworthy to bear in mind that the predicted faults by the ratio methods are accurate if and only if a prediction is achievable.

Table 3.8: Fault indications using IGR, DR, and RR analysis.

Sample	Fault Indication		
	IGR	RR	DR
A1	Discharges	NoP	NoP
B1	Discharges	NoP	NoP
C1	Discharges	NoP	NoP
D1	Discharges	NoP	NoP
E1	Discharges	NoP	NoP
A2	DHE	NoP	High intensity PD
B2	DLE	NoP	High intensity PD
C2	Discharges	NoP	NoP
D2	Discharges	NoP	NoP
E2	Discharges	NoP	NoP

NoP = No prediction;

3.3.3.2.2. Fault Analysis using Duval Triangles and Pentagons

Duval triangles 1 and 3 are used to characterize faults and their intensity for MO and non-MOs respectively. The triangles 4-7 and pentagons 1-3 can be used for extracting additional information such as the occurrence of single or multiple faults and to classify the thermal faults with more accuracy [121]. Therefore, triangles (1 and 3) and pentagons (1 and 3) are used in this subsection to study their effectiveness in predicting electrical faults for BOs.

TH-3272_186151014

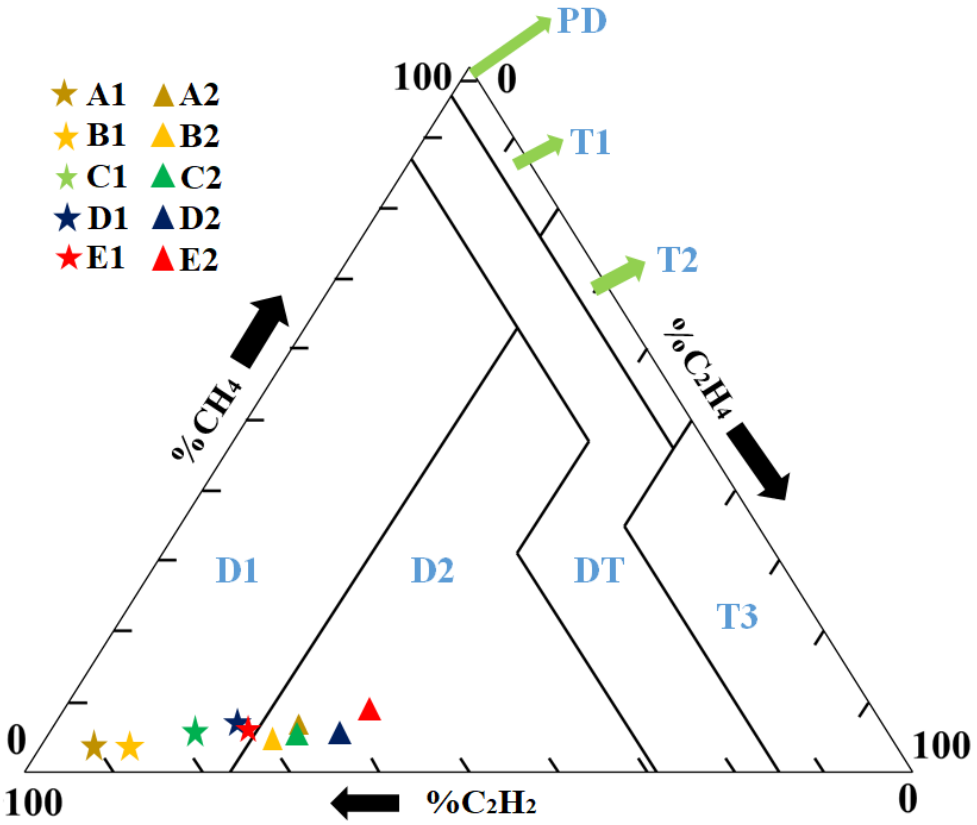

Figure 3.9: Duval triangle 1 for fault prediction in BOs.

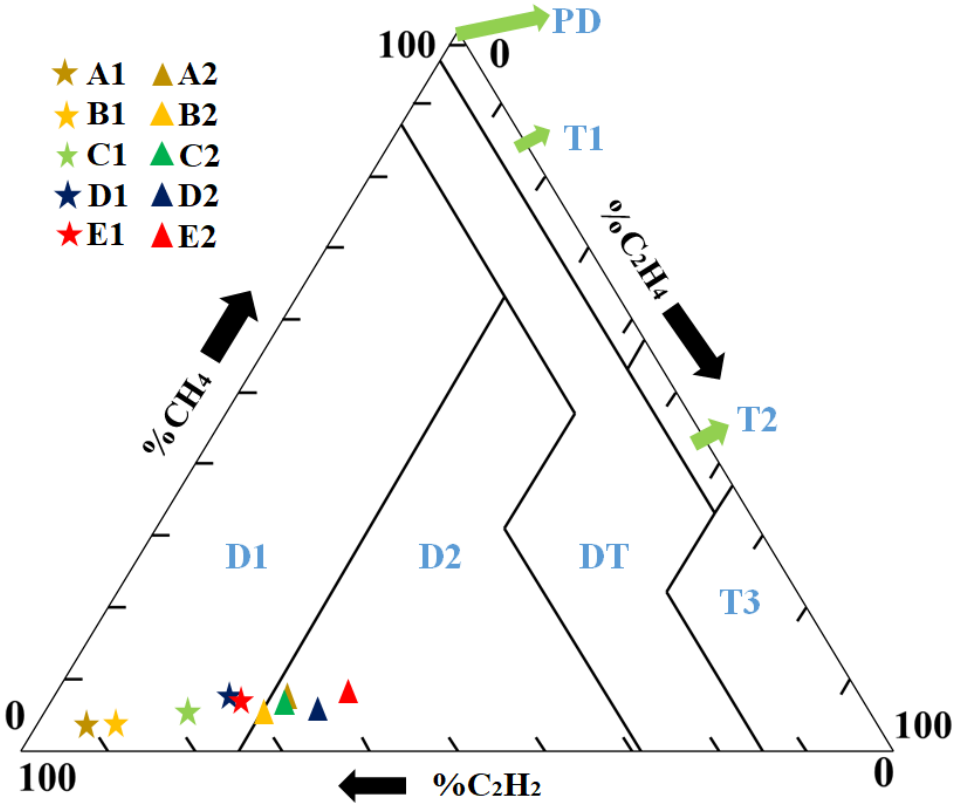

Figure 3.10: Duval triangle 3 for fault prediction in BOs.

TH-3272_186151014

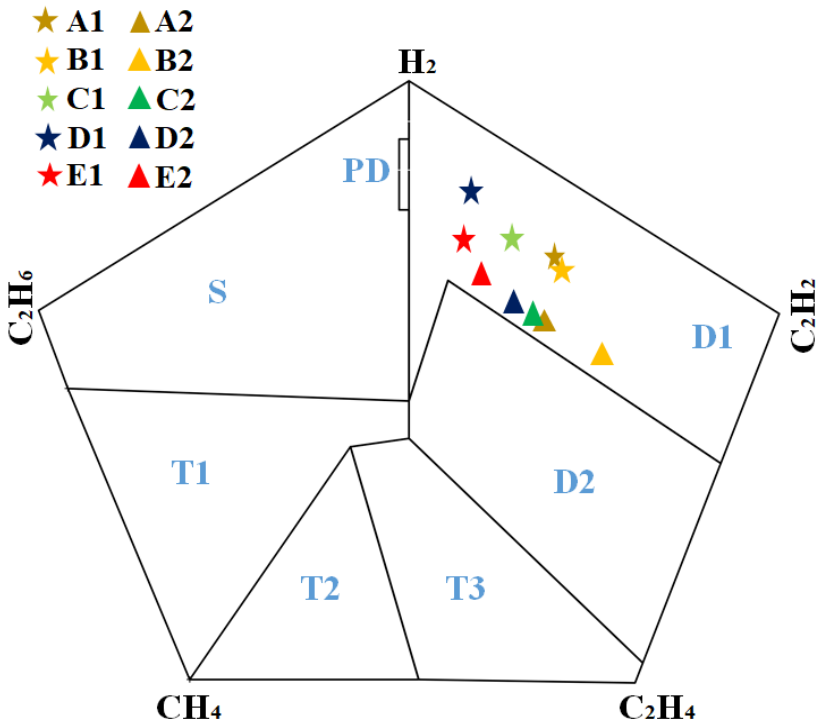

Figure 3.11: Duval pentagon 1 for fault confirmation in BOs.

The DG data pertaining to all the fresh and aged BOs are positioned on Duval triangles 1 and 3 using algorithms procured from Dr. Duval on request and are presented in Figures 3.9 and 3.10. These figures manifest the electric discharges as low intensity discharges i.e., D1 for fresh oils, and high intensity discharges i.e., D2 for aged oils. The shift in locus corresponding to samples A1 to E1 towards the D1-D2 boundary indicates the increase in the intensity of discharge in the oil with the increase in ester percentage. The aged samples are located in the D2 region of Duval triangles 1 and 3 indicating a substantial increase in the electric discharge magnitude. The increase in discharge is due to polar contaminants formed from aging. The polar contaminants are responsible for the decrease in specific resistance of the aged BOs as shown in Table 3.2. Since the increase in three key gases (CH_4, C_2H_4, and C_2H_2) is proportional, the intensity and type of discharges predicted by both Duval triangles 1 and 3 are the same. Therefore, the reliable prediction of electric faults in BOs is achievable by Duval triangles 1 and 3.

The pentagons are generally used in conjunction with triangles for drawing out complementary information. The pentagons 1 and 3 for MO and FR3 respectively are used in addition to triangles 1 and 3 to confirm the occurrence of fault, specifically the electric discharge in this case as shown in Figures 3.11 and 3.12. The five gases form the five vertices of the pentagon with seven fault zones (PD, D1, D2, stray gassing at temperatures below 200°C (S), T1, T2, and T3). Both Duval pentagons 1 and 3 confirm the occurrence of electric

TH-3272_186151014

discharges in all the fresh as well as aged BOs but of low intensity. All the locus points are in the D1 region of both pentagons, with those corresponding to aged BOs shifting towards the D1-D2 boundary compared to fresh oil samples. This potentially indicates an increase in discharge magnitude for aged oils.

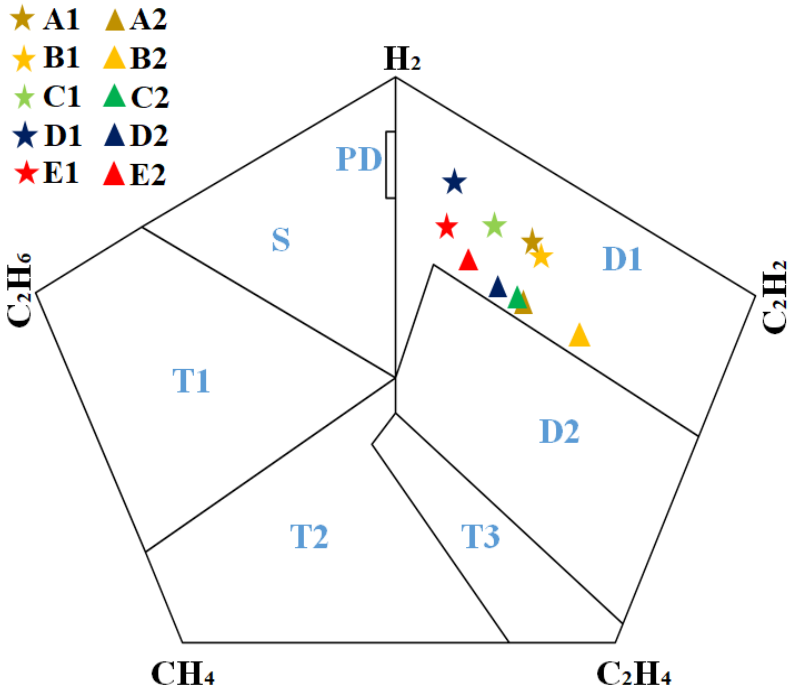

Figure 3.12: Duval pentagon 3 (FR3) for fault confirmation in BOs.

3.3.3.2.3. Comparison of TDCG in BOs

The variation in the total amount of gas generated with aging and the change in ester percentage can be analyzed from the TDCG comparison. The TDCG of all the BOs after sparking is calculated from Table 3.6 and presented in Figure 3.13. The TDCG in fresh oils on sparking follows a decreasing trend from A1 to E1. This is in agreement with the results obtained by other researchers [101, 115]. The TDCG in aged oils is approximately 1.5 times for MO and 3 times for EO compared to their respective fresh oils. The TDCG of aged oils is a combination of gases generated due to aging as well as sparking. However, the TDCG of aged BO samples does not establish any pattern.

As a large number of field observations are not available to clearly define the gassing behavior of retrofilled and BO based transformers, this study is of much importance in effectively evaluating their gassing performance and monitoring such transformers. In addition, this study presents data to develop a new DG interpretation method for BOs. It also helps in defining set values for gas relays and alarms for transformers filled with BOs. The MO in the BOs can be easily extracted by lowering the temperatures and freezing EOs. Therefore, the

TH-3272_186151014

BOs may not pose any threat to the environment if carefully disposed of. This work is beneficial for utilities and manufacturers in determining the insulating oil with optimized cost and performance. This study endorses the development and usage of BOs in power apparatus.

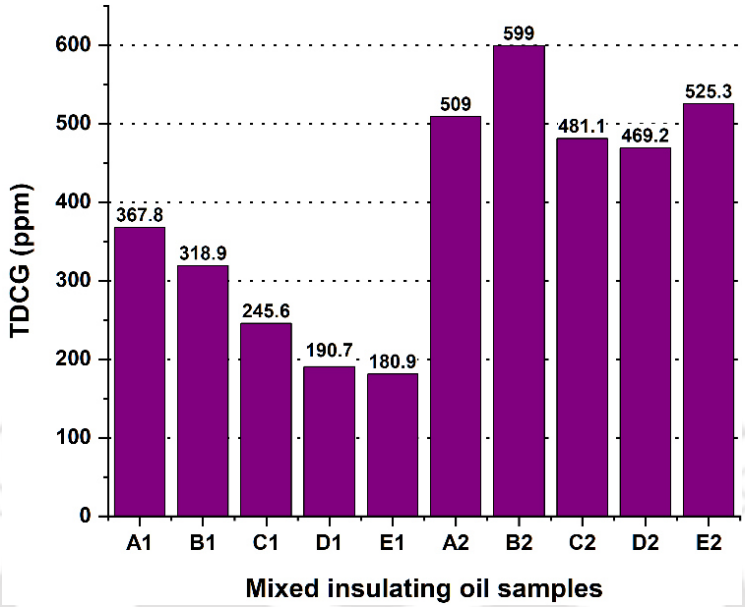

Figure 3.13: TDCG in sparked BOs.

3.4. Surface study of solid insulation aged in natural ester

The solid and liquid insulation together comprise the insulation coordination of the transformer. The use of VO in the transformer slows the degradation of the solid insulation in comparison to MO. There are two major hypotheses that support the slower degradation. One of them suggests the higher moisture saturation capability of the VO is responsible for avoiding the degradation of cellulose [11]. However, higher temperatures could still result in the breakage of the cellulose. The second hypothesis suggests the formation of a gel on the solid insulation surface protecting it from moisture and temperature [122]. An attempt has been made to study the gel formed on the kraft paper from thermal aging FR3.

Figure 3.14: Gel balls formed on the surface of the pressboard.

TH-3272_186151014

The VO, kraft paper, and copper conductors are added in 20:1:1 proportion and are subjected to thermal stress at 180°C for 500 hours. This aging resulted in the formation of multiple spherical gel balls on the walls of the aging cell and pressboard. Figure 3.14 presents the gel balls formed on the pressboard surface. The gel balls are separated from the pressboard and are studied for their crystalline composition using a single crystal X-ray diffractometer (Make: Agilent; Model: Single source supernova E) available at the Central Instrument Facility (CIF), IIT Guwahati which is capable of providing information on the unit cell dimensions, bond-lengths, bond-angles and site-ordering details of single crystal unit that form the internal lattice of the substances. The result obtained is presented in Figure 3.15.

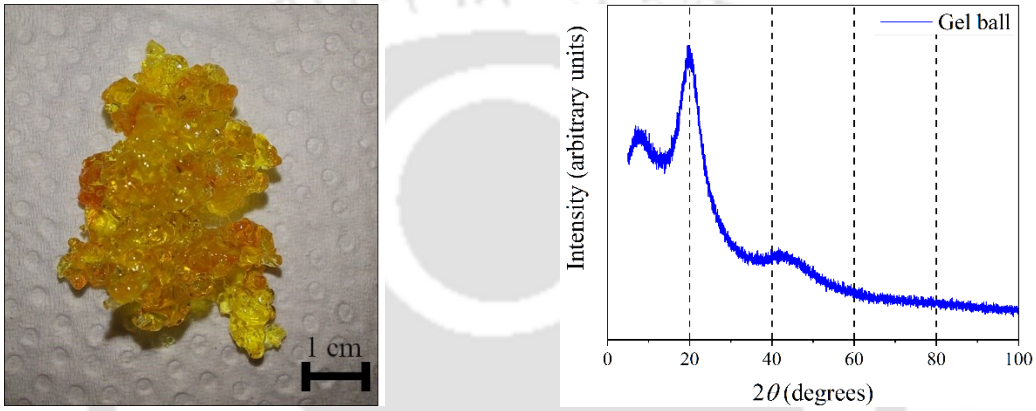

(a) (b)

Figure 3.15: (a) Gel balls (b) Single crystal X-ray diffraction of gel balls.

The results show that the gel balls are amorphous in nature indicating they are a byproduct of oil and/or paper reaction as there is no trace of any metal. It is interesting to note that these gel balls remain intact even after three years of being subjected to storage in a dehumidified room.

(a) (b) (c)

Figure 3.16: (a) Fresh and dry solid insulation (b) fresh solid insulation subjected to moisture equilibrium with VO for 96 hours and (c) solid insulation aged for 500 hours at 180 °C in VO.

TH-3272_186151014

Further, the surface of kraft paper is studied for surface smoothness on thermal aging in VO. The surface smoothness of the kraft paper aged in VO is studied using the atomic force microscope (AFM) of Oxford make and Cypher model available at the CIF, IIT Guwahati. AFMs are very high-resolution scanning probe microscopes with three-dimensional accuracy up to 0.1nm. AFMs generally measure the lateral and vertical deflection of the cantilever using an optical lever operated by reflecting a laser beam that strikes the position-sensitive photo-detector. The surface study is performed on fresh and dry solid insulation with 100% of life remaining, the fresh solid insulation subjected to moisture equilibrium with VO for 96 hours, and solid insulation aged for 500 hours at 180 °C, and the samples are presented in Figure 3.16.

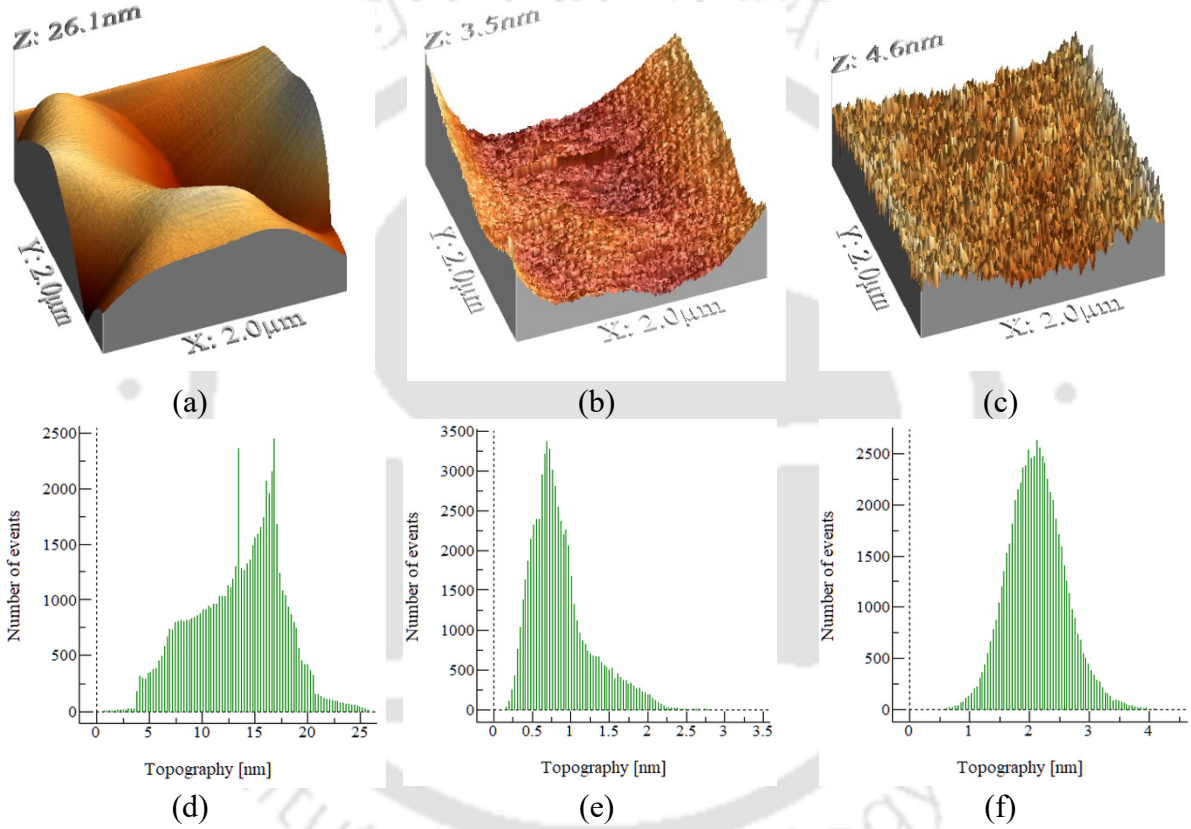

Figure 3.17: (a) 3D image of fresh dry solid insulation (b) 3D image of fresh solid insulation immersed in VO (c) 3D image of solid insulation after thermal aging for 500 hours (d) Topography of fresh dry solid insulation (e) Topography of fresh solid insulation immersed in VO (f) Topography of solid insulation after thermal aging for 500 hours.

The surface profile of the samples is studied using AFM and the results are presented in Figure 3.17. The AFM imaging of the sample is done on a dimension of 2 µm × 2 µm. Further, the number of events versus topography is plotted for each sample and shown in Figure 3.17. The surface roughness of sample (a) shown in Figure 3.16 has an RMS of 4.2516 nm and a maximum of 26.0645 nm. The surface roughness of sample (b) shown in Figure 3.16 has an RMS of 0.4185 nm and a maximum of 3.5216 nm. The surface roughness of sample (c) shown

TH-3272_186151014

in Figure 3.16 has an RMS of 0.4937 nm and a maximum of 4.5533 nm. The topography results show that the surface smoothening occurs on immersion of solid insulation sample in the VO and remains smooth even after a long duration of thermal aging.

Considering the XRD and AFM, it can be concluded that the thermal aging of VO at higher temperatures leads to the formation of gel balls as well as gel deposition on the kraft paper. The formed gel might obstruct the moisture from entering the solid insulation thereby slowing its degradation. Slower degradation indicates a longer transformer life. This study opens a new area to be explored by varying many parameters such as aging temperature, presence of oxygen, aging duration, and the type of VO. Further analysis into this area is not delved as it does not fall under the scope of this thesis.

3.5. Summary of the chapter

The physiochemical properties of MO, FR3, and their mixtures in different ratios are studied. Further, the PD and DGs in BOs are extensively studied subjecting them to electric stress. The outcomes of this work are as follows:

- The retrofilling of MO based transformer with FR3 or blended oil does not pose any danger to its operation. In addition, it provides better electrical and physiochemical characteristics.
- The FR3 is found to have higher PDIV compared to MO and their blends among the fresh oils. On the other hand, an equal amount of MO-FR3 blend has higher PDIV among aged oils.
- The PD pulses are irregular for all the insulating oils. However, low pulse count and discharge magnitude are characteristics of MO and large pulse count and discharge magnitude are characteristics of VO. BOs provide a middle ground.
- MO is sensitive to aging and hence PDIV variation is very high for fresh and aged MO samples.
- The PD is predominantly found to occur during the negative half cycle and the number of pulses increases with the voltage.
- PDIV and PDEV are reproducible subject to the same method of preparation of samples and testing.
- The amount of gases generated in BOs is different for each individual combination of MO and EO.
- The findings confirm that the application of gas ratio methods existing for MO cannot be directly used for BOs and requires modifications.

TH-3272_186151014

- Rogers ratios method fails to interpret the electric faults in BOs.
- Sparking in fresh BOs leads to low energy discharges, whereas sparking in aged BOs results in high energy discharges as interpreted by IEC ratios and Duval triangle methods.
- The thermal aging of kraft paper in vegetable oil leads to the gelling of oil on the surface of the solid insulation at high temperatures. It also leads to the formation of gel balls.

This study provides critical information on the short and long term behaviour of various BOs. Various studies performed on the chosen mixtures establish their performance as a suitable alternate transformer insulation. These studies support the fact that the proposed technique is being used on validated insulation rather than arbitrarily selected samples. This study also helps transmission system operators and transformer manufacturers choose the appropriate insulation in terms of technical and financial feasibility. The EOs and BOs provide an improved electric breakdown characteristic compared to mineral oil. However, the ACBDV can be further improved by the addition of nanoparticles to these oils. The following chapter deals with nanofluids as an alternative transformer insulation.

Note 1: A part of this work, "Study of Partial Discharges in Fresh and Oxidative Aged Mineral-Natural Ester Blended Oils," has been published in IEEE Transactions on Dielectric and Electrical Insulation, 2023, vol. 30, no. 5, pp. 2325-2333.

Note 2: A part of this work, "Gassing Tendency of Fresh and Oxidative Aged Mixed Insulating Oils on Electric Sparking," has been accepted for publication in IEEE Transactions on Dielectric and Electrical Insulation.

TH-3272_186151014

4

Nanofluids as alternate transformer insulation

Contents

4.1	Introduction	70
4.2	Preparation of nanofluids	71
4.3	Thermal conductivity studies of the nanofluids	72
4.4	Simulation of electric field around NPs dispersed in oil	74
4.5	Dielectric frequency response of nanofluids	78
4.6	Magnetic profiling of NPs and NFs possessing potential transformer application	81
4.7	Conjecture on benefits of using VO and NFs over MO	98
4.8	Summary of the chapter	99

TH-3272_186151014

4.1. Introduction

Transformers are important devices in the electrical power system network as they allow the efficient stepping up/down of voltage levels. The operating voltage levels and the power demand are increasing at a larger rate day by day, increasing the requirements for performance and reliability. Particularly, the integrity and reliability of the insulation of HV equipment play a key role in reaching those rising demands. MO is generally used as a coolant and insulation in transformers. Researchers have proposed using VO as it possesses better electrical properties compared to the MO [70, 123]. VOs also have the additional advantage of better biodegradability than MOs. Furthermore, studies have proved that NFs prepared by sonicating NPs in the base oils (MO, VO) have superior electrical and thermal characteristics [52, 124, 125]. The NPs are electrically classified as conducting (e.g. Fe_3O_4, Fe_2O_3), semiconducting (e.g. ZnO, TiO_2, CuO), and insulating (e.g. Al_2O_3, SiO_2, Eh-BN) [124]. Despite the nature of each particle, the nanofluid as a whole is electrically insulating in nature [124, 125]. Although some NFs have better electrical breakdown characteristics than the base liquid, the physical mechanisms involved are not yet well understood [126].

The NPs are generally prepared by two methods namely top down and bottom up methods. They are prepared by abrasion, crushing, sol gel technique, gas phase condensation, and liquid solid state reaction methods in the industry [127]. On dispersing the NPs into base oils, electrical breakdown strength and thermal conductivity increase resulting in a wide range of applications such as an insulant in high voltage apparatus, coolant for industrial, nuclear as well as for vehicular modules, geothermal energy, and microscale fluidic applications [128].

The NF preparation can be classified into single and two step methods. In the former method, the NFs are produced in a single step in which NPs are developed within the base oil by methods such as vacuum evaporation onto a running oil stream, physical vapor deposition, and submerged arc nanoparticle synthesis system [129]. Due to the high costs involved and the practical limitations in large scale production, the two step method is preferred. NPs are procured and added to base oil by ultra-sonication in two separate steps in the two step method. Due to the ease of preparation and the costs involved, the two step method is the choice of NF preparation method for many researchers [129]. Extensive research has been performed on the electrical breakdown and partial discharges of NFs by researchers across the globe [129]. Therefore, in this work, a few NPs are selected and their NFs are studied for thermal, magnetic, and dielectric frequency response behavior. In order to reduce the complexity in the

TH-3272_186151014

preparation, testing, and analysis of the samples, NFs are limited to MO and VO as base oils. The blends of base oils are not considered.

4.2. Preparation of nanofluids

The NF preparation process is shown in Figure 4.1. The nanoparticles used in this study are procured from Sigma-Aldrich and are added to the base oil in a predetermined quantity. The ultra-sonication is performed on this mixture using a 1500-Watt digital sonicator with a 3/4-inch diameter solid tip. It has provision for full amplitude and temperature control along with pulse sequencing. A continuous pulse train (ON and OFF times of 10 and 5 seconds, respectively) is used to thump the oil at 50% of the rated power and temperature of 25°C for 45 minutes to prepare uniformly dispersed nanofluids. Sonication is performed in a room with 40% RH to reduce moisture ingress into the oil. The sonicated fluid is subjected to shaking and vacuum drying as a conditioning process.

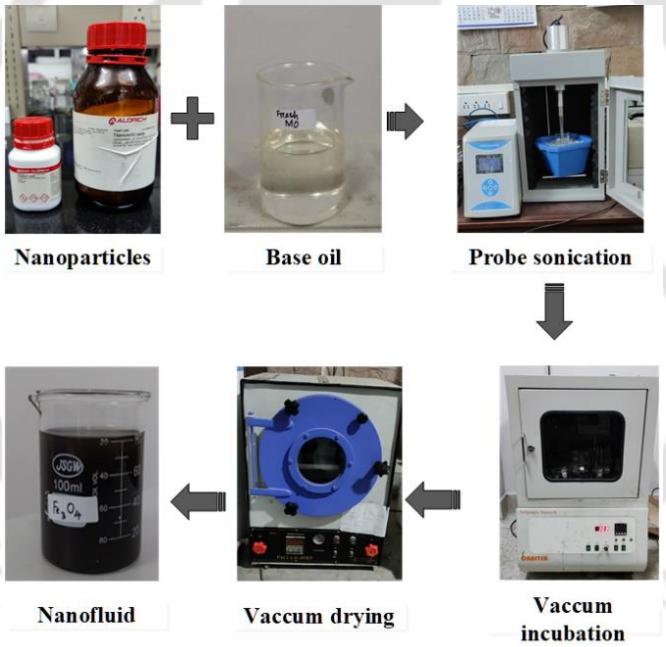

Figure 4.1: Preparation of nanofluids.

The nanofluids were hermetically sealed immediately after preparation to avoid any contact with atmospheric air. The moisture content of nanofluids is measured just after preparation, and it is the same as that of their respective base oil. Since the weighing of nanoparticles, mixing, magnetic stirring, and sonication in oil were done in a room with low RH, the nanofluids were not affected by the atmospheric moisture during their preparation. The NF samples were stable for at least 12 hours when kept idle. However, the nanofluids were tightly sealed and placed in a shaking incubator rotating at 140 RPM to avoid agglomeration until experimentation. UVS is performed to check the stability and uniformity of the NFs [130].

TH-3272_186151014

The UVS is performed on NFs immediately after preparation and after every 48 hours. The absorption spectrum was unchanged for six weeks, indicating the NFs were stable due to shaking in the incubator.

4.3. Thermal conductivity studies on the NFs

The electrical transformer efficiency and safety depend on the working temperature of the coolant, i.e., insulating oil. The increase in temperature causes the formation of hotspots which ultimately leads to the breakdown of oil. Adding NP to the oil shows a major trend in the enhancement of the heat transfer property. The TC of the NFs is investigated individually by varying concentration and temperature in this section. In this section, emphasis is placed on the TC regardless of the NP to ensure the usage of multiple NPs to demonstrate the behavior of NFs.

4.3.1. With variation in NP concentration

NFs are prepared by dispersing CuO NP in various concentrations (0, 0.01, 0.02, 0.05, and 0.1 %w/v) with MO and FR3 as base oils according to the procedure mentioned in Section 4.2 and are shown in Figure 4.2. The TC of the prepared samples is measured using KD-2 pro (single probe, make Decagon Inc.) at room temperature and is presented in Figure 4.3.

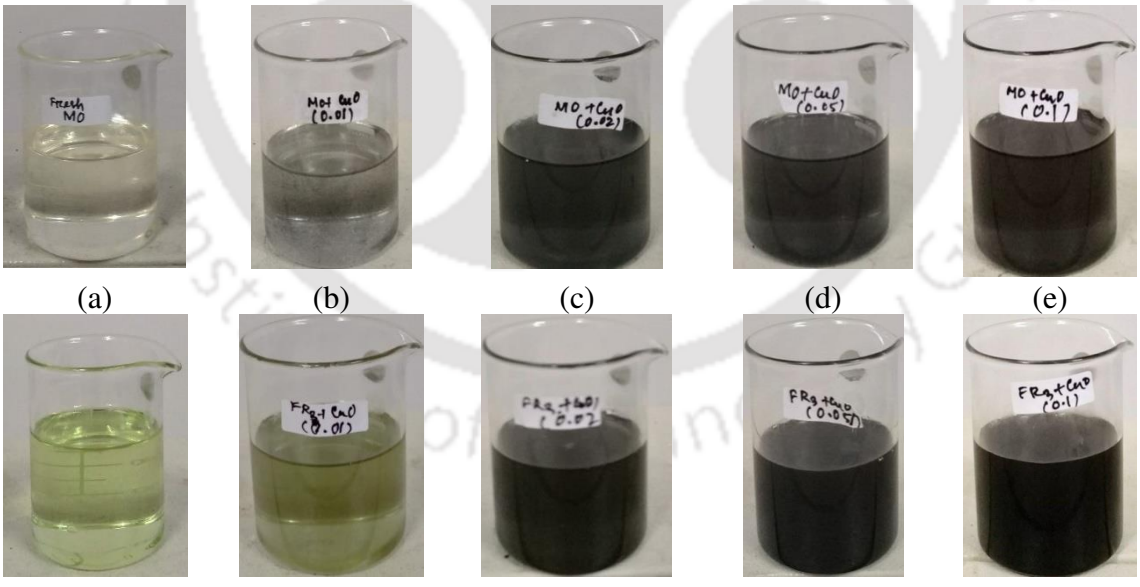

(a) (b) (c) (d) (e)

(f) (g) (h) (i) (j)

Figure 4.2: Samples of (a)fresh MO (b)MO+0.01wt.%NP (c)MO+0.02wt.%NP (d)MO+0.05wt.%NP (e)MO+0.1wt.%NP (f) fresh FR3 (g) FR3+0.01wt.%NP (h)FR3+0.02wt.%NP (i)FR3+0.05wt.%NP (j)FR3+0.1wt.%NP.

The TC tends to increase with the increase in particle concentration for both FR3 and MO. The TC is higher for FR3 in comparison to MO. Although the increase in TC is highest

TH-3272_186151014

for a concentration of 0.1 %w/v among the measured samples, this concentration is practically not feasible due to the quick agglomeration of the samples. The sample with 0.01 %w/v is optimal in terms of NF stability which is found using UVS.

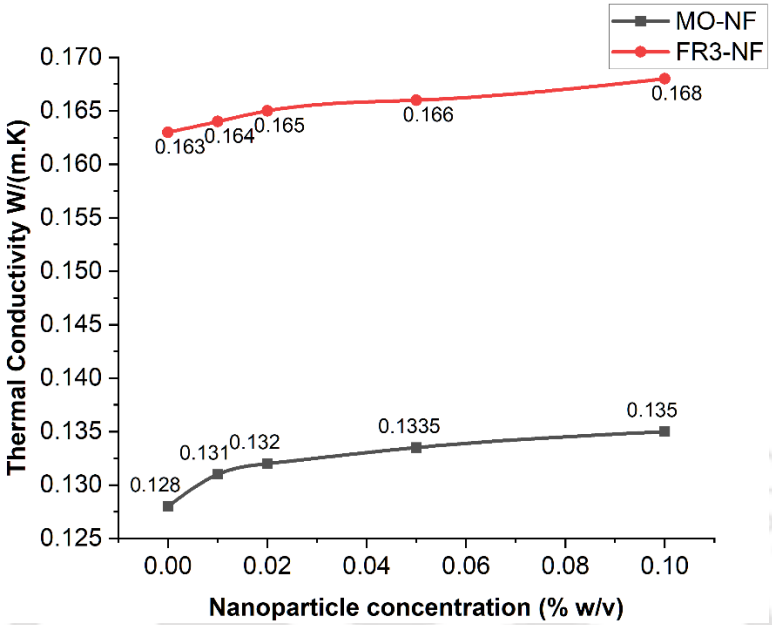

Figure 4.3: Thermal conductivity of base oils and nanofluids.

4.3.2. With variation in temperature

NF is prepared by dispersing a 0.01 %w/v ZnO NP according to the procedure mentioned in Section 4.2 to study the effect of temperature on the TC of NFs. This study is limited to one NP and base oil to demonstrate the efficacy of NF in heat transfer with variation in temperature. The temperature of the NF is varied from 25 to 75°C and the TC is measured at every 5°C interval and the results are presented in Figure 4.5. The TC increases with the increase in temperature for a fixed amount of NP concentration. The TC of NF is higher than that of its base oil at all tested temperatures. The higher TC indicates a quick dissipation of heat from the transformer enabling it to support high loads and long working life.

(a) (b)

Figure 4.4: Samples of (a) fresh MO (b) MO+0.01wt.%NP.

TH-3272_186151014

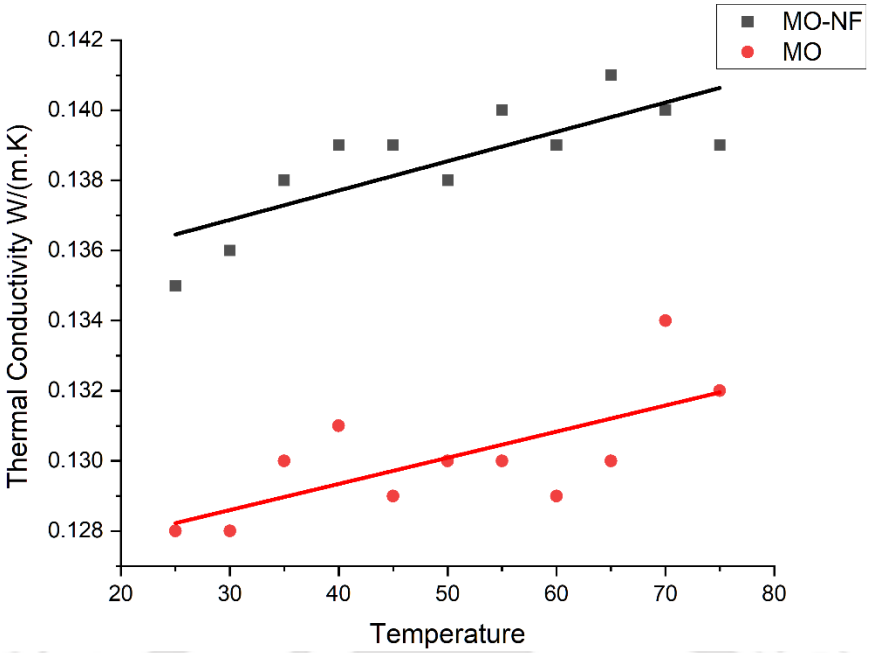

Figure 4.5: Thermal conductivity of MO and its nanofluid with increase in temperature.

Therefore, NFs prove to have better thermal properties with variation in concentration and with variation in temperature at a fixed concentration in comparison to the base oils. The following sections elucidate further effects of the addition of NPs to the base oil.

4.4. Simulation of electric field around nanoparticles dispersed in oil

Simulation work is carried out using the COMSOL Multiphysics tool to understand the distribution of the electric field around NP subjected to DC HV. COMSOL is a finite element analysis tool to find numerical solutions to partial differential equations with boundary values for complex geometries. The tool can solve problems by using multiple physics simultaneously and hence is very useful in analyzing the streamer initiation and growth in dielectric liquids. Finite element methods enable us to find an approximate solution to a complex boundary value problem by dividing the domain into many sub-domains called finite elements. There are a few stages in solving a model with COMSOL. Firstly, the space and dimensions of the model are designed, followed by choosing the necessary physics based on the scope of the study which is further followed by the selection of the study. The geometry of the model is now divided into finite elements by meshing and computed to simulate the defined conditions.

The electric field in the insulating medium of the HV equipment is of concern when a heterogeneous NP is added to the homogeneous liquid insulating medium. Due to the heterogeneity, NP distorts the surrounding local electric field which might lead to breakdown or PD. A simulation model is developed in COMSOL Multiphysics to understand the distribution of the electric field in the liquid dielectric filled with NPs. The model consists of

TH-3272_186151014

two parallel plate electrodes with a gap of 0.6 µm as shown in Figure 4.6. The gap between the electrodes is filled with the MO. The liquid dielectric used in modeling is assumed to be fresh and the electrical properties of MO are intact. The MO represented in modeling has a relative permittivity of 2.2 and conductivity of 1×10^{-12} S/m. The parallel plate electrodes are made of copper whose electrical conductivity is 5.998×10^{7} S/m and RP is 1. The nanoparticles chosen for the study are Fe_3O_4, TiO_2, and Eh-BN representing conductive, semi-conductive, and insulating nanoparticles. The insulating oil along with three different NPs is modeled individually and the electric field distribution is observed on excitation with DC voltage. The electric currents physics is applied for a stationary field study and the model is divided into 5720 elements for calculating the field. The model is optimized until the mesh independence is achieved. Certain assumptions such as all the NPs are spherical in shape with a radius of 50 nm, dispersed in MO, located midway between electrodes, and static spatially are made to simplify the model.

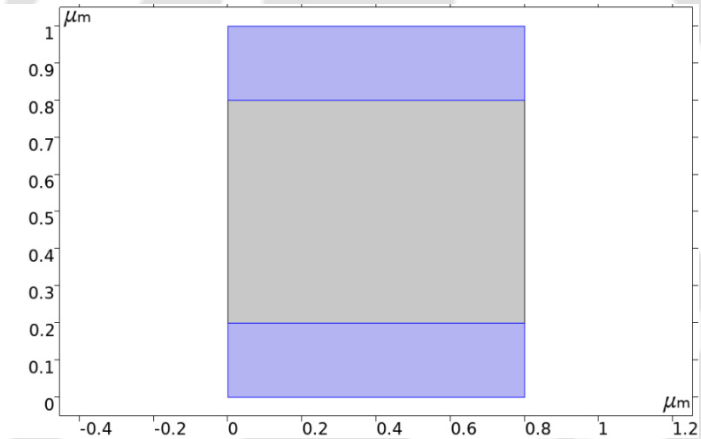

Figure 4.6: Parallel plate electrodes with MO in between.

A DC voltage of 1 kV is applied to the top electrode and the bottom electrode is connected to the ground terminal in this vertical configuration. The electric field in the absence of NP is found to be uniform with a magnitude of 1.67×10^{9} V/m all along the gap between the electrodes as shown in Figure 4.7 (a). In the presence of NP, the application of voltage results in polarization of the NP [131]. The polarization results in distortion of the electric field. The change in radial and tangential components affects the net electric field in its innate direction.

A conductive NP of RP 80 and electrical conductivity 1×10^{4} S/m introduced in between the electrodes is found to increase the electric field intensity to a maximum of 8.3367×10^{9} V/m along the direction of the field and above the NP. The NPs capture the free electrons due to polarization or ionization occurring from the applied electrical stress [132]. During the electron-capturing process, the stray electrons generated by the application of electrical stress

TH-3272_186151014

are deposited on the surface of the NPs. However, after a certain threshold of surface deposition, no more electrons are adsorbed by the surface [131-133]. When this threshold is reached, the NP is completely negatively charged and thus the field lines from the positive electrode are directed to the NP in all directions as shown in Figure 4.7(b). The field around the NP is observed to be impacted up to 350 nm from the surface of the NP. Since the concentration of electric field lines around the NP is different, it results in different space charge densities outside the NP which results in different positive and negative peak magnitudes of electric field for conductive NP. A semi-conductive NP of RP 31 and electrical conductivity 1×10^{-3} S/m introduced in between the electrodes is also found to increase the electric field with a maximum intensity of 3.4091×10^{9} V/m along the direction of the field. The field around the NP is observed to be impacted up to 50 nm from the surface of the NP as shown in Figure 4.7(c). Further, an insulating NP of RP 4 with an electrical conductivity of 1×10^{-13} S/m introduced in between the electrodes is also found to increase the electric field intensity to a maximum of 2.9785×10^{9} V/m perpendicular to the direction of the field. The field around the NP is observed to be impacted up to 50 nm from the surface of the NP.

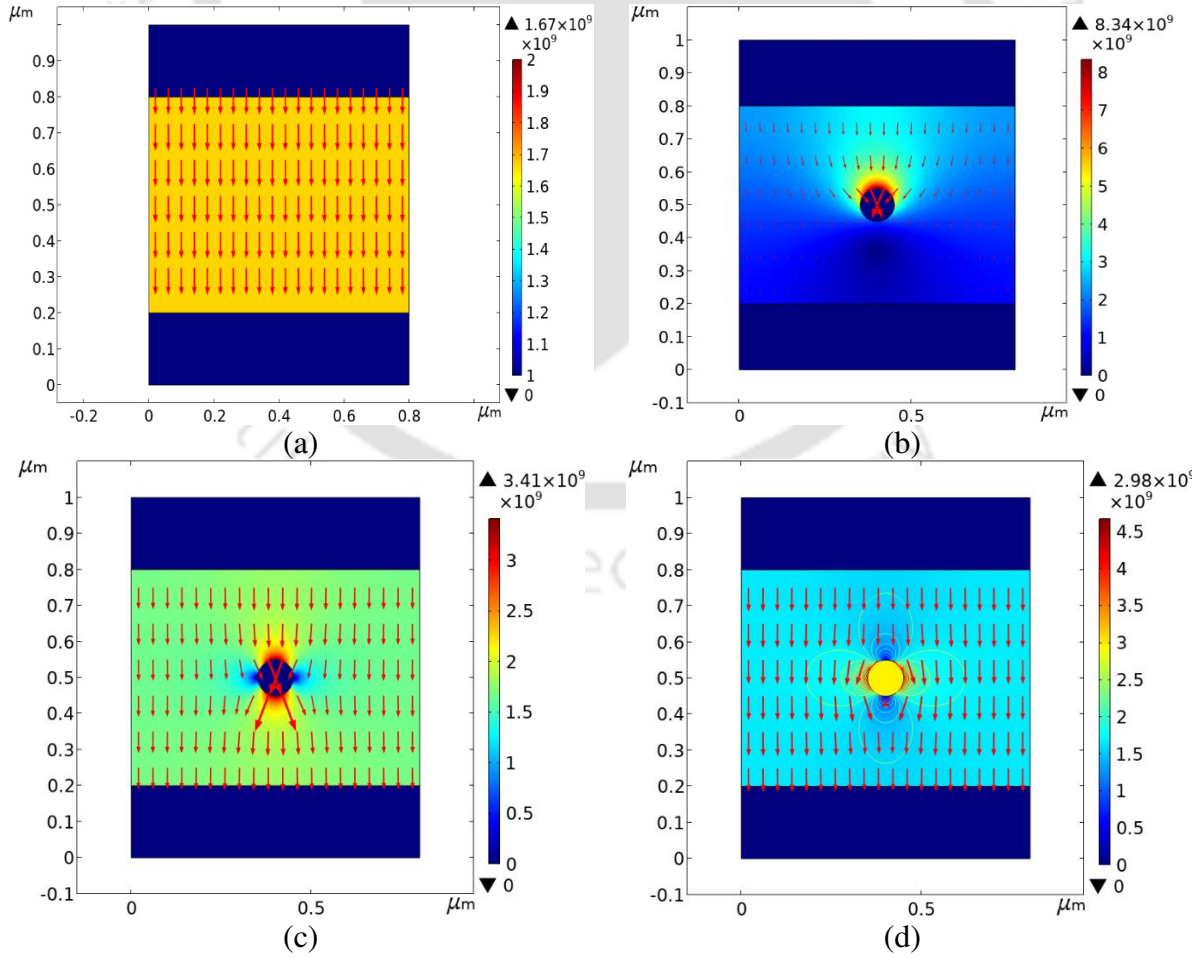

Figure 4.7: Electric field distribution in (a) MO (b) MO with conducting NP (c) MO with semi-conducting NP and (d) MO with insulating NP.

TH-3272_186151014

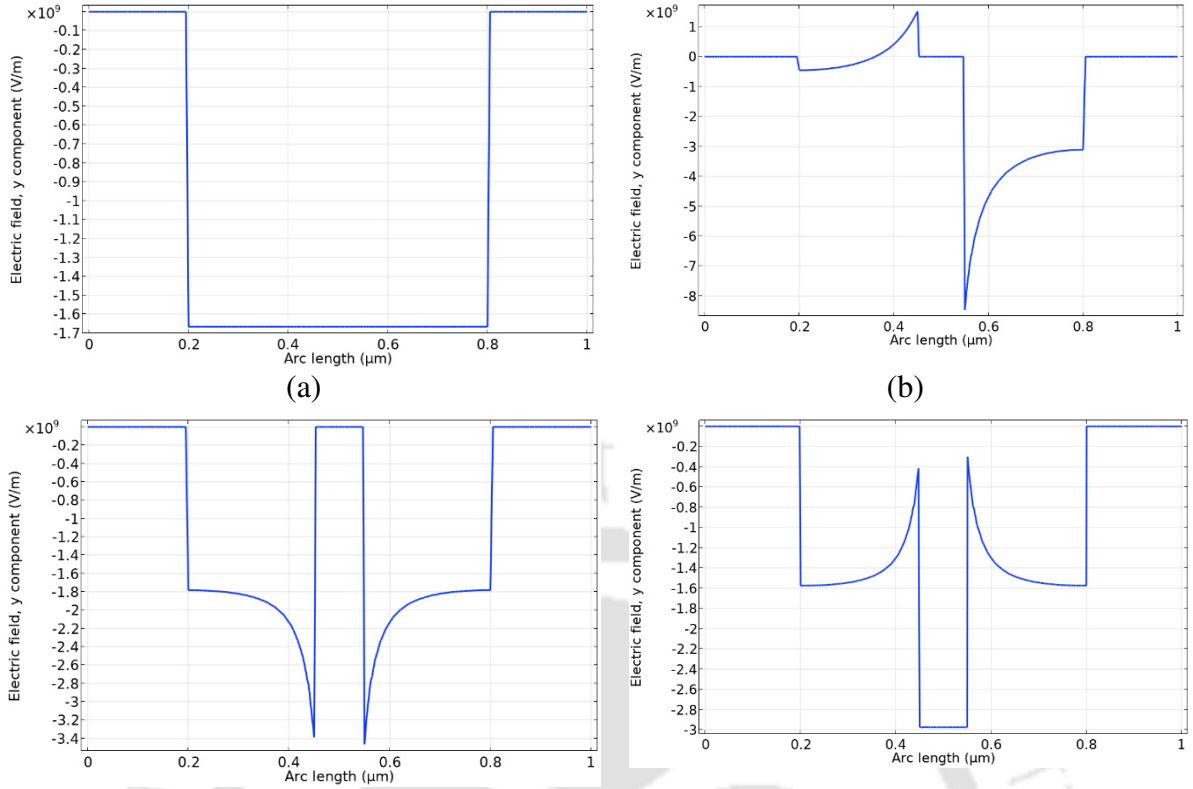

Figure 4.8: Electric field distribution along the electrodes in (a) MO (b) MO with conducting NP (c) MO with semi-conducting NP and (d) MO with insulating NP.

The electrical field magnitude along the dielectric from the top to the bottom electrode is plotted and presented in Figure 4.8. The conducting NP enhanced the electric field intensity around its surroundings by 5 times compared to that in the base oil, which could be a reason for faster charging of this NP as observed in [131]. The electric field around the conducting NP is determined by the space charge formed on its surface due to field ionization. The uneven space charge distribution around the NP as observed in Figure 4.7(b) is responsible for the difference in positive and negative peak magnitudes of the electric field. For the semi-conductive NP, the electric field intensity is enhanced by 2 times compared to that in base oil, which also could lead to charging of the NP but at a slower rate. However, insulating NP enhanced the electric field intensity around itself by 1.5 times compared to that in base oil. The field distortion in the case of insulating NP is the lowest among the NPs. The electric field lines are observed to divert from the insulating NP unlike for conducting and semi-conducting. The increase in electric field intensity due to conducting and semi-conducting NPs may result in local field enhancement followed by PD. Moreover, theories suggest the alignment of conducting NP with the electric field leading to breakdown channel formation. The results support the proposition that the addition of NPs to the base oil affects the electric field in the vicinity of the NP. It is established that using an insulating NP does not enhance the electric

TH-3272_186151014

field multifold, unlike other NPs. Therefore, the distortion in the electric field in the vicinity of the insulating NP is not enormous. Further, the conducting and semiconducting NPs tend to align with the electric field and might lead to a partial or complete breakdown of the insulation. Hence, the usage of insulating NP is endorsed. However, there is very little literature available on the DDF and RP of the insulating NP based NFs. The following section deals with the study of the dielectric frequency response of insulating NP based liquid insulation with the change in NP concentration.

4.5. Dielectric frequency response of nanofluids

The dielectric frequency response is an advanced non-destructive and offline technique to characterize the insulation. It is a representation of insulation response to the frequency variation. It gives information on moisture content in solid dielectric and liquid insulation conductivity. The frequency response of the liquid insulation (FRI) depends on the condition and type of oil, which in turn signifies the general status of the liquid insulation. It is preferably performed in the frequency range of 1 kHz to 1 mHz. For another one-tenth decrease in frequency towards the lower limit, the measurement time increases by 10 times for each data point. This large measurement time may introduce random errors, and repetition of this experiment for zero error is tedious. In this section, the FRI is performed in the frequency range of 10 kHz to 1 mHz. The measurement commences at 10 kHz, brought down to 1 mHz, and not vice versa to avoid the polarization memory in the insulating oils. The obtained response is unique to the condition of the liquid insulation. The effect of moisture and contaminants is dominant at lower frequencies. The oil conductivity is generally represented in the frequency range of 10 Hz to 0.01 Hz. The liquid losses are determined in this range of frequency [52, 134]. Interfacial polarization is responsible for the response at a low frequency range [46]. The FRI can also be used to detect carbon tracking, contamination, the presence of corrosive sulphur, and the effect of stray and creepage currents [61]. In this section, the effect of NP concentration on the FRI is studied by choosing three different concentrations, and their corresponding properties such as dissipation factor and RP are plotted.

(a) (b) (c) (d)

Figure 4.9: Samples of (a) MO (b) MO+0.01 %w/v Eh-BN (c) MO+0.05 %w/v Eh-BN and (d) MO+0. 1 %w/v Eh-BN.

TH-3272_186151014

NFs with 0.01, 0.05, and 0.1 %w/v of Eh-BN are prepared as mentioned in section 4.2 and are shown in Figure 4.9. The FRI is performed using a Solartron make SI 1260A impedance analyzer, in conjunction with the dielectric interface 1296A. For this equipment, the measurement is accurate in the range of 1 μHz to 10 MHz. The *tanδ* measurements are accurate down to 0.0001. The test setup is shown in Figure 4.10. The liquid insulation sample is filled in a test cell with a pair of parallel plate electrodes. The meticulous filling of NFs in the test cell ensures that there is no air bubble formation in the test cell. The RH is maintained at 50% during experimentation to avoid random errors in the measurements. The experiments are conducted in an EMI shielded room. The frequency domain spectroscopy measurements are highly sensitive to temperature variation. Therefore, the test cell is immersed in a temperature-controlled chamber during the experimentation as shown in Figure 4.10. All the measurements are noted at a room temperature of 23°C. The frequency response of each and every sample is tested three times and the average value is plotted in order to minimize the error. The MO exhibits linear ohmic response only at low voltage. In particular, the minimum frequency before altering the linearity of frequency response is proportional to the voltage stress. For a minimum frequency of 1 mHz, non-linearity in oil insulation is observed to be achieved for 3.9 V/mm AC stress at 23ºC [61]. Therefore, the voltage stress has to be below 3.9 V/mm which is the critical value for linearity. The complex permittivity (ϵ) of a sample can be calculated as shown in (4.1). Where ϵ' is the real part of complex permittivity that represents the charge storage in the insulation and ϵ'' represents the imaginary part of the complex permittivity that represents the losses in the dielectric. The imaginary part incorporates both the dielectric (polarization) and resistive (DC conduction) losses.

$$\epsilon(\omega) = \epsilon'(\omega) - j\epsilon''(\omega) \tag{4.1}$$

$$\epsilon''(\omega)\ \alpha\ \frac{\sigma}{\omega\epsilon} \tag{4.2}$$

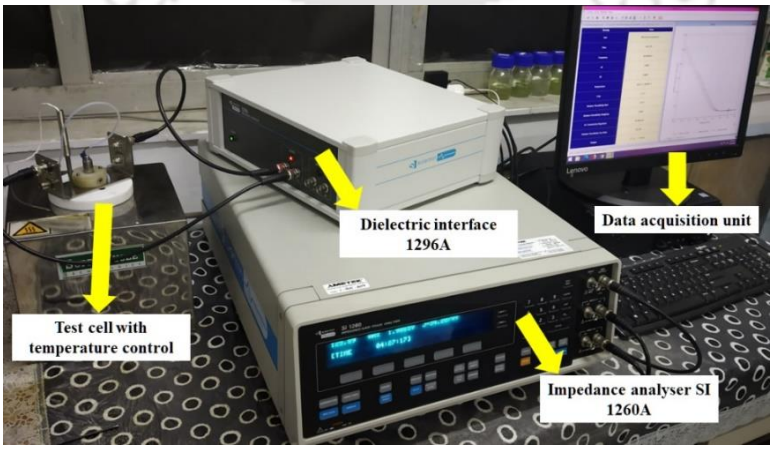

Figure 4.10: Impedance analyzer and dielectric interface for dielectric frequency response measurement.

TH-3272_186151014

Equation (4.2) points to the effect of conductivity (σ) on loss (ϵ'') which is significant at low frequencies (ω). As the moisture content decreases, the real and imaginary relative permittivity tends to reduce due to net reduction in the polarization process. The frequency response is dominated by the liquid conductivity in the frequency range of 0.1 Hz to 0.01 Hz. As mentioned earlier, the frequency is varied from 10 kHz to 1 mHz and the variation in real and imaginary components of complex RP of the NFs and base oil are measured and presented in Figure 4.11. Both the real and imaginary RP show a similar trend of decrease in the permittivity with the increase in the concentration of the NPs due to the interfacial polarization. Differences in conductivity lead to interfacial polarization and its contribution is much larger than that of dipole polarization. This trend is observed below 1 kHz for real permittivity and below 1 Hz for imaginary permittivity. The RP should be lower for the use of dielectric as a combined insulation to avoid higher capacitances. It is important to note that the measurements are performed at room temperature. When the oil insulation temperature rises, the RP increases. Since the RP of NFs is lower compared to base oil, the RP of the nanoliquid inches closer to that of the pressboard at transformer operating temperature. Hence, the addition of NP to the base oil is advantageous as it results in an even distribution of electric stress.

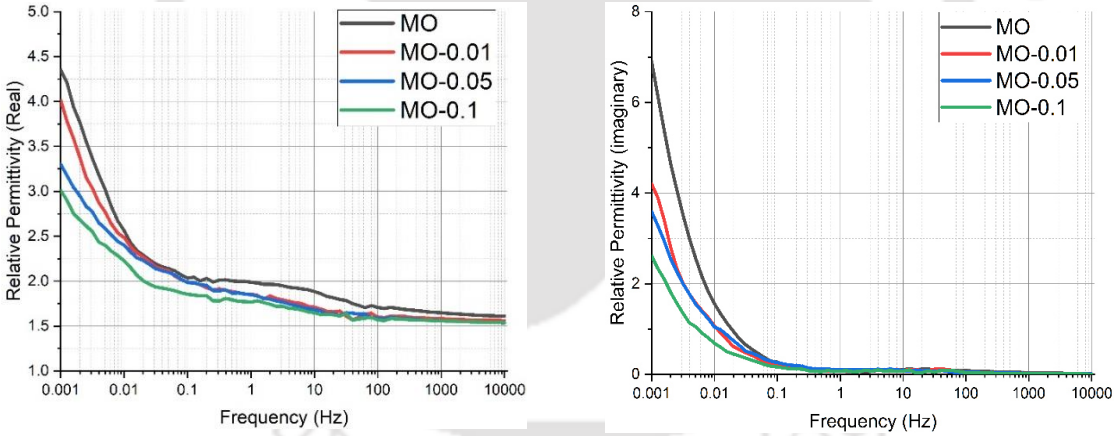

(a) (b)

Figure 4.11: Variation of (a) real and (b) imaginary relative permittivity of nanoliquids with frequency.

The variation in dissipation factor (*tanδ*) of the nanoliquids with frequency is shown in Figure 4.12. The *tanδ* tends to decrease with an increase in NP concentration. The dissipation factor measurements are independent of the geometry of the insulation in high voltage equipment. A low value of *tanδ* implies low losses in the liquid and also a low level of soluble polar ionic or colloidal contaminants. The increase in dielectric losses at lower frequencies is due to the increase in interfacial polarization. Therefore, the decrease in dissipation factor

TH-3272_186151014

indicates lower contamination/ ionic impurities/ lower moisture content. The frequency domain spectroscopy of the NFs is limited to the study of RP and *tanδ* to limit the scope of the thesis.

All the above characterization techniques give insight into the change in behavior of base oils with the addition of NPs. However, commercialization of the NFs requires extensive study into the various stresses they encounter during real time operation and the stability of the NFs. Most of the research published until now is focused on the response of NFs to electric fields such as BDV, PD, and charge trapping [123, 125]. It is evident that the magnetic field coexists with the electric field in the transformer and therefore the behavior of the NF in the presence of magnetic field needs to be studied.

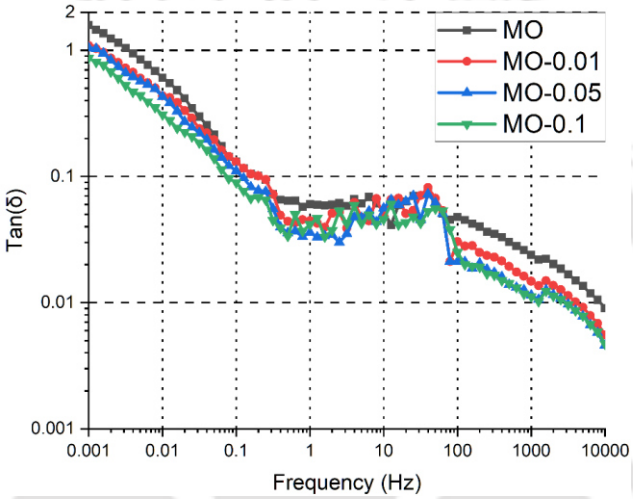

Figure 4.12: Variation in *tanδ* of nanoliquids with frequency.

4.6. Magnetic profiling of conducting, semi-conducting, and insulating nanoparticles and their nanofluids

4.6.1. Introduction

Magnetic-thermal-fluidic studies have shown that some NFs with high NP concentration can reduce the operating temperature of power transformers by 5°C [135, 136]. The reduction in operating temperatures by magnetic fluids is higher due to magneto-convection [135]. The reduction in operating temperature by other NFs is dominated instead by electrophoresis [137]. Thus, researchers have studied the application of NFs for power transformers, microactuators, bearings, sensors, transducers, and miniature planar spiral transformers [138].

In transformers, the windings are magnetically coupled and they are designed in such a way that most of the magnetic flux is directed through the core. In practice, some of the flux diverges from the core due to design limitations causing leakage fluxes. The leakage flux in power transformers results in circulating currents in windings, gassing of oil, and eddy currents in metal clamps and the transformer tank. This leakage flux passes through both the solid and

TH-3272_186151014

liquid insulation of the power transformer. The magnetic fields are inevitable during charge transfer as they are the result of the electric currents in the devices. Since magnetic fields affect the electrical discharges in the liquid insulation [139], it is relevant to study the impact of magnetic fields on insulation. Preliminary studies have shown that the interaction of magnetic flux with the fresh, aged, and base oil as well as NF samples gives a distinct response. The interphase, which is the vicinity of the NP-base oil boundary is expected to contribute to the change in the properties of a nanocomposite [140]. Charge redistribution occurs in the interphase when an NP is added to the base oil [140]. Lewi's and Tanaka's multicore model explains the composition, dimension, behavior, and influence of the interphase region [140, 141]. The interphase modeling provides an understanding of the application of nanocomposites. Simulations are performed to understand and interpret the space charge formation, prebreakdown, and breakdown phenomena in insulation. Applying multiphysical analysis helps incorporate thermal, electrical, magnetic, chemical, and physical effects simultaneously in the simulation to study the insulation breakdown. Most of the research published until now is focused on the response of NFs to electric fields such as BDV, PD, and charge trapping [123, 125, 140, 141]. In order to move one step closer to the application of NFs in high voltage equipment and improve the multiphysics mathematical models representing the interphase region, there is a need to study the response of NPs and NFs to the magnetic fields.

The magnetic nature and the interaction of a material with a magnetic flux are defined by its magnetic susceptibility. A heterogeneous mixture may have a different magnetic susceptibility compared to individual materials with which it is formed. Therefore, the addition of NPs to base oils might result in a different magnetic nature for NFs. It is necessary to establish the magnetic response of the NFs to understand their behavior when used in equipment having active dynamic magnetic fields. In addition, the NPs have a high affinity to agglomerate and sediment when kept idle. There is also a need to understand if the magnetic field can influence agglomeration in NFs.

Electron spin resonance spectroscopy (ESR) and vibrating sample magnetometers (VSM) are generally used to obtain magnetic parameters such as magnetic susceptibility and resonance field by subjecting samples to static and dynamic magnetic fields. ESR is a technique to study the dynamic magnetic behavior of materials that gives information about the valence state of the paramagnetic ions, magnetic interactions, spin correlation, and the local symmetry of the lattice host [142, 143]. It is also very effective in probing local and microscopic magnetic states compared to mere magnetic measurements [143]. In addition, VSMs are used for studying the quasi-static magnetic properties of materials [144].

TH-3272_186151014

4.6.2. Description of experimental techniques

4.6.2.1. Vibrating sample magnetometer spectroscopy

VSM analysis, also called Foner magnetometer analysis, is performed using a Lake Shore magnetometer (VSM7410) available at CIF of IIT Guwahati. The VSM is shown in Figure 4.13 (a). The VSM operation is based on Faraday's law of induction. Electromagnets are used to apply a magnetic field on the sample, resulting in the induction of a magnetic moment. The electromagnets generate varying magnetic fields. The dipole moment is induced in the sample proportional to the applied magnetic field and the sample's magnetic nature. Electromotive force (EMF) is generated in the gradient coils due to the vibration of the sample. This EMF is proportional to the vibration frequency, amplitude, and magnetic moment of the sample. The schematic of the experimental setup is shown in Figure 4.13(b).

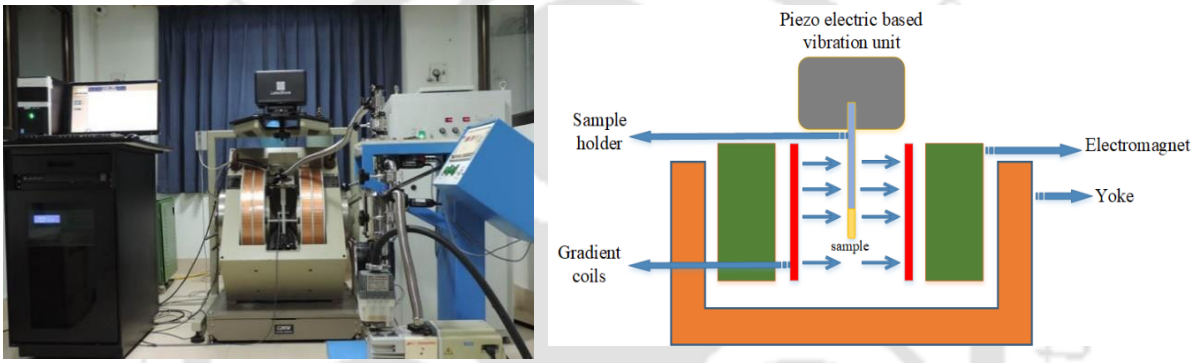

(a) (b)

Figure 4.13: (a) Experimental setup of VSM and (b) Schematic of VSM.

The dielectric liquid samples are loaded into the VSM in a sample tube which has a cup at the bottom to hold the insulating oil sample. After every single use, the sample cup is cleaned properly, rinsed with the sample, and inserted into VSM at room temperature of 27°C and nearest zero magnetic field. The VSM automatically centers the sample for detection in detection coils using the touchdown technique. The magnetic moment is displayed in e.m.u units. The magnetic moment is sample specific and hence varies with the quantity of the sample. So, it is necessary to provide a more standard comparison for dielectric samples and this can be achieved by taking the mass magnetization (MM) value of the sample which is a moment density and is independent of scale. Therefore, the magnetic moment obtained from the experimentation is converted to MM and plotted with respect to magnetic field strength.

4.6.2.2. Electron spin resonance spectroscopy

The ESR spectroscopy is performed using a JEOL X-band spectrometer (JES-FA200) available at the CIF of IIT Guwahati and is shown in Figure 4.14. The ESR is similar to the nuclear magnetic resonance (NMR) except that the electrons are excited in ESR, unlike the

TH-3272_186151014

nuclei in NMR. The unpaired electrons of the material in the presence of a magnetic field and radio frequency electromagnetic energy transits between the two spin states. The transition energy is expressed in terms of Bohr magnetron (μB), electron spin (*g*-factor), and applied magnetic field (B).

Figure 4.14: Experimental setup of ESR spectrometer.

4.6.3. Sample preparation

Transformer grade commercial MO is procured from M/s Savita Oil Technologies Limited, and commercial VO (FR3) is procured from M/s Cargill India. The oil samples are initially vacuum dried to degas and dehumidify, conforming with IEEE C57.637. The drying reduced moisture from 18 to 6 ppm in MO and from 102 to 32 ppm in FR3. The MC is measured using a Metrohm coulometric Karl Fischer titrator following ASTM D1533. These pre-processed oils are used in the experiments. The properties of these vacuum-dried MO and VO are presented in Table 4.1.

Table 4.1: Specification of the liquid insulation.

Property	Liquid insulation	
	Mineral Oil	FR3
Density at 25°C (kg/m^3)	0.828	0.9
Kinematic viscosity at 27°C (cSt)	12.82	16.25
Moisture content (ppm)	12	92
Flashpoint (°C)	145	275
Pour point (°C)	-25	-10
Dielectric constant at 90°C, 50 Hz	0.00055	0.00085
Interfacial Tension at 27°C (N/m)	0.047	0.0223

TH-3272_186151014

Table 4.2: Specification of the nanoparticles.

Property	Nanoparticle		
	Fe_3O_4	**CuO**	**Al_2O_3**
Name	Iron (II, III) oxide	Copper (II) oxide	Aluminum oxide
Purity	97%	--	≥ 99.9%
Size (nm)	50-100	< 50	< 50
Color	Black	Black	White
Form	Powder	Powder	suspension
Mol. Wt. (g/mol)	231.53	79.55	101.96
Brand	Aldrich	Aldrich	Aldrich
CAS number	1317-61-9	1317-38-0	1344-28-1
EC number	215-277-5	215-269-1	200-661-7
PCode	1002834758	101627599	1001961649
Product number	637106	544868	702129
pH	--	--	7.5-9.5

Three NPs (Fe_3O_4, CuO, and Al_2O_3), each from a different electrical category, are used to prepare NFs. The NFs are produced by adding each NP to each base fluid (MO and VO) in a concentration of 0.01% weight/volume (%w/v) following the procedure mentioned in Section 4.2. The prepared NF samples are shown in Figure 4.15. The NF samples are hermetically sealed after preparation until experimentation. The NPs used to prepare NFs are procured from Sigma-Aldrich, with properties stated in Table 4.2. The NP concentration of 0.01 %w/v is chosen considering the stability of all NFs at the maximum possible concentration. UVS is performed to check the stability and uniformity of the NFs [130]. The UVS absorption spectrum of MO-NFs and FR3-NFs is studied using an Agilent Cary 60 UV-Visible Spectrophotometer and is shown in Figure 4.16. The UVS is performed on NFs immediately after preparation and after every 48 hours. The absorption spectrum was observed to be unchanged for six weeks, indicating the NFs were stable due to shaking in the incubator. Also, the same %w/v of all NPs is chosen for correlative comparison. The electrical and thermal properties of the NFs are higher compared with the base liquid at this chosen concentration [52, 145]. Higher concentrations are practically not feasible for transformer applications due

TH-3272_186151014

to agglomeration and reduction in electro-thermal characteristics [145]. The higher and lower concentrations of NPs in the base oils lead to agglomeration as examined by UVS.

(a) (b) (c) (d) (e) (f)

Figure 4.15: Different kinds of nanofluids prepared in the laboratory (a) MO-Fe_3O_4 (b) MO-CuO (c) MO-Al_2O_3 (d) FR3-Fe_3O_4 (e) FR3-CuO and (f) FR3-Al_2O_3.

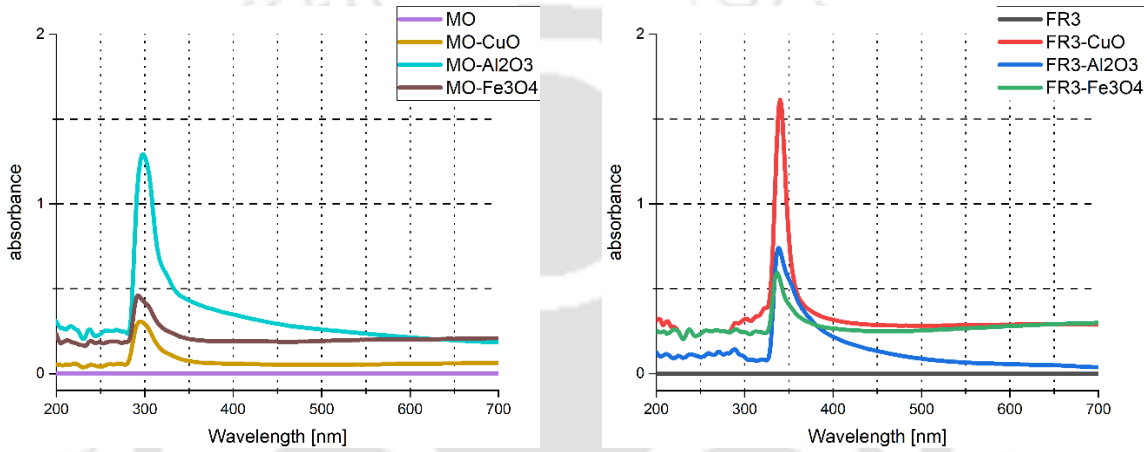

(a) (b)

Figure 4.16: UV-visible spectroscopy of (a) MO-NFs and (b) FR3-NFs.

The nanoparticles are not subjected to any pretreatment such as heating since some of the nanoparticles have low flash points (for example: Al_2O_3 in suspension form has a flash point of 12°C). Also, there is no standardized method to measure moisture in NPs according to the author's knowledge. Therefore, the moisture in NPs cannot be ascertained. However, the effect of moisture in NP on the NF can be studied by observing changes in the MC of the NF. The MC in NF is measured just after preparation and is observed to be the same as that in the base oil. The MC is tested using a Metrohm coulometric Karl Fischer titrator in accordance with ASTM D1533. An average of 3 readings of MC is provided in Table 4.3. Since the variation in MC is within the accuracy range of the equipment, the effect of moisture in NPs (if any) can be ignored.

Also, the NPs were recently procured and are stored in a room with 40% RH. The weighing of NPs and sonication of the NFs are done in a room with 40% RH. The NFs were hermetically sealed immediately after preparation to avoid any contact with atmospheric air. The above measures helped in achieving NFs with low moisture content. Kindly note that there

TH-3272_186151014

is no standardized method to nullify the influence of atmospheric humidity on samples. However, some standards provide consensus on maintaining low relative humidity to avoid the influence of humidity on samples. For example:

- ASTM D923 (Standard Practices for Sampling Electrical Insulating Liquids) says, "It is undesirable to collect samples that are exposed to the atmosphere when the relative humidity exceeds 50 % or under conditions of rain or snow."
- ASTM D924 (Standard Test Method for Dissipation Factor and Relative Permittivity of Electrical Insulating Liquids) says, "Samples to be subjected to test should preferably be obtained through a closed system. If exposed to atmospheric conditions, it is preferable to take the sample when the relative humidity is 50 % or less. If it is not feasible, the length of time the sample is exposed to atmospheric conditions must be kept to a minimum."
- IEEE C57.93 says, "The transformer should not be opened under circumstances that permit the entrance of moisture, such as on days of high relative humidity (80% or higher), without precautions to limit the entrance of moisture."

The above practices help in achieving repeatability. Taking note of the consensus from all the above standards, a low RH (40%) is chosen to avoid the influence of moisture.

Table 4.3: Moisture content in nanofluids.

Property	Sample							
	MO	MO-Fe_3O_4	MO-CuO	MO-Al_2O_3	FR3	FR3-Fe_3O_4	FR3-CuO	FR3-Al_2O_3
MC (ppm)	12	12	13	12	92	94	93	92

4.6.4. Magnetic profiling of nanoparticles and nanofluids

The magnetic response of the NPs, base oils, and NFs is presented in this section. All the experiments are performed five times to prove repeatability. The experiments are performed in a dehumidified (RH of 30%) room at a constant temperature (20°C).

4.6.4.1. Magnetic study using vibrating sample magnetometer spectroscopy

The VSM spectroscopy is initially used on the three NPs (Al_2O_3, CuO, and Fe_3O_4). Since the results obtained from VSM spectroscopy are in CGS units, they are converted into SI units according to IEEE Magnetics Society guidelines. A quasi-static magnetic field as shown in Figure 4.17(a) is applied and the magnetic moment of the NPs is obtained. The CGS to SI unit conversion factor for magnetic field strength (H) is $10^3/4\pi$ and the SI units are A/m. The

TH-3272_186151014

magnetic moment is normalized as the mass magnetization (MM) (magnetic moment/mass). The CGS to SI unit conversion factor for MM is 1 with units in $A.m^2/kg$. The measured MM of the tested NPs is independent of time as the field is quasi-static. For this reason, it is shown as a function of the measured data point in Figure 4.17(b-d).

The peak magnetic field intensity in power transformers can reach a few hundred kA/m depending on the geometry of the coil assembly [146, 147]. The operational magnetic flux density in the transformer core is generally close to 1.5 T and the leakage flux density is around 0.15 T [80, 148]. The magnetic flux density (B) in Tesla and the mass susceptibility (χ_p) in m^3/kg can be obtained from MM with the following relations:

$$B = \mu_0(MM + H) \tag{4.3}$$

$$\chi_p = \frac{MM}{H} \tag{4.4}$$

where μ_0 is the absolute permeability of free space ($4\pi\times10^{-7}$ H/m). The magnetic field intensity is varied from -1196.5 kA/m to 1196.5 kA/m in order to cover a broad range of operations. In this manner, the magnetic response of the NPs and NFs at transformer operational conditions can be established.

The MM response of the insulating NP shows that it has a diamagnetic nature as presented in Figure 4.17(b) which is due to the unavailability of unpaired electrons in the valence band. When subjected to an external magnetic field, a weak dipole moment is induced in the direction opposite to the applied field in the insulating Al_2O_3 NP resulting in a negative magnetic moment of 3.33×10^{-8} m^3/kg.

The MM response of the semi-conducting NP CuO to the incident field shows a paramagnetic nature as shown in Figure 4.17(c). The paramagnetic nature is established by the weak magnetic moment, a small and positive magnetic susceptibility of 4.58×10^{-8} m^3/kg. The paramagnetic nature is due to the Cu^{2+} ion having a single unpaired electron in the orbital.

Whereas the MM response of the conducting NP Fe_3O_4 shows a ferromagnetic nature. Fe_3O_4 nanoparticle exhibits Verwey transition and is a highly spin polarized conductor at room temperature [149]. The ferromagnetic nature is substantiated by the large magnetic moment and magnetic saturation as shown in Figure 4.17(d). The positive magnetic susceptibility in this case ranged between 5×10^{-9} and 7.2×10^{-6} m^3/kg.

The corresponding M-H curve of the tested NPs is shown in Figure 4.18. The magnetic susceptibility of Al_2O_3 and CuO NPs is small, whereas it is too large and saturated for the Fe_3O_4 NP. Now that the magnetic response of the NPs has been characterized, the MM of the base

TH-3272_186151014

oils (MO, FR3) and the corresponding NFs are studied. The M-H curve of the MO and MO-NFs is shown in Figure 4.19. The base oil MO and the nanofluids MO-CuO, MO-Al_2O_3 are found to be purely diamagnetic in nature. Unsurprisingly, the addition of Al_2O_3 NP to MO has increased the diamagnetic nature of the NF compared with the base liquid. Similarly, the CuO NP has reduced the diamagnetic nature of the base oil. This is due to the mutually opposing magnetic nature of CuO NP and MO as established in Figure 4.17(c).

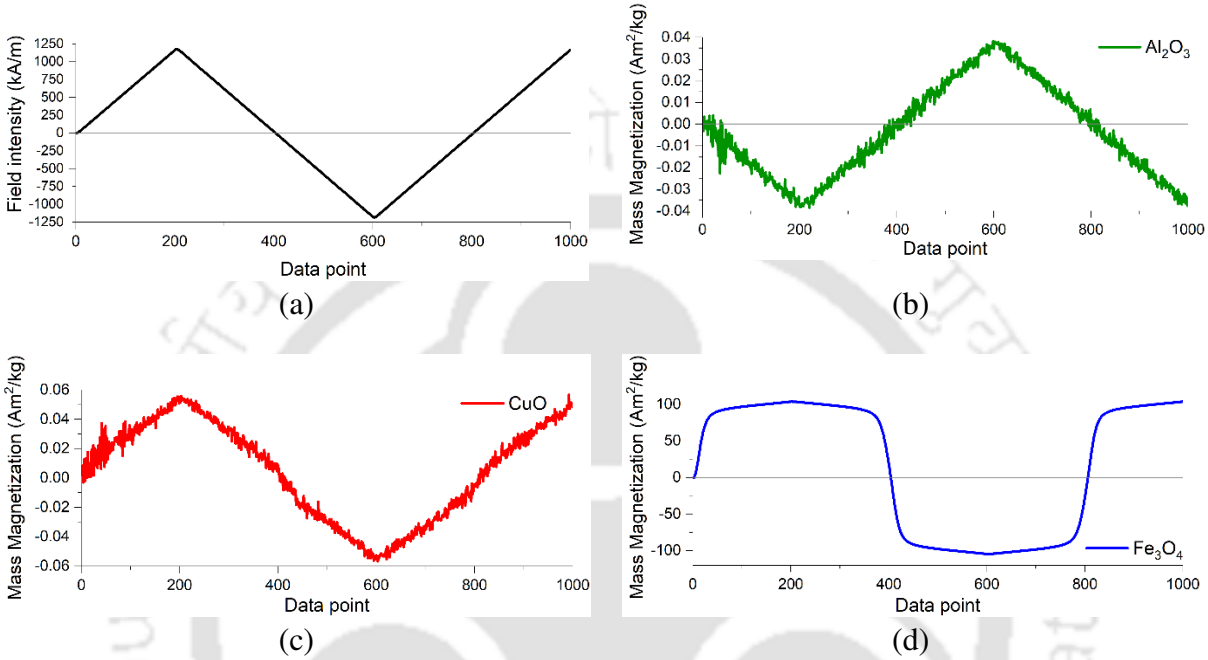

Figure 4.17: (a) Incident magnetic field, (b) Magnetic moment/mass of Al_2O_3 nanoparticle, (c) Magnetic moment/mass of CuO nanoparticle, and (d) Magnetic moment/mass of Fe_3O_4 nanoparticle.

The MM response of the MO-Fe_3O_4 NF shows a ferromagnetic response at low magnetic field intensity while a diamagnetic nature at higher magnetic field intensity. The magnetic field at which the MO-Fe_3O_4 NF showed the ferromagnetic nature is the linear region corresponding to the M-H curve of Fe_3O_4 NP that is from -125 to 125 kA/m in Figure 4.18. As the MM of Fe_3O_4 NP saturates beyond this field, the NF tends to become diamagnetic in nature due to the dominating magnetic moment of MO. Since the concentration of NP is low, the overall nature of the NF remains diamagnetic in nature at higher field strengths. However, the diamagnetic nature of MO-Fe_3O_4 is less compared to the MO-CuO NF. It implies that the total magnetic susceptibility of Ferro nanofluids (FNF) is due to both diamagnetic and ferromagnetic components. To extract the ferromagnetic nature incorporated in the FNF, the diamagnetic contribution is to be subtracted. The diamagnetic contribution in the M-H curve of NFs could be due to the sample holder and/or the base oil.

TH-3272_186151014

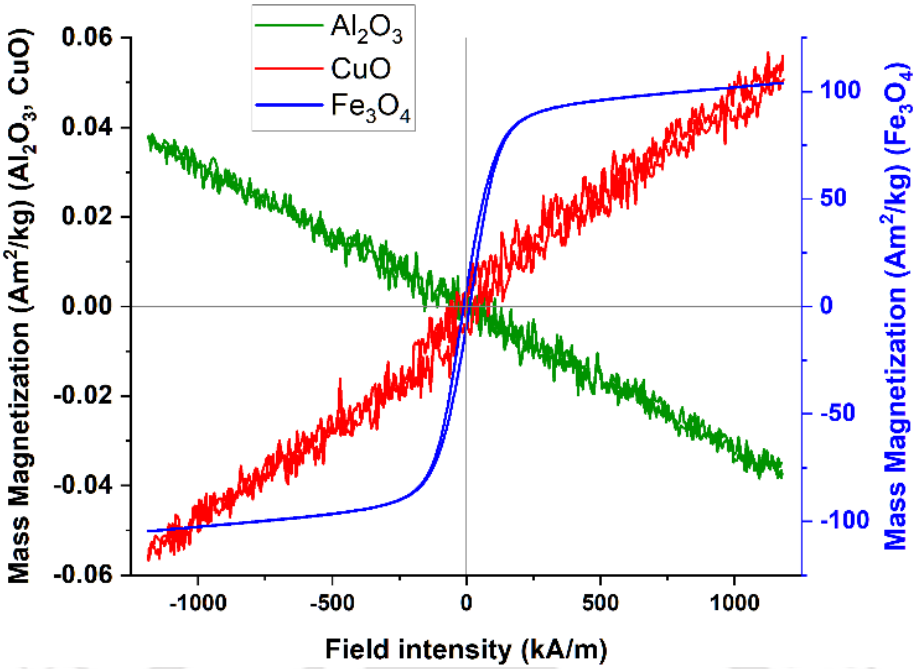

Figure 4.18: M-H curve of nanoparticles.

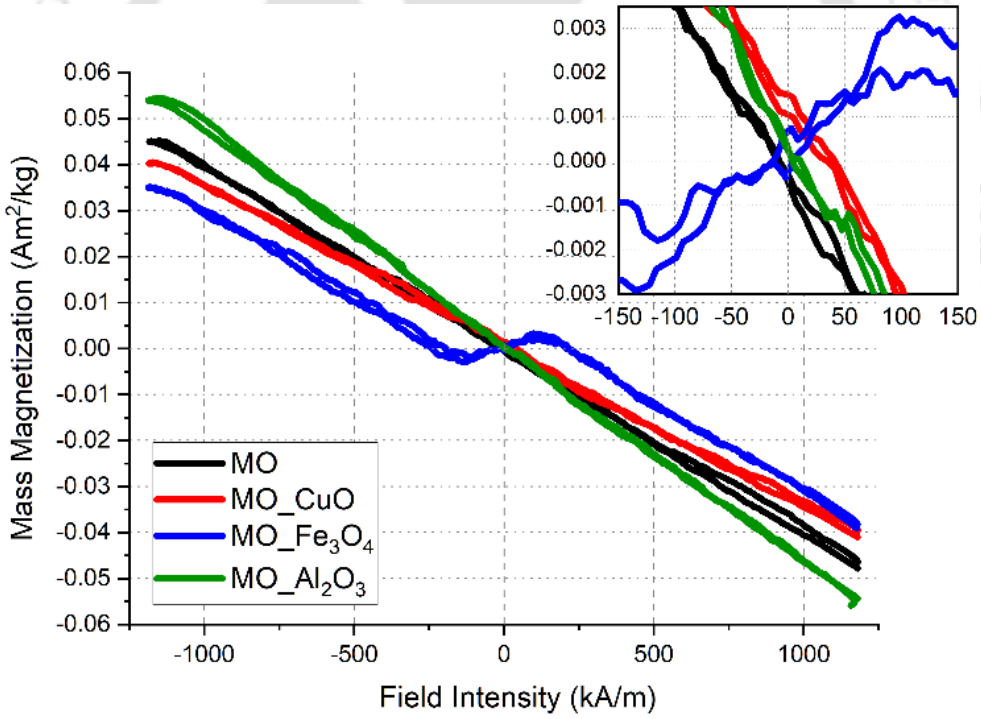

Figure 4.19: M-H curve of MO and MO-NFs.

To ascertain the impact of the sample holder, samples are tested in a Polychlorotrifluoroethylene tube (PCTET) and a glass capillary tube (GCT). The measured M-H curve is the same for both the sample holders. VSM spectroscopy of the empty PCTET and GCT are performed and it is observed from their M-H curve that the magnetic moment of both sample holders is very low compared to the magnetic moment of the samples. Therefore, the sample holder is not responsible for the change in the magnetic moment between NPs and NFs.

TH-3272_186151014

When the diamagnetic contribution of the base oils is subtracted from their respective NFs, the resultant magnetic moment is found to be similar to the magnetic moment of the NPs. The M-H curve of the NFs after subtracting the diamagnetic contribution of the base oil (MO) is shown in Figure 4.20. Observe that the resultant MM has a lower amplitude compared to that shown in Figure 4.18 only for the NPs. The reduction is due to the surface interaction of NP and the base oil leading to the formation of an interaction zone around the NP [150, 151]. The MM shown in Figure 4.20 is therefore an effective MM of the NP and its interaction zone with the liquid. The distortions in the M-H curve are due to the continual motion of the NPs in the NF which is confirmed by performing the experiment multiple times.

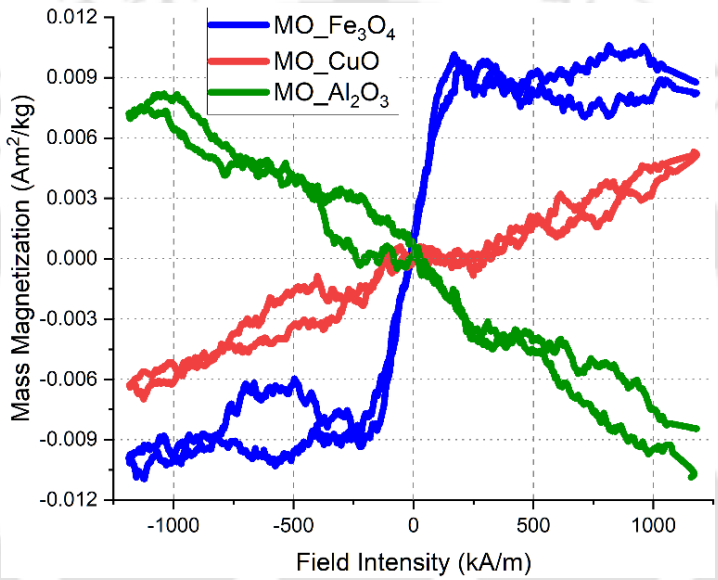

Figure 4.20: M-H curve of MO-NFs after removing the diamagnetic component due to base oil.

The magnetic susceptibility (χ_p) is extracted from the data in Figure 4.19 and presented in Table 4.4. The χ_p of MO and two of its nanofluids (MO-Al_2O_3, MO-CuO) are negative and constant for the entire tested magnetic intensity range. Whereas the χp of MO-Fe3O4 is positive at lower field intensity and negative at higher field intensity, which implies the FNF behaves as a ferromagnetic material for leakage fluxes and a diamagnetic material at higher flux densities.

The M-H curve of the FR3-NFs is shown in Figure 4.21. Although the nature of the MO-NFs and the FR3-NFs is similar, the magnitude of the magnetic moment of the FR3-NFs is smaller compared to that of MO-NFs. The higher viscosity of FR3 compared to MO is a factor for the reduced magnetic response. Due to the higher viscosity of FR3, the NPs observe friction to align with the magnetic field increases, reducing the overall moment of the FR3-NFs. The explanation of the MO-NFs is also valid for FR3-NFs. The diamagnetic component due to the

TH-3272_186151014

base oil (FR3) is subtracted from the MM of the NFs and the resultant MM is shown in Figure 4.22. The distortion in this M-H curve is also due to the movement of the NPs in the NF. Similarly, the reduction in the magnitude of the resultant MM compared to the original MM of NPs is due to the interaction zone formed between the NP and the base oil. The χ_p of FR3 and its NFs is extracted from Figure 4.21 and is also tabulated in Table 4.4. The χ_p of FR3-NFs follows the same trend as MO-NFs but with a lower magnitude. The χ_p is reduced at least two-fold for the FR3-NFs compared to MO-NFs.

Table 4.4: Magnetic susceptibility of nanofluids.

Fluids	Mass magnetic susceptibility (χ_p) (m^3/kg)	Fluids	Mass magnetic susceptibility (χ_p) (m^3/kg)
MO	-3.78×10^{-8}	FR3	-1.48×10^{-8}
MO-Al_2O_3	-4.61×10^{-8}	FR3-Al_2O_3	-1.67×10^{-8}
MO-CuO	-3.34×10^{-8}	FR3-CuO	-1.27×10^{-8}
MO-Fe_3O_4		FR3-Fe_3O_4	
(a) up to 0.16 T	$+2.55\times10^{-8}$	(a) up to 0.16T	$+0.85\times10^{-8}$
(b) 0.16 to 1.5 T	-3.58×10^{-8}	(b) 0.16T to 1.5T	-1.45×10^{-8}

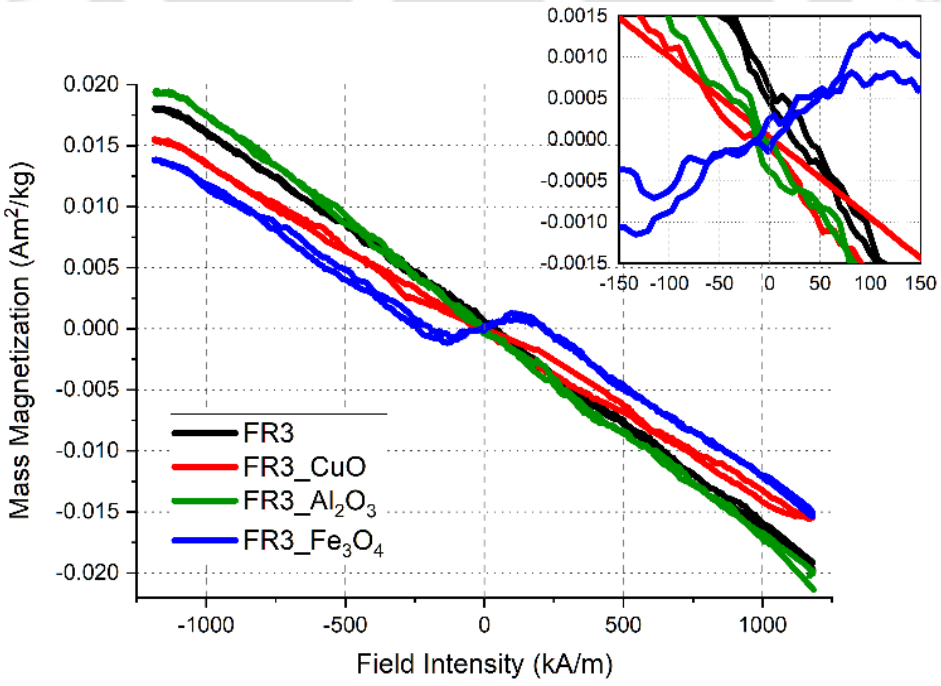

Figure 4.21: M-H curve of FR3 and FR3-NFs.

TH-3272_186151014

Charge redistribution occurs in the interphase when new particles are introduced in the base matrix [140]. Both Van der Waals' attractive and electrostatic repulsive forces continuously act on the NPs. London dispersion forces are a type of Van der Waal force that exists when two non-polar molecules, such as base oil molecule and NP, come in contact, resulting in a dipole moment due to electron positions despite zero net dipole moment. This causes polarization in the neighboring molecule [152]. In addition, due to the Brownian motion of NPs, there is a chance of an increase in ionic concentration due to the overlapping of interfacial regions. All the above effects are a result of the addition of NPs. The presence of interfacial regions and their interactions result in liquids with different magnetic properties. The positive magnetic susceptibility of the semi-conducting and the conducting NPs indicate that they tend to align with the operating magnetic field of the HV equipment which eventually creates a path for electrical breakdown [153]. Furthermore, the magnetic nanofluids can generate EMF in their vicinity [154, 155]. Therefore, both MO-Fe_3O_4 and FR3-Fe_3O_4 FNFs can generate EMF, leading to the formation of space charge in the transformer. These charges may sufficiently distort the operational electric fields to produce streamers and/or PD, which may lead to fatal static discharges. Also, the FNFs may generate EMFs on the tank of the transformer and metal clamps. In such cases, special insulation coating needs to be done to avoid accidents, which will increase production costs. The magnetic study suggests that the leakage flux may align the conducting NPs close to conductors and may distort the electric field distribution which might eventually result in breakdown. Hence usage of the conducting NFs in the transformer is not suggested considering its magnetic behavior.

On the other hand, the magnetic properties of the NFs can also influence the leakage fluxes around the transformer core. High leakage fluxes can in turn produce local overheating of the transformer and produce circulating currents in the windings due to unequal induced voltages [80]. The leakage flux increases in proportion to the square root of the power rating and the reactance of the transformer. The stray flux also leads to the generation of gas from insulation by the side of metallic parts when the transformer is overloaded, the frequency is lowered, and/or in the presence of power frequency over voltages [80].

The leakage flux can be controlled by using appropriate NF whose magnetic properties push the NPs away from windings and NPs force the flux through the core. This effect is driven by the magnetic force ($\boldsymbol{F}$) on the NP in the NF, given by [153]:

$$\boldsymbol{F} = \mu_0 V_n \chi_p (\boldsymbol{\nabla}.\boldsymbol{H})\boldsymbol{H} \tag{4.5}$$

TH-3272_186151014

where μ_0 is the absolute permeability of free space ($4\pi\times10^{-7}$ H/m), V_n is the volume of NP, χ_p is the magnetic susceptibility, and $\boldsymbol{H}$ is the applied magnetic field. Based on the M-H curves reported above, Al_2O_3 based NF would be a suitable candidate as it has a negative χ_p. Therefore, an Al_2O_3 based NF does not lead to agglomeration on the windings and transformer core as the diamagnetic material prevents the magnetic lines from passing through it [139]. It could help in reducing the leakage flux in transformers. Therefore, an efficient design of a transformer using insulating NP based NFs might also help in reducing the number of taps due to improved voltage regulation. Hence insulating NP (Al_2O_3) based NFs may be suitable for usage in transformers based on their magnetic behavior.

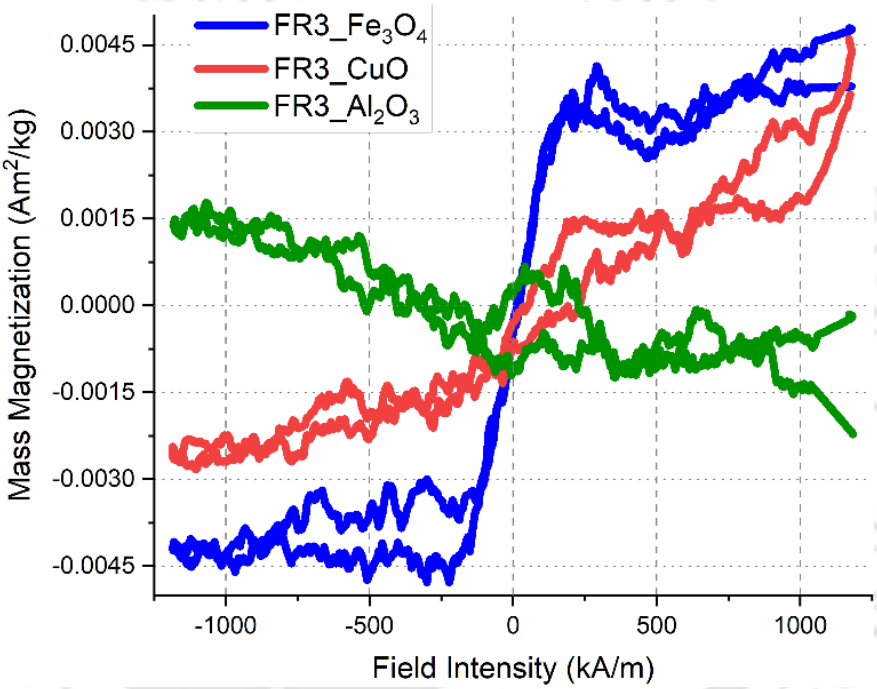

Figure 4.22: M-H curve of FR3-NFs after removing the diamagnetic component due to base oil.

4.6.4.2. Magnetic study using electron spin resonance spectroscopy

The ESR spectrum is a plot of the first derivative of electromagnetic radiation absorption as a function of the incident magnetic field. The first derivative of the absorption curve is preferred for the analysis as it provides the advantage of easy extraction of information. ESR spectroscopy is used on all the NPs and the NFs samples to study their response to the dynamic magnetic field. However, the CuO and Fe_3O_4 NPs as well as the FNFs are the only samples found to respond to the ESR spectroscopy. The ESR spectroscopy results in this case are shown in Figure 4.23.

To extract the line shape parameters such as Lande's g-factor (g), the peak-to-peak line width ($\Delta B_{p\text{-}p}$), the resonance flux density (B_0), and the spin-spin relaxation time (T_2) from the

TH-3272_186151014

experimental data, mathematical functions are fitted to the experimental data based on their line shape [143, 156-158]. The curve fits generated using mathematical functions are overlapped with the experimental data shown in Figure 4.23.

The ESR spectrum of the CuO NP is fitted by the two-component Dysonian line shape function given in (4.6). Lorentzian line shape function is used when the spectroscopy curve is symmetrical with respect to the x-axis. The Dysonian is preferred to Lorentzian as the former can incorporate the asymmetry (if any exists). Whereas, the ESR absorption spectrum of Fe_3O_4 nanoparticle, MO-Fe_3O_4, and FR3-Fe_3O_4 nanofluids are best fitted by the two component Gaussian function given in (4.7). The first term in the above line shape function equations signifies clockwise polarization and the second term signifies the counterclockwise polarization of the linearly polarized incident signal [143, 156, 157].

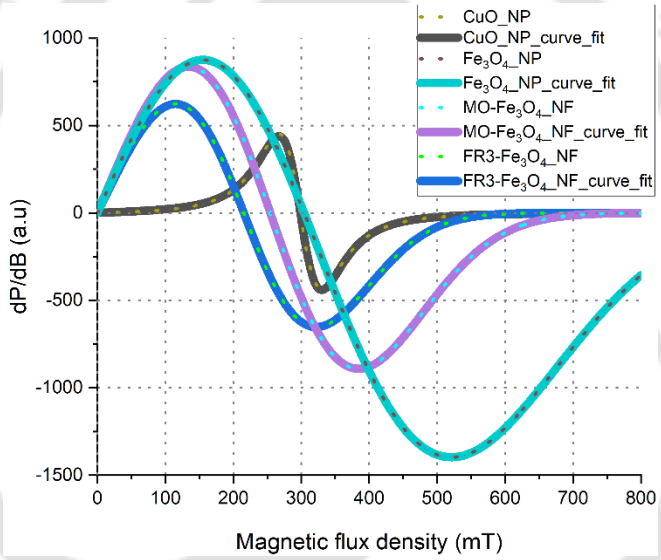

Figure 4.23: ESR spectra of NPs and NFs.

$$\frac{dP}{dB} = \frac{d}{dB}\left[\frac{2A}{\pi}\left(\frac{\Delta B+\alpha(B-B_0)}{4(B-B_0)^2+(\Delta B)^2} + \frac{\Delta B+\alpha(B+B_0)}{4(B+B_0)^2+(\Delta B)^2}\right)\right] \quad (4.6)$$

$$\frac{dP}{dB} = \frac{d}{dB}\left[A\frac{\sqrt{\ln 2}}{(\Delta B).\sqrt{\pi}}\left[\exp\left(-(B-B_0)\frac{\ln 2}{(\Delta B)^2}\right) + \exp\left(-(B+B_0)\frac{\ln 2}{(\Delta B)^2}\right)\right]\right. \quad (4.7)$$

where A is the area under the absorption curve and α is the asymmetry parameter. The resonance frequency and width at half height of the absorption peak (ΔB) are obtained from (4.6) and (4.7). The other line parameters such as peak-to-peak line width, Lande's g-factor, and spin-spin relaxation time are obtained using the relations given in (4.8), (4.9), and (4.10) respectively, and are tabulated in Table 4.5.

TH-3272_186151014

$$\Delta B_{p-p} = \frac{\Delta B}{\sqrt{3}} \tag{4.8}$$

$$g = \frac{h\upsilon}{\mu_B B_0} \tag{4.9}$$

$$T_2 = \frac{\hbar}{g\mu_B \Delta B} \tag{4.10}$$

where $h(\hbar)$ is Planck's constant (6.625×10^{-34} J-s (1.054×10^{-34} J-s)), μ_B is Bohr magnetron (9.274×10^{-24} J/T), υ is the frequency of the electromagnetic radiation, spin-spin relaxation time (T_2) is the time taken by the electron in the process of reaching ground state from an excited state.

Table 4.5: Parameters extracted from ESR spectroscopy.

Nanoparticle/ Nanofluid	Effective g-factor (g)	Peak-to-peak line width (ΔB_{p-p}) (mT)	Resonance flux density (B_0) (mT)	Spin-spin relaxation time (T_2) ($\times10^{-15}$ secs)
CuO	2.256	62.93	299	46.22
Fe_3O_4	2.163	284.90	312	10.65
MO-Fe_3O_4	2.646	176.67	255	14.04
FR3-Fe_3O_4	3.138	144.92	215	14.43

The spin resonance of the CuO NP is due to the single valence electron in Cu^{2+}. When the CuO NP is dispersed in the base oils, the overall response is dominated by the base oil. This can be explained by the characteristics obtained in the VSM study. The diamagnetic component due to the base oil is dominant over the contribution of the NP. Therefore, the CuO based NFs are irresponsive to the ESR spectroscopy. The Al_2O_3 based NFs are irresponsive due to the diamagnetic nature of the base oil as well as Al_2O_3 NP as seen in VSM spectroscopy. The spin resonance of the Fe_3O_4 NPs is due to the five unpaired electrons in Fe^{3+}. When Fe_3O_4 NP is dispersed in the base oils, the peak-to-peak line width and resonance frequency are reduced for both the FNFs. The decrease is much greater in FR3 based NF.

A low peak-to-peak line width (ΔB_{p-p}) indicates lower magnetic losses, better homogeneity, increased demagnetization, and a change of nature from hard to soft magnetic material [159]. The FR3 FNF has a higher demagnetizing nature than MO FNF, which supports the findings from VSM spectroscopy. The soft magnets easily magnetize and demagnetize. Furthermore, low ΔB_{p-p} implies high saturation values and hence the saturation of FNFs is not

TH-3272_186151014

observed in VSM spectroscopy. Therefore, the FNFs in close proximity to windings provide a high magnetic permeable path which may result in increased leakage flux. Consequently, the dynamic magnetic study shows that FNFs may lead to higher leakage fluxes in transformers. The decrease in line width also corresponds to lower magnetic dipolar interactions [160, 161], which indicates the magnetic dipolar interactions are lower in FR3 FNF. Therefore, the use of FNFs is not suggested considering their dynamic magnetic response.

The parameter B_0 signifies the field at which the magnetic resonance of the material occurs. At magnetic resonance, the maximum radiation is observed by the sample. The resonance field of Fe_3O_4 NP is found to decrease when adding it to base oils. The resonance field is observed to further decrease with an increase in the viscosity of the NF. The FR3-FNF resonates at a lower magnetic field compared to MO-FNF. Therefore, B_0 is an important factor to consider when designing the insulation to avoid resonance in the operating field of the equipment.

The g defines the contribution of angular momentum to the total magnetic moment of an unpaired electron [158]. The decrease in the g-factor corresponds to the increase in magnetic dipole interactions, and therefore the increase in magnetic moment [162]. The increase in g-factor is observed in FNFs with higher g-value for FR3-FNF, indicating a decrease in magnetic moment for FNFs compared to NP. The lower magnetic moment for FNFs compared to NPs is in accordance with the findings in VSM spectroscopy.

Since the diamagnetic materials are insensitive to ESR spectroscopy [158], the principal nature of the NFs can be studied sensitively only in paramagnetic and ferromagnetic NPs. As observed in the VSM spectroscopy, the FNFs show ferromagnetic response at lower field strength in ESR spectroscopy too.

The spin-spin relaxation time (T_2) shows that the relaxation time for the FNFs is higher compared to the NP. T_2 is relatively higher for the FR3-NF compared to MO-NF. Since the PD in the transformers occurs at a nanosecond time scale [163], it generates an electromagnetic pulse of very high frequency [148]. The FNFs in close proximity to PD may align with the electromagnetic fields due to their short relaxation times. Under either static or dynamic magnetic fields, the ferromagnetic response in the case of the FNFs is only found at lower magnetic field magnitude.

The electrical charge relaxation time is short for conducting NP, followed by semiconducting and insulating NPs [152]. Similarly, the magnetic relaxation time of conducting NP is observed to be smaller compared to semiconducting NP, whereas the insulating NP has no response to the high-frequency fields. In other words, the magnetic

TH-3272_186151014

relaxation time of the insulating NP can be assumed to be infinite.

All the NFs are observed to be stable after interaction with the quasi-static and dynamic magnetic fields. There was no visual agglomeration or sedimentation of NPs in the NFs during experimentation. As the nanoparticles are insoluble in base oils, it is hard to prepare NFs that do not agglomerate for a long time.

Although it is known that Fe_3O_4 based NFs can increase the TC when subjected to magnetic fields [164], there is a risk of insulation failure due to the EMF generation and orientation of NPs with the field. The transformer vibrations and the near stray magnetic fields could lead to increased degenerative effects. Therefore, the usage of FNFs in transformers may be considered subject to the above issues being addressed.

4.7. Conjecture on benefits of using VO and NFs over MO

The primary and secondary windings (PSW) of the transformer are magnetically coupled. The magnetic flux linking the PSW is intended to flow through the core of the transformer. The magnetic flux chooses the path of the lowest reluctance. In general, the transformers are designed such that most of the magnetic flux flows through its core. The magnetic flux will experience low reluctance if the medium through which it is flowing is ferromagnetic. The core in the transformer is generally made up of cold rolled grain oriented (CRGO), a ferromagnetic material to reduce the reluctance to the magnetic flux linkage, to maintain high flux density, to maximize magnetic induction, to minimize specific core loss at no load, and low magnetostriction [80]. However, the flux leakages are inevitable due to design constraints and insulation placement. The leakage flux is responsible for voltage drop in the transformer, thus its reduction shall improve the voltage regulation. It also affects the excitation demands of salient poles, the leakage inductance of windings, stray losses, circulating currents in transformer walls, and metallic clamps [165, 166]. In converter transformers, this leakage flux is responsible for the hotspot formation and the failure of the converter transformers [167]. Therefore, leakage flux is responsible for the voltage dip on the secondary side. Hence, its reduction is important to maintain good voltage regulation and efficiency. The leakage flux also flows through the liquid dielectric used for insulation and cooling purposes in the transformer. Therefore, the magnetic nature of liquid dielectric is very important to analyze its impact on leakage flux.

The diamagnetic material repels the magnetic lines of force as shown in Figure 4.24 due to its completely filled sub shells. The fresh VO being more diamagnetic in nature compared to MO, could distort the magnetic flux in the gap between the PSW and between the winding-

TH-3272_186151014

core assembly of the transformer. A liquid insulation with a greater diamagnetic nature opposes the flow of leakage through it. The leakage flux due to current flowing in the windings of the transformer does not tend to flow through the dielectric liquid with a high diamagnetic nature and is forced to enter the core of the transformer to complete the magnetic circuit. The more diamagnetic a liquid insulator is, the more leakage flux lines are forced to flow through the core of the transformer. Using a suitable liquid dielectric could potentially reduce the voltage drop in the secondary winding of the power transformer. The reduction in leakage flux reduces the circulating currents in transformer tank walls and metallic clamps. Since the VO, semi-conducting, and insulating NP based NFs are found to have a greater diamagnetic nature compared to MO, their application in transformers may help achieve a reduction in leakage fluxes.

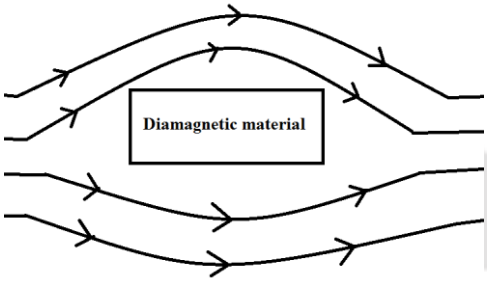

Figure 4.24: Magnetic field lines in the presence of diamagnetic material.

4.8. Summary of the chapter

NFs are prepared in the laboratory and their thermal conductivity is studied by varying temperature as well as concentration. The electric field around various NPs dispersed in MO is simulated to study the impact of NP on the electric field around it. Further, the dielectric frequency response of NFs is studied by varying its concentration. Finally, the VSM and ESR spectroscopies are performed on three types of NPs, and their NFs to ascertain the static and dynamic magnetic properties of the insulation. The outcomes of this chapter are:

- The thermal conductivity of NF increases with an increase in temperature as well as with an increase in NP concentration.
- The electric field around all the nanoparticles gets distorted with the least distortion in the case of insulating NP.
- The dielectric frequency response study on nanofluids infers that the dissipation losses decrease with an increase in NP concentration.
- The ferromagnetic nature is found to dominate in FNFs at lower magnetic field strengths. MO and FR3 FNFs have magnetic susceptibilities of 2.55×10^{-8} and

TH-3272_186151014

0.85×10^{-8} respectively, in this region.

- Regardless of the nature of the NPs, all NFs are diamagnetic in nature between a magnetic field strength of 150 kA/m and 1250 kA/m. However, the MO-NFs possess approximately 2.5 times higher magnetic susceptibility than FR3-NFs.
- CuO, Fe_3O_4 NPs, and FNFs have shown resonance to the dynamic magnetic field, while Al_2O_3 NP and all other NFs are irresponsive. The resonance field is 18.2% and 31.1% smaller for MO-FNF and FR3-FNF compared to Fe_3O_4 NP.
- The FNFs tend to be soft magnetic materials in comparison to the Fe_3O_4 NP. Therefore, the magnetic dipolar interactions and magnetic moment are lower in FNFs.
- The insulating NP makes its base oil further diamagnetic, resulting in a solution that provides high reluctance to the magnetic flux and potentially avoids settling of NP on or near the magnetic core.
- The NPs in NFs do not agglomerate/sediment upon subjecting them to quasi-static and dynamic magnetic fields.

Considering the electric field distortion and the magnetic response, insulating NP based NF is a preferred alternate liquid insulation among the NFs. Various studies conducted in this chapter establish the magnetic behaviour and performance of NFs as suitable alternate transformer insulation. These studies support the fact that the proposed technique is being used on validated insulation rather than arbitrarily selected samples. They also provide key input parameters for mathematical models of the interaction of NPs in NFs under magnetic fields and the corresponding interaction zones around the NPs. Such models should also complement the assessment of the dielectric, thermal, and fluid mechanical performance of NFs in power transformers. These studies will help design engineers in the multiphysics modeling of the breakdown in liquid insulation and choosing an appropriate NF as a transformer insulant. With the extensive study on various alternate liquid insulations in Chapters 3 and 4, the next chapter deals with the application of non-intrusive and non-destructive technique presented in Chapter 2 for condition assessment of these alternate liquid insulations.

TH-3272_186151014

भारतीय प्रौद्योगिकी संस्थान गुवाहाटी • Indian Institute of Technology Guwahati •

Note: This work, "Magnetic Profiling of Conducting, Semi-conducting, and Insulating Nanoparticles and their Nanofluids Possessing Potential Transformer Application," has been published in IEEE Transactions on Dielectric and Electrical Insulation, 2022, vol. 30, no. 2, pp. 649-657, Apr. 2023.

TH-3272_186151014

5

The non-intrusive and non-destructive technique for condition assessment of alternate liquid insulating oils

Contents

5.1	Introduction	103
5.2	Non-intrusive and non-destructive technique for condition assessment of nanofluids	103
5.3	Non-intrusive and non-destructive technique for condition assessment of blended oils	107
5.4	Summary of the chapter	111

TH-3272_186151014

5.1. Introduction

The aging and consequential degradation occur due to the thermal, electrical, and environmental stresses acting on the liquid insulation [28, 29]. Aging is no exception to the alternate liquid insulation such as NFs, EOs, and BOs [16, 28, 29, 72, 74]. However, the relative aging of such insulation is different compared to MO despite being subjected to a similar individual or multiple stresses over time [13, 33]. Regardless of the time taken by the various insulations to age, the insulation eventually degrades, leading to the formation of byproducts. The variation in physiochemical and electrical properties of BOs on aging as presented in Chapter 3 supports the proposition. The investigation of short and long term performance of such insulation helps avoid the sudden failure of the equipment and increases the grid reliability. There are no defined standard test methods for assessing the aging status of BOs according to the author's knowledge. However, researchers have analyzed the electrical properties of BOs using the testing equipment employed for MO [16]. A quick and cost-effective assessment of insulation is always an advantage as it aids in carrying out swift assessment and countermeasures to avoid equipment failure. This chapter deals with the applicability of the non-intrusive and non-destructive condition assessment technique proposed in Chapter 2 for alternative liquid insulation such as NFs, EO, and BOs.

5.2. Non-intrusive and non-destructive technique for condition assessment of nanofluids

MO and FR3 based NFs are prepared in accordance with the process described in Section 4.2. The prepared NFs include MO-Fe_3O_4, MO-CuO, MO-Al_2O_3, FR3-Fe_3O_4, FR3-CuO, and FR3-Al_2O_3 with 0.01 %w/v of NPs as shown in Figure 5.1. The MC and TAN in the base oils and NFs are measured according to ASTM D1533 and IEC 62021 standards respectively and the data is shown in Table 5.1. A negligible variation in the MC and TAN are observed in the NFs compared to base oils and can be ignored for practical reasons. The MO-NFs and FR3-NFs are now tested using the calibrated test setup presented in Section 2.2.2. The frequency responses obtained from testing of the MO-NFs and FR3-NFs using the non-intrusive and non-destructive condition assessment technique are presented in Figures 5.2 and 5.3 respectively.

Although there is no change in the TAN, the resonance corresponding to the first resonance point is observed to change with the change in NP for both oils. As manifested in Chapter 4, the NPs affect the electric and magnetic nature of the base oils. The reflections from the oil increase with the increase in conductivity of the NP. The relationship between the cut-

TH-3272_186151014

off frequency (f_c) of the horn antenna and the effective relative permittivity (ϵ_r) of the oil is given by (2.1), wherein, the cut-off frequency is inversely proportional to the square root of the relative permittivity. The addition of NPs to MO and FR3 leads to a change in the overall conductivity of the NF. The change in conductivity results in a change in relative permittivity as given by (5.1) [168].

$$\sigma = i\omega\epsilon_0\epsilon_r \tag{5.1}$$

where $i = \sqrt{-1}$, σ is complex electrical conductivity, ϵ_r is complex relative permittivity and ϵ_0 is the permittivity of free space (8.85 x 10^{-12} F/m). Interestingly, the change in conductivity due to the addition of NPs is reflected at the first resonance point in the chosen frequency band. The addition of conducting and semi-conducting particles increases the overall conductivity of the insulation sample leading to greater reflection of signal to the antenna and is evident from Figures 5.2 and 5.3. However, the addition of insulating NPs resulted in a lower reflection of signal indicating a decrease in the overall electrical conductivity of the insulation. Further, since there is no significant variation in the moisture of NFs compared to base oils, the frequency response corresponding to the moisture at the second resonant frequency does not have any notable variation.

Table 5.1: MC and TAN in nanofluids.

Property	Sample							
	MO	MO-Fe_3O_4	MO-CuO	MO-Al_2O_3	FR3	FR3-Fe_3O_4	FR3-CuO	FR3-Al_2O_3
MC (ppm)	12	12	13	12	92	94	93	92
TAN (mg KOH/g)	0.012	0.013	0.012	0.011	0.03	0.035	0.033	0.028

(a) (b) (c) (d) (e) (f)

Figure 5.1: Nanofluids prepared in the laboratory (a) MO-Fe_3O_4 (b) MO-CuO (c) MO-Al_2O_3 (d) FR3-Fe_3O_4 (e) FR3-CuO and (f) FR3-Al_2O_3.

TH-3272_186151014

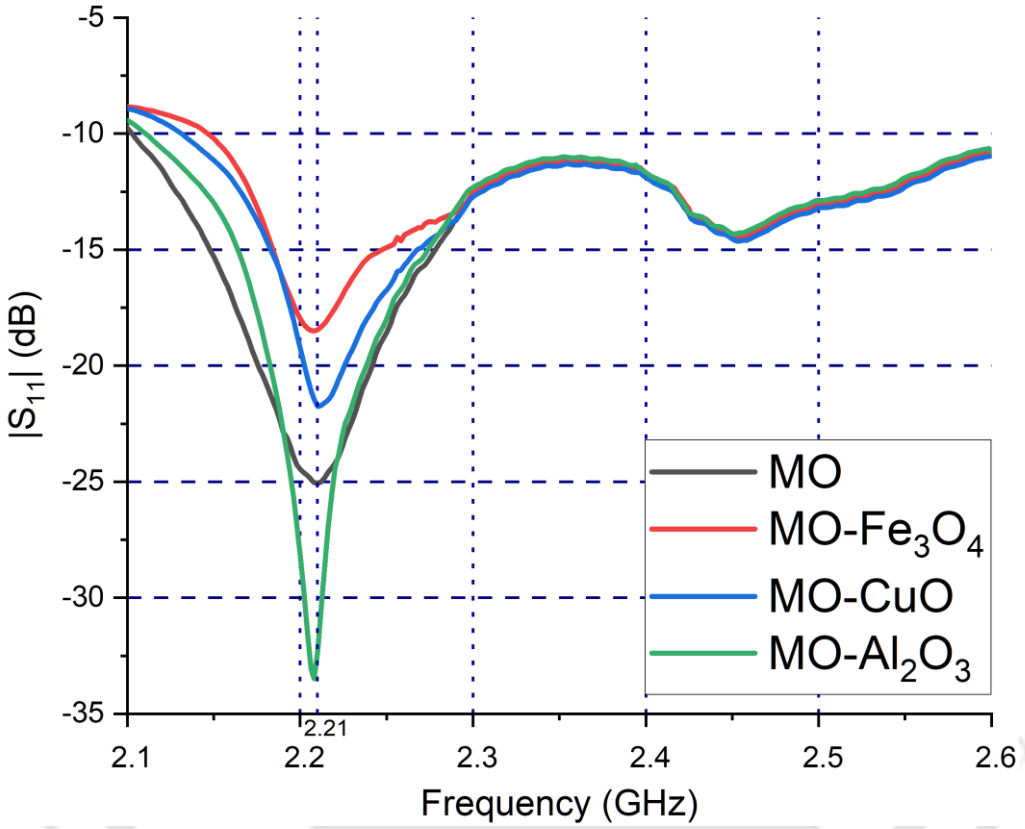

Figure 5.2: Frequency response analysis of MO based nanofluids.

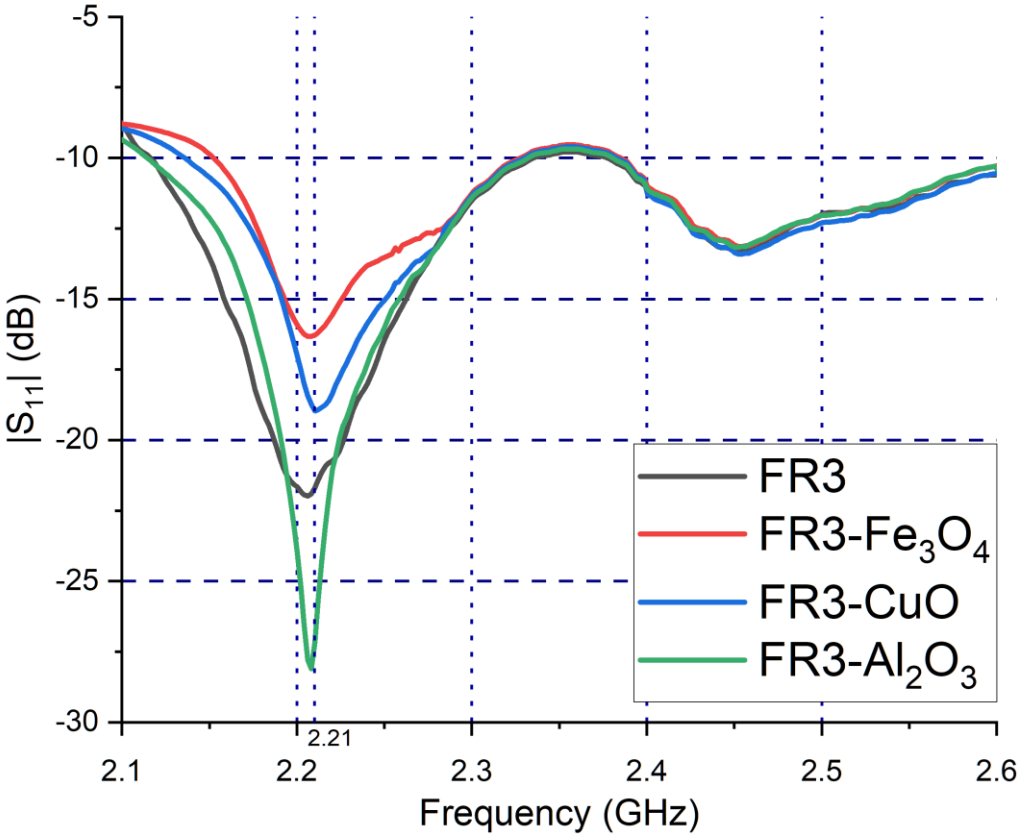

Figure 5.3: Frequency response analysis of FR3 based nanofluids.

TH-3272_186151014

Further, care should be taken while cleaning the test cell between each consecutive experiment as the NPs tend to adhere to the walls and corners of the test cell potentially contaminating the next sample. Therefore, the test cell must be cleaned and dried multiple times to ensure there are no NPs on its walls before loading the next sample. It is important to mention that the adherence of NPs to the walls of the test cell cannot be verified sometimes directly with the naked eye and also the precision microscopes do not reach the edges of the test cell. Therefore, in order to avoid the errors creeping in from contamination of the samples, it is advised to use a different test cell for each type of NF. One of the test cells with Fe_3O_4 NPs adhered to its walls after removing the oil sample is shown in Figure 5.4.

Figure 5.4: Fe_3O_4 NPs adhered to the test cell after removing the nanofluid.

Further, to understand the effect of aging on NFs and the efficacy of the proposed condition assessment setup in establishing the aging status of NFs, all the NFs should be aged and tested. An attempt is made to age the NFs by accelerated thermal aging and oxidative aging methods presented in Sections 2.2.1.1 and 2.2.1.2. On aging, the NPs are found to adhere to the materials such as copper, pressboard, and kraft paper resulting in an unpredictable concentration of NP left in the base oil. Test results of such oil samples with unknown concentrations cannot be compared with reference curves obtained in establishing a conclusion. Hence, it is not possible to extend the aging studies to study the long-term performance of the NFs. It is noteworthy to mention that the application of non-intrusive and non-destructive condition assessment technique for the aged NFs is not limited by the technique but by the challenges faced in aging the NFs to prepare test samples. Pressboards aged along with the NFs

TH-3272_186151014

are shown in Figure 5.5. This agglomeration of NPs may have serious consequences on introducing them into the transformer due to possible settling in radiator tubes, core, and valves.

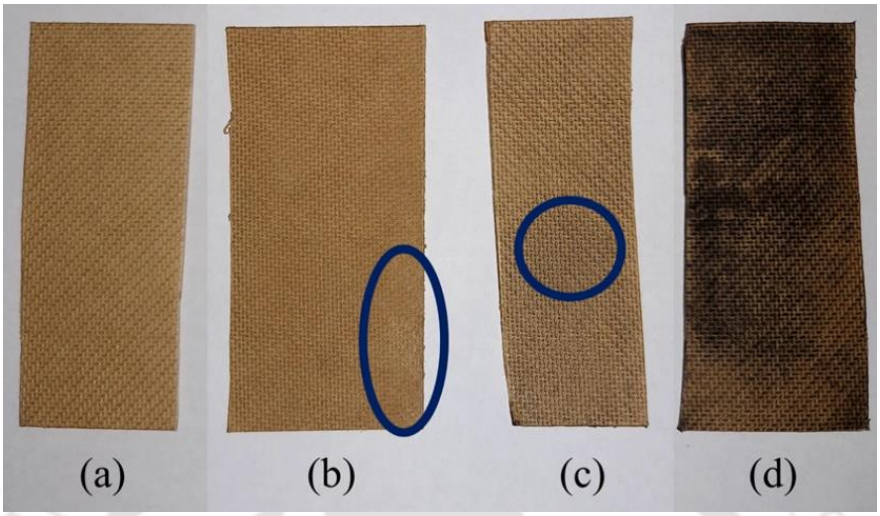

Figure 5.5: (a) Dried fresh pressboard (b) Pressboard aged in MO-Al_2O_3 NF (c) Pressboard aged in MO-CuO NF and (d) Pressboard aged in MO-Fe_3O_4 NF.

5.3. Non-intrusive and non-destructive technique for condition assessment of VO and BOs

The BOs prepared in Section 3.2.1 are tested using the non-intrusive and non-destructive condition assessment technique setup to check its applicability. The fresh and oxidative aged oil samples are shown in Figure 5.6 and their corresponding codes are in Table 5.2. The MC and TAN of all oils are tested according to ASTM D1533 and IEC 62021 standards respectively and the results are presented in Table 5.3. The TAN and MC in the fresh oils increase with an increase in ester content from A1 to E1. However, the increase in MC and TAN in the aged oils from A2 to E2 is not linear due to the presence of esters in various ratios and their response to the aging in terms of the amount of by-products produced.

Table 5.2: Samples of blended oils.

Fresh sample	Sample code	Oxidative aged sample	Sample code
MO	A1	MO	A2
MO- FR3 (3:1)	B1	MO- FR3 (3:1)	B2
MO- FR3 (1:1)	C1	MO- FR3 (1:1)	C2
MO- FR3 (1:3)	D1	MO- FR3 (1:3)	D2
FR3	E1	FR3	E2

TH-3272_186151014

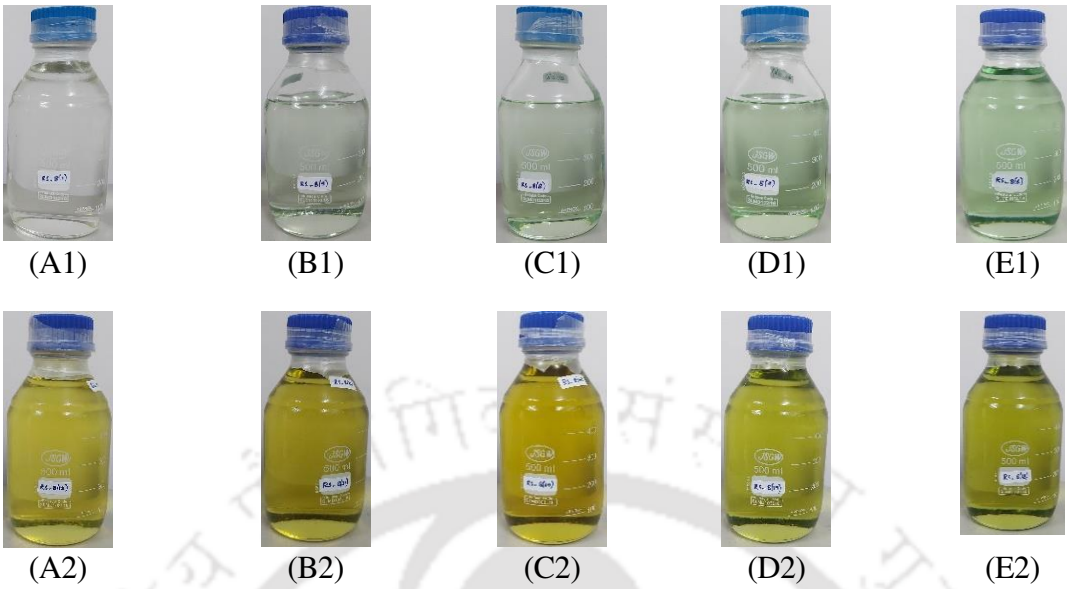

Figure 5.6: Hermetically sealed fresh and oxidative aged liquid insulation samples.

The frequency responses of the fresh and aged oils obtained by testing the oil samples using the non-intrusive and non-destructive condition assessment technique are shown in Figures 5.7 and 5.8 respectively. The reflection of the signal from the oil increases proportionally with the increase in the MC and TAN at their corresponding resonant frequencies. The frequency response of aged oils is found to be differing and irregular for the samples D2 and E2 due to the exceedingly greater amounts of MC and TAN present in them.

Table 5.3: MC and TAN in blended oils.

Sample	MC	TAN
A1	12	0.012
B1	38.3	0.0175
C1	71.1	0.0255
D1	91.5	0.0285
E1	99.2	0.0352
A2	29.9	0.025
B2	72.8	0.063
C2	112.9	0.082
D2	163.2	0.141
E2	316.4	0.254

TH-3272_186151014

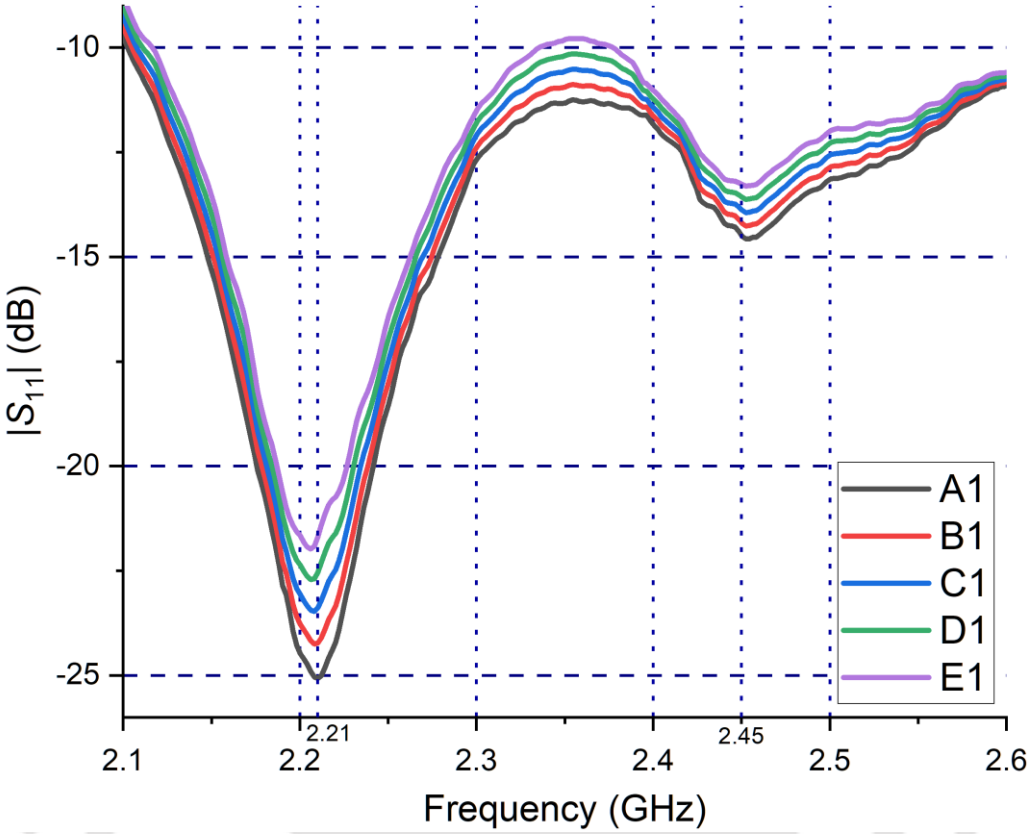

Figure 5.7: Frequency response analysis of fresh MO, FR3 and their BOs.

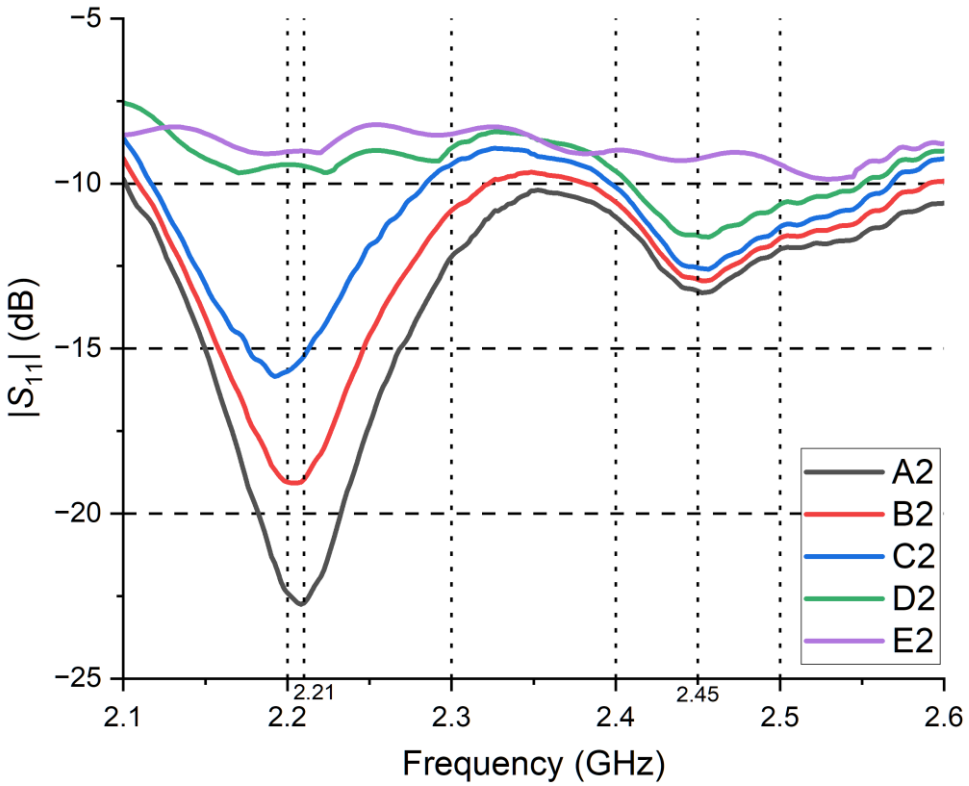

Figure 5.8: Frequency response analysis of aged MO, FR3 and their BOs.

TH-3272_186151014

5. The non-intrusive and non-destructive technique for condition assessment of alternate liquid insulating oils

The linear prediction graphs for MC and TAN presented in Figures 2.9 and 2.10 are used to compare the $|S_{11}|$ data corresponding to the first and second resonance points obtained from the frequency response of BOs to predict their MC and TAN. The percentage error between the estimated and measured values is calculated and shown in Table 5.4.

Table 5.4: Predicted and measured MC and TAN in MO, EO, and BOs.

Sample	TAN (mg KOH/g)			MC (ppm)		
	Predicted value	Measured value	% error	Predicted value	Measured value	% error
A1	0.0126	0.0126	0	12.4	12.4	0
B1	0.0176	0.0175	0.56	29	38.3	24.28
C1	0.0246	0.0255	3.52	65	71.1	8.57
D1	0.0278	0.0285	2.45	79	91.5	13.72
E1	0.0327	0.0352	7.10	90	99.2	9.27
A2	0.0262	0.0259	1.14	37	29.9	18.91
B2	0.0612	0.0631	3.01	90	72.8	19.11
C2	0.0725	0.0820	11.58	120	112.9	5.91
D2	NoP	0.141	NoP	170	163.2	4
E2	NoP	0.254	NoP	NoP	316.4	NoP

NoP = No prediction

There is no prediction error for sample A1 since the prediction graphs are trained on the fresh MO sample. The prediction of TAN is accurate at lower magnitudes and the error increases with an increase in the magnitude. However, for MC, the prediction is accurate at higher magnitudes which implies a reduction in error with an increase in MC. The average errors in the prediction of TAN and MC in BOs are found to be 3.26% and 11.53%, respectively. Good accuracy in the prediction of MC and TAN in BO samples is possible because of the dependency of the frequency response only on the MC and TAN rather than the composition of the oil sample or the structure of the oil molecule. Therefore, the linear graphs developed for MO in Chapter 2 are also suitable for predicting MC and TAN in the EO and BOs. However, the applicability of the technique and linear graphs for aged oil samples with MC and TAN above 300 ppm and 0.085 mg KOH/g is limited by the overwhelming reflection from the oil samples due to excessive contaminants.

TH-3272_186151014

5.4. Summary of the chapter

In this chapter, the proposed non-intrusive and non-destructive technique in Chapter 2 is applied to the MO-NFs, VO-NFs, VOs, and BOs for predicting the MC and TAN present in them. The following conclusions are drawn from this chapter:

- Each NF has a different frequency response compared to its base oil despite having the same MC and TAN.
- The application of the proposed technique in the assessment of NFs is limited by the adherence of NPs to the solid insulation, copper strips, and the walls of the beaker during the aging process.
- The linear graphs for MC and TAN developed in Chapter 2 are also suitable for estimating MC and TAN in EO and BOs.
- The average errors in the prediction of TAN and MC in BOs are found to be 3.26% and 11.53%, respectively.
- The applicability of the technique and linear graphs for aged oil samples with MC and TAN above 300 ppm and 0.085 mg KOH/g is limited by the overwhelming reflection from the oil samples due to excessive contaminants.

Considering the applicability of the developed technique and the linear prediction graphs for estimating the MC and TAN in MO, EO, and BOs and its good prediction accuracy, the non-intrusive and non-destructive technique proves to be a potential alternative condition assessment technique that provides two chemical parameters almost immediately.

Note: This work has been awarded the 2022 IEEE DEIS Graduate Student Fellowship.

TH-3272_186151014

6

Conclusion and Future Work

Contents

6.1	**Summary of the present work**	**113**
6.2	**Contribution of the thesis**	**115**
6.3	**Suggestions for future research work**	**115**

TH-3272_186151014

6.1. Summary of the present work

This thesis presents a novel condition assessment technique that can simultaneously detect the moisture and acid content in a liquid insulation sample and generate a unique response based on the amount of moisture and acid present in it. The technique is found to be suitable for detecting the moisture and acid in mineral oil, ester oil, and mineral-ester BOs.

In Chapter 2, a non-intrusive and non-destructive setup, which comprises an S-band horn antenna placed over the test cell filled with an insulating oil sample, is placed in an anechoic chamber to avoid external noises such as EMI from various sources. A radio frequency signal in the band of 2.1 to 2.6 GHz is passed onto the test sample, and the amount of reflected signal is collected by the antenna connected through a vector network analyzer. The chosen frequency band shows two resonant points corresponding to the TAN and MC of the test sample. Multiple fresh insulating oil samples with different acids are tested to confirm the same. Further, numerous laboratory aged samples are prepared by thermal and oxidative aging MO and tested with the developed setup. It is found that the amount of signal reflected back from the oil at the first and second resonant frequencies is dependent on the TAN and MC in it. The actual TAN and MC in the oil samples are tested according to ASTM D1533 and IEC 62021 respectively using the conventional apparatus. The reflection coefficient obtained from testing of the laboratory aged samples is used to generate individual linear prediction graphs for both TAN and MC. Further, TAN and MC in any unknown sample can be predicted by obtaining the reflection coefficient of the sample and comparing it to the linear prediction graphs. To validate the concept, insulating oil samples from the service transformers of IIT Guwahati and ASEB are procured and the reflection coefficient of these oil samples is obtained using the developed setup. The TAN and MC of these transformer oil samples are predicted by comparing the reflection coefficient with linear prediction graphs. In addition, all these samples are conventionally tested for TAN and MC by following ASTM D1533 and IEC 62021 standards. The actual and predicted values are compared and the percentage error is calculated. The TGA of aged solid insulation samples is performed and it is found that merely performing TGA will not provide precise information on the aging status of the solid insulation.

In Chapter 3, multiple BOs are prepared by mixing MO and a commercial natural ester FR3 in various ratios and their physiochemical as well as electrical properties such as moisture, AC BDV, DDF, RP, specific resistance, density, flash and fire points are studied according to ASTM D1533, D1816, D924, D1169, D1298, D93, and D971 respectively. In addition, to evaluate their long-term performance, the oils are oxidative aged according to ASTM D1934,

TH-3272_186151014

and all the above characteristics are studied. The change in the properties of BOs is correlated to the variation in ester content. Further, PD in these oils is studied by subjecting the samples to electrical stress in accordance with IEC 60270. For this purpose, a test cell with a needle plane electrode system containing nylon nuts and bolts is used to fasten the connections at HV and ground electrodes in order to avoid corona at the junctions and ensure the PD is certainly due to the needle. The experiments are performed in a temperature and humidity controlled EMI free room. PDIV and PDEV of the samples are interpreted according to IEC 60270 and IEC TR 61294. The PRPD and minimum phase angle at which PDIV occurs are also analyzed to conclude that the EOs have better PDIV and PDEV compared to MO and BOs among fresh oils. However, an equal mixed ratio of MO and FR3 has better PDIV and PDEV among the aged oils. Furthermore, DG in the fresh and aged oils is studied by subjecting them to multiple electrical sparks. The DGs are used to predict the type and intensity of faults using various ratios and graphical methods. Among all the methods, the graphical methods are found to be suitable for predicting the type and intensity of electrical faults in BOs. The above studies show that retrofilling a MO based transformer with FR3 or BOs does not pose any danger to its operation. In addition, it provides better electrical and physiochemical characteristics. Further, the surface roughness of the solid insulation thermally aged in ester oil is studied. It is observed that the gelling occurs on the surface of solid insulation which potentially rescues the solid insulation from moisture and damage.

In Chapter 4, NFs are studied for their thermal conductivity by varying the NP concentration and temperature. It is found that the thermal conductivity increases in both cases. The electric field distribution around various types of NPs is simulated using COMSOL, and it is found that the least distortion of the electric field occurs when insulating NP is used. The dielectric frequency response of NFs is studied by varying the insulating NP concentration and the dielectric losses are found to reduce with the increase in NP concentration. Later, a 0.01 %w/v of various NPs is added to MO and VO individually to prepare multiple NFs. The prepared NFs are studied for their magnetic behaviour by subjecting them to quasi-static and dynamic magnetic fields using VSM and ESR spectrometers. The parameters such as magnetic susceptibility, Lande's *g* factor, peak-to-peak line width, resonance flux density, and spin-spin relaxation time are extracted from the magnetic studies. Finally, a conjecture on the benefits of using VO and a few NFs over MO in terms of their magnetic behaviour is presented.

Chapter 5 presents the applicability of the non-intrusive and non-destructive condition assessment technique and the linear prediction graphs for NFs, VO, and BOs. The NFs, VO, and BOs prepared in Chapters 3 and 4 are tested using the experimental setup developed in

TH-3272_186151014

Chapter 2, and the results are presented. The applicability of the non-intrusive and non-destructive condition assessment technique for the NFs is limited by the challenges faced in aging the NFs. The analysis of the reflection coefficient of BOs shows that the technique and linear graphs developed for MO in Chapter 2 are also suitable for predicting the MC and TAN in EO and BOs. The average errors in the prediction of TAN and MC in BOs are found to be 3.26% and 11.53%, respectively. However, the applicability of the technique and linear graphs for aged oil samples with MC and TAN above 300 ppm and 0.085 mg KOH/g is limited by the overwhelming reflection from the oil samples due to excessive contaminants. Therefore, the non-intrusive and non-destructive technique proves to be a potential alternative condition assessment technique that provides two chemical parameters almost immediately.

6.2. Contribution of the thesis

The major contributions of the thesis to the development of a non-intrusive and non-destructive technique for condition assessment of transformer liquid insulation are as follows:

- An EMI free, compact, rapid responsive test setup is developed and tested on various laboratory aged MO samples to construct individual prediction graphs to predict MC and TAN in various service aged MO samples.
- Mixtures of MO and FR3 are studied for various electrical and physiochemical properties and found to be suitable for usage in MO based transformers.
- Various NFs prepared from different NPs are studied for their magnetic behaviour and several magnetic parameters are deduced from the studies.
- The EMI free, compact, rapid responsive test setup developed for MO is used to test the NFs, VO, and BOs and is found to be suitable for detecting MC and TAN in alternate insulating oils.

6.3. Suggestions for future research work

The suggestions for future research are as follows:

- Machine learning models may be applied to the frequency response curves obtained from antenna analysis to replace the linear prediction graphs.
- The accuracy of prediction in samples may be improved by aging the samples simultaneously with thermal and electrical stress. Such multi-stress aging bestows one step closer to the representation of the in-service transformer aging phenomena.
- Various analyses on kraft paper can be explored that can be used in conjunction with TGA to predict its aging status accurately.

TH-3272_186151014

- The effect of transformer construction materials on the short and long-term performance of BOs can be explored.
- The surface discharge characteristics of various solid insulations immersed in BOs can be a topic of research.
- Nanofluids of BOs can be studied extensively for their electrical, physiochemical properties and dissipation factor.
- The stability of NFs and their adsorption to the transformer construction materials is also a challenging issue that can be addressed.
- The effect of NFs on the stray gassing behaviour of the EO and BOs can also be explored.
- Low temperature partial discharge behaviour of the mixed insulating oils needs to be studied to understand any detrimental effects of partial discharges during the start of the transformer in cold regions.
- A potential connection of PD and DGA with the frequency response can be investigated to improve the reliability of insulation diagnosis.
- A potential connection of multiple parameters such as IFT, DDF, and specific resistance with the frequency response can also be explored.

TH-3272_186151014

Bibliography

[1] T. O. Rouse, "Mineral insulating oil in transformers," *IEEE Electr. Insul. Mag.*, vol. 14, no. 3, pp. 6-16, May-June 1998, doi: 10.1109/57.675572.

[2] C. Krause, "Power transformer insulation – history, technology and design," *IEEE Trans Dielectr. Electr. Insul.*, vol. 19, no. 6, pp. 1941-1947, Dec. 2012, doi: 10.1109/TDEI.2012.6396951.

[3] D. M. Nail and P. H. Shoun, "Retrofilling" - a technique to reduce polychlorinated biphenyls (pcb's)," *IEEE Pow. Eng. Rev.*, vol. 4, no. 3, pp. 26-26, March 1984.

[4] I. Webber, D. B. Pilgrim and M. A. Thompson, "The safe disposal of polychlorinated biphenyls," *IEEE Trans. Ind. Appl.*, vol. IA-20, no. 1, pp. 159-166, Jan. 1984.

[5] S. K. Das, S. U. S. Choi, W. Yu, T. Pradeep, *Nanofluids: Science and Technology*, John Wiley & Sons, Inc., New Jersey, USA, 2008.

[6] Y. Xuan and Q. Li, "Heat transfer enhancement of nanofluids," *Int. J. Heat and Fluid Flow*, vol. 21, no. 1, pp. 58-64, Feb. 2000.

[7] C. Choi, H. S. Yoo and J. M. Oh, "Preparation and heat transfer properties of nanoparticle in transformer oil dispersions as advanced energy-efficient coolants," *Curr. Appl. Phy*., vol. 8, no. 6, pp. 710-712, Oct. 2008.

[8] T.J. Lewis, "Nanometric dielectrics," *IEEE Trans. Dielectr. Electr. Insul.*, Vol. 1, no. 5, pp. 812-825, Oct. 1994.

[9] I. Fofana, "50 Years in the Development of Insulating Liquids," *IEEE Electr. Insul. Mag.*, vol. 29, no. 5, pp. 13–25, Sept.-Oct. 2013.

[10] C. Rakesh and M. J. Thomas, "Pongamia oil, an eco-friendly alternative for mineral oil used in high voltage transformers," in *Proc. 2016 IEEE Int. Conf. Dielectr. ICD 2016*, 2016, pp. 959–962.

[11] M. Martins, "Vegetable oils, an alternative to mineral oil for power transformers-experimental study of paper aging in vegetable oil versus mineral oil," *IEEE Electr. Insul. Mag.*, vol. 26, no. 6, pp. 7–13, Nov.-Dec. 2010.

[12] R. A. Farade, N. I. B. A. Wahab, D. A. Mansour, N. B. Azis, J. Jasni, N. R. Banapurmath, and M. E. M. Soudagar, "Investigation of the Dielectric and Thermal Properties of Non-Edible Cottonseed Oil by Infusing h-BN Nanoparticles," *IEEE Access*, vol. 8, pp. 76204–76217, 2020.

[13] M. A. G. Martins, "Correction to "Vegetable Oils, an Alternative to Mineral Oil for Power Transformers–Experimental Study of Paper Aging in Vegetable Oil Versus Mineral Oil"," *IEEE Electr. Insul. Mag.*, vol. 27, no. 1, pp. 46-46, Jan.-Feb. 2011.

TH-3272_186151014

[14] H. M. Wilhelm, M. B. C. Stocco, L. Tulio, W. Uhren, and S. G. Batista, "Edible natural ester oils as potential insulating fluids," *IEEE Trans. Dielectr. Electr. Insul.,* vol. 20, no. 4, pp. 1395–1401, Aug. 2013.

[15] A. K. Das, D. C. Shill, and S. Chatterjee, "Potential of coconut oil as a dielectric liquid in distribution transformers," *IEEE Electr. Insul. Mag.*, vol. 36, no. 6, pp. 36–46, Nov.-Dec. 2020.

[16] U. M. Rao, I. Fofana, R. Sarathi, *Alternative Liquid Dielectrics for High Voltage Transformer Insulation Systems: Performance Analysis and Applications*, IEEE-Wiley, New Jersey, USA, 2022.

[17] N. Beltrán, E. Palacios, and G. Blass, "Potential of Jatropha curcas oil as a dielectric fluid for power transformers," *IEEE Electr. Insul. Mag*., vol. 33, no. 2, pp. 8–15, Mar.-Apr. 2017.

[18] J. Carcedo, I. Fernandez, A. Ortiz, F. Delgado, C. J. Renedo, and A. Arroyo, "Quantitative study on the aging of kraft paper in vegetable oils," *IEEE Electr. Insul. Mag.*, vol. 32, no. 6, pp. 29–35, Nov.-Dec. 2016.

[19] R. Saidur, K. Y. Leong, H. A. Mohammad, "A review on applications and challenges of nanofluids," *Renewable and Sustain. Energy Rev*., vol. 15, no. 3, pp. 1646–1668, Apr. 2011.

[20] D. Wen and Y. Ding, "Natural convective heat transfer of suspensions of titanium dioxide nanoparticles (nanofluids)," *IEEE Trans. Nanotech*., vol. 5, no. 3, pp. 220-227, May 2006.

[21] L. Yu and D. Liu, "Study of the thermal effectiveness of laminar forced convection of nanofluids for liquid cooling applications," *IEEE Trans. Compon., Packag. And Manufacturing Techno*., vol. 3, no. 10, pp. 1693-1704, Oct. 2013.

[22] D. Liu, Y. Zhou, Y. Yang, L. Zhang and F. Jin, "Characterization of high performance AlN nanoparticle-based transformer oil nanofluids," *IEEE Trans. Dielectr. Electr. Insul*., vol. 23, no. 5, pp. 2757-2767, Oct. 2016.

[23] H. B. H. Sitorus, A. Beroual, R. Setiabudy, and S. Bismo, "Pre-breakdown phenomena in new vegetable oil - Based jatropha curcas seeds as substitute of mineral oil in high voltage equipment," *IEEE Trans. Dielectr. Electr. Insul*., vol. 22, no. 5, pp. 2442–2448, Oct. 2015.

[24] P. Trnka, V. Mentlik, and M. Svoboda, "Ecologically acceptable insulating liquids for electrical appliances," in *Proc. 2014 IEEE 18th Int. Conf. Dielectr. Liq. ICDL 2014*, 2014, pp. 3–6.

TH-3272_186151014

[25] B. X. Du and X. L. Li, "Dielectric and thermal characteristics of vegetable oil filled with BN nanoparticles," *IEEE Trans. Dielectr. Electr. Insul*., vol. 24, no. 2, pp. 956–963, Apr. 2017.

[26] S. Ab Ghani, Z. A. Noorden, N. A. Muhmad, H. Zainuddin, M. A. Talib, "A Review on the Reclamation Technologies for Service-Aged Transformer Insulating Oils," *Indonesian J. Electr. Eng. And Comp. Sci*., vol. 10, no. 2, pp. 426-435, May 2018.

[27] S. Chakravorti, D. Dey, B. Chatterjee, *Recent Trends in the Condition Monitoring of Transformers*, Springer, London, UK, 2013.

[28] T. K. Saha, P. Purkait, *Transformer Ageing: Monitoring and Estimation Techniques*, IEEE-Wiley, New Jersey, USA, 2017.

[29] M. Schaible, "Electrical insulating papers – an overview," *IEEE Electr. Insul. Mag*., vol. 3, no. 1, pp. 8–12, Jan. 1987.

[30] T. V. Oommen, "Vegetable oils for liquid-filled transformers," *IEEE Electr. Insul. Mag*., vol. 18, no. 1, pp. 6-11, Jan.-Feb. 2002.

[31] T. S. Ramu, H. N. Nagamani, *Partial Discharge based Condition Monitoring of High Voltage Equipment*, New Age International Publishers, New Delhi, India, 2010.

[32] J. Li, Z. Zhang, S. Grzybowski, and M. Zahn, "A new mathematical model of moisture equilibrium in mineral and vegetable oil-paper insulation," *IEEE Trans. Dielectr. Electr. Insul*., vol. 19, no. 5, pp. 1615–1622, Oct. 2012.

[33] C. Perrier, M. Marugan, and A. Beroual, "DGA comparison between ester and mineral oils," *IEEE Trans. Dielectr. Electr. Insul.*, vol. 19, no. 5, pp. 1609–1614, Oct. 2012.

[34] M. Jovalekic, D. Vukovic, and S. Tenbohlen, "Dissolved Gas Analysis of Alternative Dielectric Fluids," in *IEEE Int. Conf. on Dielectr. Liq. (ICDL),* 2011, pp. 2–5.

[35] Z. Wang, X. Yi, J. Huang, J. Hinshaw, and J. Noakhes, "Fault gas generation in natural-ester fluid under localized thermal faults," *IEEE Electr. Insul. Mag*., vol. 28, no. 6, pp. 45–56, Nov.-Dec. 2012.

[36] D. Martin, N. Lelekakis, and V. Davydov, "Preliminary Results for Dissolved Gas Transformer," *IEEE Electr. Insul. Mag.*, vol. 26, no. 5, pp. 41–48, Sept.-Oct. 2010.

[37] N. V. Dung and H. L. Huong, "The effect of antioxidants on the physical and chemical properties of rice oil, corn oil, peanut oil and Kraft paper," *IEEE Trans. Dielectr. Electr. Insul*., vol. 27, no. 5, pp. 1698–1706, Oct. 2020.

[38] M. A. Talib, N. A. Muhamad, Z. A. Malek, and B. T. Phung, "Fault identification of in-service power transformer using depolarization current analysis," *Int. J. Electr. Comput. Eng*., vol. 7, no. 2, pp. 559–567, Apr. 2017.

TH-3272_186151014

[39] W. M. S. C. Samarasinghe, J. R. S. S. Kumara, M. A. R. M. Fernando, and A. U. A. W. Gunawardena, "Aging assesment of transformer pressboard insulation by micro-strip ring resonator at GHz frequencies," *IEEE Trans. Dielectr. Electr. Insul.*, vol. 24, no. 3, pp. 1923-1930, June 2017.

[40] A. P. Gregory and R. N. Clarke, "A review of RF and microwave techniques for dielectric measurements on polar liquids," *IEEE Trans. Dielectr. Electr. Insul.*, vol. 13, no. 4, pp. 727-743, Aug. 2006.

[41] S. I. Al-Mously and A. Y. Ahmed, "An alternative test for evaluating transformer-oil deterioration using microwaves," in *1999 Asia Pacific Microwave Conf. APMC'99. Microwaves Enter the 21st Century. Conf. Proc. (Cat. No.99TH8473)*, 1999, pp. 884-887.

[42] A. H. El-Hag, N. Qaddoumi, R. Mourtada, E Murawwi, A. Nimer, K. AlMazam, M. Hirzallah, and A. Huwair, "Multi-purpose RF antenna for partial discharge and oil quality monitoring," in *2013 3rd Int. Conf. Electr. Pow. Energy Conversion Sys.,* 2013, pp. 1-5.

[43] M. Siegel, M. Beltle, S. Tenbohlen, and S. Coenen, "Application of UHF sensors for PD measurement at power transformers," *IEEE Trans. Dielectr. Electr. Insul.*, vol. 24, no. 1, pp. 331-339, Feb. 2017.

[44] M. A. Benaissa, A. Mokraoui and H. Moulai, "Development of a microstrip antenna for dielectric constant measurement in liquid insulations," in *2017 IEEE 19th Int. Conf. Dielectr. Liq. (ICDL),* 2017, pp. 1-5.

[45] M. A. Benaissa, A. Mokraoui, H. Moulai, and O. Idir, "Microwave-based sensor for power transformers' insulation oil monitoring," *IET Sci. Meas. & Technol.,* vol. 13, no. 7, pp. 1068-1074, Sept. 2019.

[46] W. S. Zaengl, "Dielectric spectroscopy in time and frequency domain for HV power equipment. I. Theoretical considerations," *IEEE Electr. Insul. Mag.*, vol. 19, no. 5, pp. 5-19, Sept.-Oct. 2003.

[47] W. M. S. C. Samarasinghe, J. R. S. S. Kumara, M. A. R. M. Fernando, A. C. M. Ahamed, and A. U. A. W. Gunawardena, "Moisture estimation of transformer pressboard by micro-strip ring resonator at GHz frequencies," *IEEE Trans. Dielectr. Electr. Insul.*, vol. 23, no. 3, pp. 1409-1417, June 2016.

[48] U. M. Rao, I. Fofana, A. Betie, M. L. Senoussaoui, M. Brahami, and E. Briosso, "Condition monitoring of in-service oil-filled transformers: Case studies and experience," *IEEE Electr. Insul. Mag*., vol. 35, no. 6, pp. 33-42, Nov.-Dec. 2019.

TH-3272_186151014

[49] M. Fischer, S. Tenbohlen, M. Schafer and R. Haug, "Determining power transformers' sequence of service in power grids," *IEEE Trans. Dielectr. Electr. Insul.,* vol. 18, no. 5, pp. 1789-1798, Oct. 2011.

[50] CIGRE Task Force 15.01.09: "Dielectric response methods for diagnostics of power transformers," *IEEE Electr. Insul. Mag.,* vol. 19, no. 3, pp. 12-18, May-June 2003.

[51] B. Kapilevich, A. Lipsky and B. Litvak, "On-line testing transformer oil using microwaves," in *2010 IEEE 26th Convention Electr. and Electron. Eng. Israel*, 2010, pp. 000006-000008.

[52] M. Maharana, N. Baruah, S. K. Nayak, N. Meher and P. K. Iyer, "Condition Assessment of Aged Ester-Based Nanofluid Through Physicochemical and Spectroscopic Measurement," *IEEE Trans. Instrum. Meas.,* vol. 68, no. 12, pp. 4853-4863, Dec. 2019.

[53] N. Baruah, S. S. Dey and S. K. Nayak, "Evaluation of dissolved gas analysis and long-term performance of non-edible natural ester," *IEEE Trans. Dielectr. Electr. Insul.*, vol. 27, no. 5, pp. 1561-1569, Oct. 2020.

[54] *IEEE Guide for Acceptance and Maintenance of Insulating Mineral Oil in Electrical Equipment*, IEEE Std C57.106-2015.

[55] *IEEE Guide for the Reclamation of Mineral Insulating Oil and Criteria for Its Use*, IEEE Std C57.637-2015.

[56] *IEEE Guide for Loading Mineral-Oil-Immersed Transformers and Step-Voltage Regulators*, IEEE Std C57.91-2011.

[57] *Standard Test Method for Oxidative Aging of Electrical Insulating Liquids by Open-Beaker Method*, ASTM Std D1934-20.

[58] *Standard Practices for Sampling Electrical Insulating Liquids*, ASTM Std D923-15.

[59] S. Ingebrigtsen, M. Dahlund, W. Hansen, D. Linhjell, L. E. Lundgaard, "Solubility of carboxylic acids in paper (Kraft)-oil insulation systems" *The 17th Annual Meeting of the IEEE Lasers and Electro-Optics Society, 2004. LEOS 2004.*, 2004, pp. 253-257.

[60] N. Lelekakis, J. Wijaya, D. Martin, and D. Susa, "The effect of acid accumulation in power-transformer oil on the aging rate of paper insulation," *IEEE Electr. Insul. Mag.*, vol. 30, no. 3, pp. 19-26, May-June 2014.

[61] L. E. Lundgaard, W. Hansen, D. Linhjell, and T. J. Painter, "Aging of oil-impregnated paper in power transformers," *IEEE Trans. Pow. Del.,* vol. 19, no. 1, pp. 230-239, Jan. 2004.

[62] *IEEE Guide for Dielectric Frequency Response Test*, IEEE Std C57.161-2018.

TH-3272_186151014

[63] M. L. Rao, S. R. Sedlmayr, R. Roy and J. Kanzius, “Polarized microwave and RF radiation effects on the structure and stability of liquid water,” *Current Sci.*, vol. 98, no. 11, pp. 1500–1504, Jun. 2010.

[64] D. F. Garcia, R. Villarroel, B. Garcia and J. C. Burgos, "A review of moisture diffusion coefficients in transformer solid insulation - Part 2: Experimental validation of the coefficients," *IEEE Electr. Insul. Mag.,* vol. 29, no. 2, pp. 40-49, Mar.-Apr. 2013.

[65] Y. E. Sari, A. D. S. Ritonga and Suwarno, "Comparative Study of Kraft Paper Aged in Natural Ester with XRD and TG/DTG Analysis," in *2019 Int. Conf. Electr. Eng. Informatics (ICEEI)*, 2019, pp. 564-569.

[66] Elmer, Perkin. "Thermogravimetric analysis (TGA) a beginners guide." United States of America: Perkin Elmer (2010).

[67] D. F. Garcia, B. Garcia, J. C. Burgos and N. G. Hernando, "Experimental determination of the diffusion coefficient of water in transformer solid insulation," *IEEE Trans. Dielectr. Electr. Insul*., vol. 19, no. 2, pp. 427-433, Apr. 2012.

[68] M. Maharana, S. K. Nayak and N. Sahoo, "Karanji oil as a potential dielectrics liquid for transformer," *IEEE Trans. Dielectr. Electr. Insul.*, vol. 25, no. 5, pp. 1871–1879, Oct. 2018.

[69] U. M. Rao, I. Fofana and E. R. Celis, "Liquid insulation for power transformers," in *Alternative Liquid Dielectrics for High Voltage Transformer Insulation Systems: Performance Analysis and Applications*, Piscataway, NJ, USA: Wiley-IEEE Press, 2021, pp.1-9.

[70] A. Beroual, H. B. H. Sitorus, R. Setiabudy and S. Bismo, "Comparative study of AC and DC breakdown voltages in Jatropha methyl ester oil, mineral oil, and their mixtures," *IEEE Trans. Dielectr. Electr. Insul.*, vol. 25, no. 5, pp. 1831-1836, Oct. 2018.

[71] I. Fofana, V. Wasserberg, H. Borsi and E. Gockenbach, "Retrofilling conditions of high voltage transformers," *IEEE Electr. Insul. Mag*., vol. 17, no. 2, pp. 17-30, Mar.-Apr. 2001.

[72] I. Fofana, V. Wasserberg, H. Borsi and E. Gockenbach, "Challenge of mixed insulating liquids for use in high-voltage transformers.1. Investigation of mixed liquids," *IEEE Electr. Insul. Mag*., vol. 18, no. 3, pp. 18-31, May-June 2002.

[73] G. Dombek and J. Gielniak, "Fire safety and electrical properties of mixtures of synthetic ester/mineral oil and synthetic ester/natural ester," *IEEE Trans. Dielectr. Electr. Insul*., vol. 25, no. 5, pp. 1846-1852, Oct. 2018.

TH-3272_186151014

[74] C. Perrier, A. Beroual and J. Bessede, "Improvement of power transformers by using mixtures of mineral oil with synthetic esters," *IEEE Trans. Dielectr. Electr. Insul.*, vol. 13, no. 3, pp. 556-564, June 2006.

[75] A. Dixit, C. Ekanayake, H. Ma, T. K. Saha and M. H. Ansari, "Thermal Analysis of Natural Cooling Type Distribution Transformer Retrofilled With Natural Ester Oil," *IEEE Trans. Dielectr. Electr. Insul.*, vol. 29, no. 1, pp. 231-239, Feb. 2022.

[76] BHEL, *TRANSFORMERS*, Second. Tata McGraw-Hill Education, 2003.

[77] P. Przybylek, Z. Nadolny and H. Moscicka-Grzesiak, "Bubble effect as a consequence of dielectric losses in cellulose insulation," *IEEE Trans. Dielectr. Electr. Insul.*, vol. 17, no. 3, pp. 913-919, June 2010.

[78] I. Atanasova-Hoehlein, T. Hammer and M. Schaefer, "Diagnostic markers for oxidation of mineral oil and ester insulating fluids," *CIGRE*, Paris, France, ref. D1 - 213, 2010.

[79] *Insulating liquids - Test methods for the determination of interfacial tension of insulating liquids - Determination with the ring method*, IEC 62961, 2018.

[80] C. Mazzetti, M. Pompili and E. O. Forster, "A study of partial discharge measurements in dielectric liquids," *IEEE Trans. Dielectr. Electr. Insul.*, vol. 27, no. 3, pp. 445-450, June 1992.

[81] M. Pompili, C. Mazzetti and R. Bartnikas, "PD pulse burst characteristics of transformer oils," *IEEE Trans. Power Del.*, vol. 21, no. 2, pp. 689-698, Apr. 2006.

[82] Z. Liu, Q. Liu, Z. D. Wang, P. Jarman, Ch. Krause, P. W. R. Smith and A. Gyore, "Partial discharge behaviour of transformer liquids and the influence of moisture content," in *2014 IEEE 18th Int. Conf. Dielectr. Liq. (ICDL)*, Bled, Slovenia, 2014, pp. 1-4.

[83] *High-voltage test techniques - Partial discharge measurements*, IEC 60270, 2015.

[84] E. O. Forster, "Partial discharges and streamers in liquid dielectrics-the significance of the inception voltage," *IEEE Trans. Dielectr. Electr. Insul.*, vol. 28, no. 6, pp. 941-946, Dec. 1993.

[85] *Insulating liquids - Determination of the partial discharge inception voltage (PDIV) - Test procedure*, IEC TR 61294, 1993.

[86] M. Pompili, C. Mazzetti and R. Bartnikas, "Simultaneous ultrawide and narrowband detection of PD pulses in dielectric liquids," *IEEE Trans. Dielectr. Electr. Insul.*, vol. 5, no. 3, pp. 402-407, June 1998.

TH-3272_186151014

[87] M. Pompili, C. Mazzetti and R. Bartnikas, "Phase relationship of PD pulses in dielectric liquids under ac conditions," *IEEE Trans. Dielectr. Electr. Insul*., vol. 7, no. 1, pp. 113-117, Feb. 2000.

[88] L. Calcara, M. Pompili, S. Sangiovanni, B. Pfeiffer, T. Renaudin and T. Welfonder, "Advances in Measuring Partial Discharge in Insulating Liquids," in *2019 IEEE 20th Int. Conf. Dielectr. Liq. (ICDL)*, Rome, Italy, 2019, pp. 1-4.

[89] L. Calcara, M. Pompili and F. Muzi, "Standard evolution of Partial Discharge detection in dielectric liquids," *IEEE Trans. Dielectr. Electr. Insul*., vol. 24, no. 1, pp. 2-6, Feb. 2017.

[90] M. Pompili, "Partial discharge development and detection in dielectric liquids," *IEEE Trans. Dielectr. Electr. Insul*., vol. 16, no. 6, pp. 1648-1654, Dec. 2009.

[91] L. Calcara, M. Pompili, M. Baur and J. Knauel, "Partial Discharge Inception Voltage in Liquid Dielectrics and its Definition," in *2021 IEEE Electr. Insul. Conf. (EIC)*, 2021, pp. 165-168.

[92] M. Pompili, C. Mazzetti, M. Libotte and E. O. Forster, "The effect of the definition used in measuring partial discharge inception voltages," *IEEE Trans. Dielectr. Electr. Insul*., vol. 28, no. 6, pp. 1002-1006, Dec. 1993.

[93] L. Calcara, K. J. Rapp, S. Sangiovanni, M. Pompili and A. Sbravati, "Influence of Water Content in Natural Ester Liquids Partial Discharge Inception Voltage," in *2021 IEEE Electr. Insul. Conf. (EIC)*, 2020, pp. 203-206.

[94] C. F. Eyring, S. S. Mackeown, and R. A. Millikan, "Fields Currents from Points," *Phys. Rev.*, vol. 31, no.5, pp. 900-909, May 1928.

[95] M. Jaroszewski and K. Rakowiecki, "Partial discharge inception voltage in transformer natural ester liquid — Effect of the measurement method in the presence of moisture," *IEEE Trans. Dielectr. Electr. Insul.*, vol. 24, no. 4, pp. 2477-2482, Sept. 2017.

[96] M. Pompili, C. Mazzetti and R. Bartnikas, "Comparative PD pulse burst characteristics of transformer type natural and synthetic ester fluids and mineral oils," *IEEE Trans. Dielectr. Electr. Insul*., vol. 16, no. 6, pp. 1511-1518, Dec. 2009.

[97] C. Thirumurugan, G. B. Kumbhar and R. Oruganti, "Surface Discharge Characteristics of Different Solid–Liquid Insulation Materials in Power Transformers," *IEEE Trans. Plasma Sci*., vol. 47, no. 11, pp. 5013-5022, Nov. 2019.

[98] T. Tanaka, "Internal Partial Discharge and Material Degradation," *IEEE Trans. Dielectr. Electr. Insul.*, vol. EI-21, no. 6, pp. 899-905, Dec. 1986.

TH-3272_186151014

[99] M. Pompili, C. Mazzetti and R. Bartnikas, "Partial discharge pulse sequence patterns and cavity development times in transformer oils under AC conditions," *IEEE Trans. Dielectr. Electr. Insul*., vol. 12, no. 2, pp. 395-403, Apr. 2005.

[100] *IEEE Guide for the Interpretation of Gases Generated in Oil-Immersed Transformers*, IEEE Standard C57.104, 2008.

[101] *IEEE Guide for the Interpretation of Gases Generated in Natural Ester and Synthetic Ester-Immersed Transformers*, IEEE Standard C57.155, 2014.

[102] L. C. Aicher, J. P. Vora, "Gas analysis – a transformer diagnostic tool," *Allis Chalmers Electr. Rev*., vol. 28, no. 1, pp. 22-24, 1963.

[103] I. Fofana, J. Sabau, D. Bussieres and E. B. Robertson, "The mechanism of gassing in power transformers," in *2008 IEEE Int. Conf. Dielectr. Liq. (ICDL)*, 2008, pp. 1-4.

[104] *Standard Test Method for Analysis of Gases Dissolved in Electrical Insulating Oil by Gas Chromatography*, ASTM Standard D3612, 2017.

[105] I. Atanasova-Höhlein and C. Schütt, "Gas-in-oil analysis and evaluation criteria for synthetic esters in offshore and traction transformers," *IEEE Electr. Insul. Mag*., vol. 36, no. 6, pp. 31-35, Nov.-Dec. 2020.

[106] *Oil-filled electrical equipment – Sampling of gases and analysis of free and dissolved gases – Guidance*, IEC Standard 60567, 2011.

[107] M. Duval, "Dissolved gas analysis: It can save your transformer," *IEEE Electr. Insul. Mag*., vol. 5, no. 6, pp. 22-27, Nov.-Dec. 1989.

[108] *Mineral oil-filled electrical equipment in service – Guidance on the interpretation of dissolved and free gases analysis*, IEC Standard 60599, 2022.

[109] R. R. Rogers, "IEEE and IEC Codes to Interpret Incipient Faults in Transformers, Using Gas in Oil Analysis," *IEEE Trans. Dielectr. Electr. Insul*., vol. EI-13, no. 5, pp. 349-354, Oct. 1978.

[110] B. Fallou, I. Davies, R. R. Rogers, E. H. Reynolds, F. Viale, A. Devaux, R. Fournie, J. Galand, P. Vuarchex, and E. Dornenburg, "Application of physico-chemical methods of analysis to the study of deterioration in the insulation of electrical apparatus," *CIGRE*, Paris, pp. 15-07, 1970.

[111] Imad-U-Khan, Z. Wang, I. Cotton and S. Northcote, "Dissolved gas analysis of alternative fluids for power transformers," *IEEE Electr. Insul. Mag*., vol. 23, no. 5, pp. 5-14, Sept.-Oct. 2007.

TH-3272_186151014

[112] N. A. Gómez, H. M. Wilhelm, C. C. Santos and G. B. Stocco, "Dissolved gas analysis (DGA) of natural ester insulating fluids with different chemical compositions," *IEEE Trans. Dielectr. Electr. Insul.*, vol. 21, no. 3, pp. 1071-1078, June 2014.

[113] F. Scatiggio and M. Pompili, "Evaluation of vegetable ester for filling large power transformers," in *2016 IEEE Int. Conf. Dielectr. (ICD)*, 2016, pp. 1052-1056.

[114] M. -L. Coulibaly, C. Perrier, M. Marugan and A. Beroual, "Aging behavior of cellulosic materials in presence of mineral oil and ester liquids under various conditions," *IEEE Trans. Dielectr. Electr. Insul.,* vol. 20, no. 6, pp. 1971-1976, Dec. 2013.

[115] C. Perrier and A. Beroual, "Experimental investigations on insulating liquids for power transformers: Mineral, ester, and silicone oils," *IEEE Electr. Insul. Mag*., vol. 25, no. 6, pp. 6-13, Nov.-Dec. 2009.

[116] M. Duval, "A review of faults detectable by gas-in-oil analysis in transformers," *IEEE Electr. Insul. Mag.*, vol. 18, no. 3, pp. 8-17, May-June 2002.

[117] M. Duval, "The duval triangle for load tap changers, non-mineral oils and low temperature faults in transformers," *IEEE Electr. Insul. Mag*., vol. 24, no. 6, pp. 22-29, Nov.-Dec. 2008.

[118] H. M. Wilhelm, M. B. C. Stocco, L. Tulio, W. Uhren and S. G. Batista, "Edible natural ester oils as potential insulating fluids," *IEEE Trans. Dielectr. Electr. Insul*., vol. 20, no. 4, pp. 1395-1401, Aug. 2013.

[119] J. Xiang, X. Y. Zhou, Q. Liu, Z. D. Wang, J. Hinshaw and P. Mavrommatis, "Correlation of hydrogen generation with sparking discharges in a mineral insulating oil," *IEEE Electr. Insul. Mag*., vol. 34, no. 3, pp. 7-12, May-June 2018.

[120] I. Atanasova-Höhlein, "Influence of copper on gassing properties of transformer insulating liquids," *IEEE Electr. Insul. Mag*., vol. 35, no. 6, pp. 15-22, Nov.-Dec. 2019.

[121] M. Duval and L. Lamarre, "The Duval pentagon-a new complementary tool for the interpretation of dissolved gas analysis in transformers," *IEEE Electr. Insul. Mag*., vol. 30, no. 6, pp. 9-12, Nov.-Dec. 2014.

[122] U. M. Rao, I. Fofana, P. Rozga, P. Picher, D. K. Sarkar and R. Karthikeyan, "Influence of Gelling in Natural Esters Under Open Beaker Accelerated Thermal Aging," *IEEE Trans. Dielectr. Electr. Insul.*, vol. 30, no. 1, pp. 413-420, Feb. 2023.

[123] B. Garcia, T. Garcia, V. Primo, J. C. Burgos and D. Urquiza, "Studying the loss of life of natural-ester-filled transformer insulation: impact of moisture on the aging rate of paper," *IEEE Electr. Insul. Mag*., vol. 33, no. 1, pp. 15-23, Jan.-Feb. 2017.

TH-3272_186151014

[124] W. Sima, J. Shi, Q. Yang, S. Huang and X. Cao, "Effects of conductivity and permittivity of nanoparticle on transformer oil insulation performance: experiment and theory," *IEEE Trans. Dielectr. Electr. Insul*., vol. 22, no. 1, pp. 380-390, Feb. 2015.

[125] N. Baruah, M. Maharana, and S. K. Nayak, "Performance analysis of vegetable oil-based nanofluids used in transformers," *IET Sci. Meas. Technol*., vol. 13, no. 7, pp. 995-1002, Sept. 2019.

[126] M. Becerra, M. Aljure, A. M. Pourrahimi and F. Roman, "High field conduction in mineral oil based ZnO nanofluids prior to negative streamer inception," *J. Phys. Commun*., vol. 5, no. 4, Art no. 045006, Apr. 2021.

[127] M. H. Esfe and M. Afrand, "An updated review on the nanofluid characteristics," *J. Therm. Anal. Calorim.*, vol. 138, no. 6, pp. 4091-4101, June 2019.

[128] K. V. Wong and O. De Leon, "Applications of nanofluids: current and future," *Adv. Mech. Eng*., vol. 2, pp. 519659, Jan. 2010.

[129] J. Jacob, P. Prabhu, S. T. Krishnan, "Natural Ester Nanofluids as Alternate Insulating Oils for Transformers," in *Alternative Liquid Dielectrics for High Voltage Transformer Insulation Systems: Performance Analysis and Applications*, Wiley-IEEE, 2022, pp.241-271.

[130] D. -E. A. Mansour and E. G. Atiya, "Application of UV/Vis spectroscopy to assess the stability of oil-based nanofluids," in *2016 IEEE Conf. Electr. Insul. Dielectr. Phen. (CEIDP)*, 2016, pp. 671-674.

[131] N. Baruah, M. Maharana, S. S. Dey and S. K. Nayak, "Nanoparticle Polarization Effect on the Permittivity of the Dielectric Liquid," in *2019 IEEE 20th International Conference on Dielectric Liquids (ICDL)*, Roma, Italy, 2019, pp. 1-4.

[132] A. Katiyar, P. Dhar, T. Nandi, L. S. Maganti and S. K. Das, "Enhanced breakdown performance of Anatase and Rutile titania based nano-oils," *IEEE Trans. Dielectr. Electr. Insul.*, vol. 23, no. 6, pp. 3494-3503, Dec. 2016.

[133] M. Maharana, N. Baruah, S. K. Nayak, N. Sahoo, K. Wu, L. Goswami, "Electrohydrodynamics Analysis of Dielectric 2D Nanofluids," *Nanomaterials,* vol. 12, no. 9, pp.1489, Apr. 2022.

[134] J. Blennow, C. Ekanayake, K. Walczak, B. Garcia and S. M. Gubanski "Field experiences with measurements of dielectric response in frequency domain for power transformer diagnostics" *IEEE Trans. Pow. Del*., vol. 21, no. 2, pp. 681-688, Apr. 2006.

TH-3272_186151014

[135] G. Jeong, S. P. Jang, H. Lee, J. Lee, S. Choi and S. Lee, "Magnetic-thermal-fluidic analysis for cooling performance of magnetic nanofluids comparing with transformer oil and air by using fully coupled finite element method," *IEEE Trans. Magn.,* vol. 49, no. 5, pp. 1865-1868, May 2013.

[136] S. Lee and H. Lee, "Numerical and experimental validation to the ability of magnetoconvection to cool vegetable-based transformer oil with magnetic nanoparticles," *IEEE Trans. Magn.,* vol. 55, no. 7, pp. 1-5, July 2019.

[137] W. Guan, M. Jin, Y. Fan, J. Chen, P. Xin, Y. Li, K. Dai, H. Zhang, T. Huang and J. Ruan, "Finite element modeling of heat transfer in a nanofluid filled transformer," *IEEE Trans. Magn.,* vol. 50, no. 2, pp. 253-256, Feb. 2014.

[138] L. P. Dănescu, A. M. Morega, G. Telipan, M. Morega, J. B. Dumitru and V. Marinescu, "Magnetic nanofluid applications in electrical engineering," *IEEE Trans. Magn.,* vol. 49, no. 11, pp. 5489-5497, Nov. 2013.

[139] S. K. Amizhtan, A. J. Amalanathan, R. Sarathi, H. Edin and N. Taylor, "Impact of Magnetic Field on Corona Discharge Behavior of Mineral Oil Under AC Voltage," *IEEE Trans. Dielectr. Electr. Insul*., vol. 29, no. 4, pp. 1417-1424, Aug. 2022.

[140] T. Lewis, "Nanometric dielectrics," *IEEE Trans. Dielectr. Electr. Insul*., vol. 1, no. 5, pp. 812–825, Oct. 1994.

[141] T. Tanaka, M. Kozako, N. Fuse, and Y. Ohki, "Proposal of a multi-core model for polymer nanocomposite dielectrics," *IEEE Trans. Dielectr. Electr. Insul*., vol. 12, no. 4, pp. 669–681, Aug. 2005.

[142] A. Abragam, and B. Bleaney, *Electron Paramagnetic Resonance of Transition Ions,* Oxford, U.K.: Clarendon, 1970.

[143] J. Yang, X. Rong, D. Suter and Y. P. Sun, "Electron paramagnetic resonance investigation of the electron-doped manganite $La_{1-x}Te_xMnO_3$ ($0.1 \leq x \leq 0.2$)," *Phys. Chem. Chem. Phys*., vol. 13, no. 36, pp. 16343-16348, Aug. 2011.

[144] K. Sun, Y. Yang, Y. Liu, Z. Yu, Y. Zeng, W. Tong, X. Jiang, Z. Lan, R. Guo and C. Wu, "Ferromagnetic resonance study on Si/NiO/NiFe films," *IEEE Trans. Magn.*, vol. 51, no. 11, pp. 1-4, Nov. 2015.

[145] E. G. Atiya, D. A. Mansour, R. M. Khattab and A. M. Azmy, "Dispersion behavior and breakdown strength of transformer oil filled with TiO2 nanoparticles," *IEEE Trans. Dielectr. Electr. Insul*., vol. 22, no. 5, pp. 2463-2472, October 2015.

[146] B. Park, T. Kim, K. Lee, R. Kim and D. Hyun, "Magnetic-field analysis on winding disposition of transformer for distributed high-speed train applications," *IEEE Trans. Magn*., vol. 46, no. 6, pp. 1766-1769, June 2010.

TH-3272_186151014

[147] R. Zanella, C. Nore, X. Mininger, F. Bouillault, J-L Guermond, "Numerical study of cooling by ferrofluids in an electrical transformer using an axisymmetric model," *IEEE Trans. Magn.,* vol. 57, no. 7, pp. 1-4, July 2021.

[148] J. M. Martínez-Tarifa, J. Rivas-Conde, G. Robles and J. Sanz-Feito, "Influence of leakage magnetic fields on partial discharge activity in power transformers," *IEEE Trans. Dielectr. Electr. Insul*., vol. 17, no. 6, pp. 1724-1730, Dec. 2010.

[149] P. Poddar, T. Fried, G. Markovich, A. Sharoni, D. Katz, T. Wizansky and O. Millo, "Manifestation of the verwey transition in the tunneling spectra of magnetite nanocrystals," *Europhys. Lett*., vol. 64, no. 1, pp. 98-103, Oct. 2010.

[150] D. A. Mansour, A. M. Elsaeed and M. A. Izzularab, "The role of interfacial zone in dielectric properties of transformer oil-based nanofluids," *IEEE Trans. Dielectr. Electr. Insul*., vol. 23, no. 6, pp. 3364-3372, Dec. 2016.

[151] R. A. Farade, N. I. A. Wahab, D. A. Mansour, N. B. Azis, J. B. Jasni, V. Veerasamy, A. Vinayagam, B. M. Kotiyal and T. M. Y. Khan, "The effect of interfacial zone due to nanoparticle–surfactant interaction on dielectric properties of vegetable oil based nanofluids," *IEEE Access*, vol. 9, pp. 107033-107045, July 2021.

[152] J. G. Hwang, M. Zahn, F. M. O'Sullivan, L. A. Pettersson, O. Hjortstam, and R. Liu, "Effects of nanoparticle charging on streamer development in transformer oil-based nanofluids," *J. of Appl. Phys.*, vol. 107, no. 1, pp. 014310, Jan. 2010.

[153] W. Wei and Z. Wang, "Investigation of magnetic nanoparticle motion under a gradient magnetic field by an electromagnet", *J. of Nanomat*., vol. 2018, Art. 6246917, Mar. 2018.

[154] I. -H. Kim, J. -C. Lee, S. Lee, G. -Y. Jeong and S. -H. Lee, "Power generation using magnetic nanofluids in millimeter-sized channel with in-phase mode of magnetization," *IEEE Trans. Magn*., vol. 51, no. 11, pp. 1-4, Nov. 2015.

[155] M. Zahn, "Magnetic fluid and nanoparticle applications to nanotechnology," *J. Nanopart. Res*., vol. 3, no. 1, pp. 73–78, Feb. 2001.

[156] J. P. Joshi, K. V. Sarathy, A. K. Sood, S. V. Bhat and C. N. R. Rao, "An electron paramagnetic resonance study of electron–hole asymmetry in charge ordered $Pr_{1-x}Ca_xMnO_3$(x= 0.64,0.36)," *J. Phys.: Condens. Matter.*, vol. 16, no. 16, pp. 2869-2878, Apr. 2004.

[157] A. K. Mall, A. Dixit, A. Garg and R. Gupta, "Temperature dependent electron paramagnetic resonance study on magnetoelectric $YCrO_3$," *J. Phys.: Condens. Matter*., vol. 29, no. 49, p. 495805, Nov. 2017.

TH-3272_186151014

[158] N. P. Crook, S. R. Hoon, K. G. Taylor and C. T. Perry, "Electron spin resonance as a high sensitivity technique for environmental magnetism: determination of contamination in carbonate sediments," *Geophys. J. Int*., vol. 149, no. 2, pp. 328-337, May. 2002.

[159] S. Thota, S. C. Kashyap, S. K. Sharma, and V. R. Reddy, "Micro Raman, Mossbauer and magnetic studies of manganese substituted Zinc Ferrite nanoparticles: Role of Mn," *J. Phys.Chem. Solids*., vol. 91, pp. 136-144, Apr. 2016.

[160] M. Deepty, C. Srinivas, E. R. Kumar, N. K. Mohan, C. L. Prajapat, T. V. C. Rao, S. S. Meena, A. K. Verma and D. L. Sastry, "XRD, EDX, FTIR and ESR spectroscopic studies of co-precipitated Mn–substituted Zn–ferrite nanoparticles," *Ceram. Int.*, vol. 45, no. 6, pp. 8037-8044, Apr. 2019.

[161] H. Bayrakdar, O. Yalçın, S. Özüm, and U. Cengiz, "Synthesis and investigation of small g-values for smart spinel ferrite nanoparticles," *J. All. Com*., vol. 869, pp. 159334, Jul. 2021.

[162] V. J. Angadi, L. Choudhury, K. Sadhana, H-L. Liu, R. Sandhya, S. Matteppanavar, B. Rudraswamy, V. Pattar, R. V. Anavekar, K. Praveena, "Structural, electrical and magnetic properties of Sc3+ doped Mn-Zn ferrite nanoparticles," *J. Magn. Magn. Mat*., vol. 424, pp. 1-11, Feb. 2017.

[163] N. Hayakawa, H. Inano, Y. Nakamura and H. Okubo, "Time variation of partial discharge activity leading to breakdown of magnet wire under repetitive surge voltage application," *IEEE Trans. Dielectr. Electr. Insul.,* vol. 15, no. 6, pp. 1701-1706, Dec. 2008.

[164] H. Cheng, P. Zhang, Q. Zhang, J. Wu, Y. Dai, W. Hu and N. M. Wereley, "Effects of surface modification on the stability of suspension and thermal conductivity enhancement of composite Fe nanofluids," *IEEE Trans. Magn.*, vol. 50, no. 11, pp. 1-4, Nov. 2014.

[165] M. G. SAY, *Alternating Current Machines,* PITMAN PUBLISHING LIMITED, 1978.

[166] J. J. Winders, *Transformers Principles and Applications,* MARCEL DEKKER, Inc., 2002.

[167] J. A. C. Forrest and B. Allard, “Thermal problems caused by harmonic frequency leakage fluxes in three-phase, three-winding converter transformers,” *IEEE Trans. Power Del*., vol. 19, no. 1, pp. 208–213, Jan. 2004.

[168] F. Kremer and A. Schönhals, *Broadband Dielectric Spectroscopy,* Springer, 2003.

TH-3272_186151014

List of publications

Patents:

[1] **Rohith Sangineni**, Shashank Satish Kulkarni and Sisir Kumar Nayak, "Design and development of an electromagnetic interference free non-intrusive test setup for condition assessment of insulating oils using antenna" Indian patent application number: 202231013474. (Under Examination)

[2] Manas Chakraborty, **Rohith Sangineni**, Niharika Baruah and Sisir Kumar Nayak, "Sandwiched non-heating filtration process for removal of moisture and Dissolved gases in transformer insulating oils using Metal Organic Framework (MOF)" Indian patent application number: 202231042371. (Under Examination)

[3] Niharika Baruah, **Rohith Sangineni**, Deepak Kanumuri and Sisir Kumar Nayak, "Long term accelerated multi-stress ageing chamber for transformer insulation" Indian patent application number: 202331008919. (Under Examination)

Journals:

[1] **R. Sangineni**, S. K. Nayak and M. Becerra, "A Non-intrusive and Non-destructive Technique for Condition Assessment of Transformer Liquid Insulation," *IEEE Trans. Dielectr. Electr. Insul*., vol. 29, no. 2, pp. 693-700, Apr. 2022.

[2] **R. Sangineni**, S. K. Nayak and M. Becerra, "Magnetic Profiling of Conducting, Semi-conducting, and Insulating Nanoparticles and their Nanofluids Possessing Potential Transformer Application," *IEEE Trans. Dielectr. Electr. Insul*., vol. 30, no. 2, pp. 649-657, Apr. 2023.

[3] **R. Sangineni**, T. Chandrasekaran and S. K. Nayak, " Study of Partial Discharges in Fresh and Oxidative Aged Mineral-Natural Ester Blended Oils," *IEEE Trans. Dielectr. Electr. Insul*., vol. 30, no. 5, pp. 2325-2333, Oct. 2023.

[4] **R. Sangineni**, M. Chakraborty and S. K. Nayak, "Gassing Tendency of Fresh and Oxidative Aged Mixed Insulating Oils on Electric Sparking," *IEEE Trans. Dielectr. Electr. Insul.,* (Accepted for publication).

[5] **R. Sangineni**, N. Baruah, S. K. Nayak, "Analysis of electric field in liquid dielectric on addition of nanoparticles," *Mater. Today: Proc.*, vol. 43, no. 6, pp. 3603-3609, Nov. 2020.

[6] M. Chakraborty, **R. Sangineni**, N. Baruah and S. K. Nayak, "A Sandwich Layer Method for Moisture Extraction in Transformer Insulating Oils Using Metal Organic Frameworks," *IEEE Trans. Instrum. Meas.,* vol. 72, pp. 1-8, July 2023, Art no. 6008108.

[7] N. Baruah, **R. Sangineni**, M. Chakraborty, S. K. Nayak, "Investigation of Natural Ester based Insulating Liquid using Statistical Hypothesis Testing," *IEEJ Trans. Fundam. Mater.*, 2021, Vol. 141, no. 10, pp. 560-566, Oct. 2021.

TH-3272_186151014

List of publications

Textbook chapter:

[1] N. Baruah, **R. Sangineni,** M. Maharana, S. K. Nayak, "Processing and Evaluation of Natural Esters," in *Alternative Liquid Dielectrics for High Voltage Transformer Insulation Systems: Performance Analysis and Applications*, U. M. Rao, I. Fofana and R. Sarathi, Eds. IEEE-Wiley Press, 2022, pp. 11-42.

Conferences:

[1] **R. Sangineni**, N. Baruah and S. K. Nayak, "Study of the Dielectric Frequency Response of Mineral Oil on addition of Carboxylic Acids," *2022 IEEE Conf. Electr. Insul. Dielectr. Phen. (CEIDP)*, 2022, pp. 143-146.

[2] **R. Sangineni**, N. Baruah and S. K. Nayak, "Influence of Concentration of Nanoparticles on the Dielectric Frequency Response of an Insulating Nanofluid," *2021 IEEE Conf. Electr. Insul. Dielectr. Phen. (CEIDP)*, 2021, pp. 418-421.

[3] **R. Sangineni**, D. Kanumuri, N. Baruah and S. K. Nayak, "Non Isothermal Thermo Gravimetric Analysis (TGA) Measurements of Oxidative Aged Solid Insulation," *2021 IEEE 5th Int. Conf. Condition Assessment Tech. Electr. Syst. (CATCON),* 2021, pp. 252-255.

[4] **R. Sangineni**, N. Baruah, D. Kanumuri and S. K. Nayak, "Comparison of Magnetic Nature of Vegetable Oil based Nanofluids," *2021 IEEE Electr. Insul. Conf. (EIC),* 2021, pp. 548-551.

[5] **R. Sangineni**, N. Baruah, M. Chakraborthy and S. K. Nayak, "Effect of magnetic properties of liquid dielectric on the leakage flux of power transformer," *2020 IEEE Conf. Electr. Insul. Dielectr. Phen. (CEIDP)*, 2020, pp. 123-126.

[6] N. Baruah, **R. Sangineni**, C. Saha, D. Kanumuri, M. Chakraborty and S. K. Nayak, "Supervised machine learning model for predictive analysis of dielectric response of insulating liquids," *2021 IEEE Conf. Electr. Insul. Dielectr. Phen. (CEIDP)*, 2021, pp. 414-417.

[7] N. Baruah, **R. Sangineni**, M. Chakraborty and S. K. Nayak, "Estimation of Dielectric Parameters of Aged Natural Ester based Insulating Liquid using Open Beaker Oxidative Ageing technique," *2021 IEEE 12th Energy Convers. Congr. Exposition - Asia (ECCE-Asia),* 2021, pp. 1833-1838.

[8] S. S. Dey, **R. Sangineni**, N. Baruah and S. K. Nayak, "Study of Heat Transfer Property of the Transformer Oils on Addition of CuO Nanoparticles," *2021 IEEE Conf. Properties Appl. Dielectr. Mater. (ICPADM)*, 2021, pp. 218-221.

[9] D. Kanumuri, **R. Sangineni**, N. Baruah and S. K. Nayak, "Study of magnetic properties of mineral oil based nanofluids," *2021 IEEE Conf. Properties Appl. Dielectr. Mater. (ICPADM)*, 2021, pp. 226-229.

[10] N. Baruah, **R. Sangineni**, M. Chakraborty and S. K. Nayak, "Data Driven Analysis of Aged Insulating Oils by UV-Vis Spectroscopy and Principal Component Analysis (PCA)," *2020 IEEE Conf. Electr. Insul. Dielectr. Phen. (CEIDP)*, 2020, pp. 451-454.

TH-3272_186151014

[11] N. Baruah, **R. Sangineni**, M. Chakraborty and S. K. Nayak, "Statistical Analysis of Natural Ester based Insulating Liquid using Hypothesis Testing," *2020 Int. Symp. Electr. Insul. Mater. (ISEIM),* 2020, pp. 347-350.

[12] S. S. Dey, **R. Sangineni**, N. Baruah, M. Maharana and S. K. Nayak, "Investigation of thermal conductivity of semiconducting nanofluid for transformer," *2019 IEEE Conf. Electr. Insul. Dielectr. Phen. (CEIDP)*, 2019, pp. 109-112.

[13] M. Chakraborty, N. Baruah, **R. Sangineni**, S. K. Nayak and P. K. Maiti, "Dissolved Gas Analysis (DGA) of Thermally Aged Blended Transformer Oil," *2020 IEEE Conf. Electr. Insul. Dielectr. Phen. (CEIDP)*, 2020, pp. 204-207.

TH-3272_186151014